UNIVERSITY OF CALIFORNIA
RIVERSIDE

Application of a Semi-Distributed Hydrologic Model to Understand Hydrologic Flux Partitioning of an Arid, Highly Managed Watershed

A Thesis submitted in partial satisfaction
of the requirements for the degree of

Master of Science

in

Environmental Sciences

by

Aarushi Jha

September 2020

Thesis Committee:
Dr. Hoori Ajami, Chairperson
Dr. Jirka Simunek
Dr. Andrew B. Gray

The Thesis of Aarushi Jha is approved:

_____

_____

_____

Committee Chairperson

University of California, Riverside

Acknowledgments

I would like to express my sincere gratitude to my advisor Dr. Hoori Ajami, for her expertise, insight, and invaluable guidance throughout this project. I would like to thank her for giving me this opportunity and for motivating me to ask the right questions and develop my skills as a scientist in the field of watershed hydrology.

I would also like to express my thanks to Dr. Adam Schreiner-McGraw, for his mentorship, feedback, and support in helping develop this project.

I would like to thank Dr. Aliasghar Montazar for his feedback and providing information on cropping and irrigation practices in the Imperial Irrigation District.

This material is based upon work partially supported by the National Science Foundation under Grant Addressing Decision Support for Water Stressed FEW Nexus
Decisions Numbered 1739977. Any opinions, findings, and conclusions or recommendations expressed in this material are those of the author(s) and do not necessarily reflect the views of the National Science Foundation." Additional support is provided by the Agricultural Experimental Station – RSAP fund from UC Riverside.

Dedication

This thesis is dedicated to my husband Michael Jhatro for his never-ending support.

And, to my parents Suraj Kumar Jha and Rimjhim Jha, for their love, belief, and guidance.

ABSTRACT OF THE THESIS

Application of a Semi-Distributed Hydrologic Model to Understand Hydrologic Flux Partitioning of an Arid, Highly Managed Watershed

by

Aarushi Jha

Master of Science, Graduate Program in Environmental Sciences
University of California, Riverside, September 2020
Dr. Hoori Ajami, Chairperson

Irrigated agriculture accounts for 70% of global freshwater withdrawals and increases in the frequency and intensity of droughts and population growth have exerted significant stress on freshwater supply in recent decades. There is a growing need to improve the quantification of hydrologic fluxes in agricultural ecosystems and reduce water use particularly in arid and semi-arid regions where irrigation contributes substantially to the region's water budget. Given the limited availability of hydrometric observations at catchment scale, hydrologic models have been widely used in research and operational applications. Recent advances in computational resources and availability of spatially distributed data have increased the use of numerical models for water balance estimation at large scale. The objective of this study is to quantify hydrologic flux partitioning of the Salton Sea Watershed, a 21,801 km^2 highly managed watershed in the arid regions of Southern California and Mexico. We apply a semi-distributed hydrologic model, Soil and Water Assessment Tool, to simulate hydrologic processes of two distinct hydrologic systems - undisturbed headwater subbasins in the mountain ranges and irrigated agricultural subbasins in the southern part of the watershed. The model setup incorporates a large endorheic lake (Salton Sea) and major irrigation canals to distribute imported Colorado River inflows across major irrigation regions. To reduce computational demand, we demonstrate a method for selecting optimal spatial discretization of Hydrologic Response Units while capturing spatial variability of hydrologic

fluxes. Model calibration for 8 undisturbed headwater subbasins is conducted on a monthly time step using the SUFI-2 optimization algorithm. We found that the suggested calibration methodology for maintaining spatial variability of parameters did not yield satisfactory model performance using Nash-Sutcliff Efficiency as an objective function (NSE < 0.5). An alternative calibration approach of replacing values of spatially distributed parameters improved model performance for 4 out of the 8 headwater subbasins (NSE ≥ 0.5) during calibration and validation periods where streamflow was perennial and mean annual streamflow was larger than 60 mm/year. Model calibration for 13 agricultural subbasins was conducted using a combination of manual and automatic calibration techniques for monthly streamflow at two major rivers draining to the Salton Sea. The calibrated model did not yield satisfactory results for either rivers (NSE < 0.5). However, temporal dynamics of streamflow is well captured by the model (linear correlation coefficient R > 0.8). We performed two simulation scenarios to assess the impacts of changes in the Colorado River inflows on the water balance. We found that under these scenarios, changes in the Salton Sea inflows were directly caused by seasonal fluctuations in the Colorado River inflows, and evapotranspiration and irrigation were not significantly impacted compared to the baseline simulation even for the low flow scenario. These findings have important implications for water and agricultural management in the Salton Sea Watershed where competing water demand exist among agriculture and urban users, and natural habitats. Future efforts will focus on improving the calibration approach by incorporating the remotely sensed evapotranspiration and soil moisture products and representing subsurface hydrologic processes using physically based modeling approaches.

TABLE OF CONTENTS

LIST OF FIGURES

LIST OF TABLES

1. INTRODUCTION

Agriculture is the single largest user of freshwater globally, accounting for 70% of global freshwater withdrawals (Wada et al., 2014). With increasing stress on freshwater resources, there is a growing need to improve the quantification of hydrologic fluxes in agricultural systems and reduce water use. This is especially important in arid and semi-arid regions of the world, where irrigation can contribute substantially to the region's water budget (McInerney et al., 2018). Since precipitation in arid and semi-arid regions is often not sufficient to support large-scale agriculture, these systems rely on limited freshwater resources. For example, in the American Southwest, the over-allocated Colorado River provides water for 40 million people and 13,000 km^2 of agriculture lands in the U.S and Mexico (Cohen et al., 2013). A recent study found that unimpaired streamflow in the Colorado River declined by 16.5% over a century (1916 - 2014), with over half of this decrease being associated with a general increase in climatic warming (Xiao et al., 2018).

With increasing demand for freshwater resources, climate change induced variability in precipitation (Kirchmeier-Young & Zhang, 2020), and its subsequent impact on freshwater supply, the need for quantifying regional scale hydrologic budget in irrigated agriculture ecosystems becomes clear. Estimating the hydrologic balance of a watershed is essential for understanding the dominant hydrologic processes of the watershed, and for water resources planning. With an increase in computational resources, hydrologic models have become a pertinent tool in understanding hydrologic processes from field to regional scales.

Hydrologic models are used widely in both research and operational applications. Hydrologic models are mathematical representations of physical processes that govern the movement and storage of water in a system. Models can be broadly classified into three categories – lumped, semi-distributed and fully distributed. Lumped models treat a watershed as a single unit with climate forcings, state variables (soil moisture, water stored in snow and groundwater) and parameters that represent watershed average condition. These models assume that model inputs and watershed

properties are uniformly applied over the entire catchment, and they ignore spatial variability of watershed properties. Lumped models such as the widely used HyMOD model (Boyle et al., 2000) have less computational and data requirements and are easy to use. Distributed hydrologic models preserve spatial variability in climate forcings and watershed properties and make spatially distributed predictions. These models divide a watershed into a gridded network of cells and perform hydrologic simulations for each cell. Some widely used distributed models include MIKE-SHE (Abbott et al., 1986), HYDRUS 3D (Simunek et al., 2006), and ParFlow (Kollet & Maxwell, 2006). These models can be computationally and data intensive for applications in large catchments. Semi-distributed models disaggregate a watershed into smaller homogenous spatial entities that are representative of catchment characteristics or hydrologic response (Khan et al., 2018). By doing so, the modeler is able to capture spatial distribution of climate and watershed properties, while reducing computational demand. The Soil and Water Assessment Tool (SWAT) (Neitsch et al., 2009) is a widely used semi-distributed model, with over 4000 publications (Tan et al., 2020). Its popularity as a modelling tool can be attributed to its semi-distributed nature, modularity, ability to use global data sets, and reliable user and developer support (Gassman et al., 2010; Griensven et al., 2012). Additionally, the model has been used widely in agricultural systems due to its ability to implement management operations such as reservoirs, irrigation, and harvest practices.

This study is focused on the Salton Sea Watershed (SSW) in California, one of the most productive and water intensive agricultural regions in the United States (Kannan et al., 2019). The SSW is an endorheic watershed, with all catchment runoff draining to the centrally located Salton Sea. The Salton Sea exists in a balance between evaporation from the lake, surface inflows and subsurface flows to or from the lake. Shallow lakes such as the Salton Sea are particularly sensitive to changes in temperature and evaporation due to their high surface area to depth ratio. The SSW lies in the

Inland Dessert Region of California, where daily maximum temperatures are projected to increase by 14-15ºC for 2006-2039, by 12-14ºC for 2040-2069, and 10-13ºC for 2070-2100 depending on future greenhouse gas emissions (Hopkins et al., 2018). This increase in temperature can be expected to increase evaporation from the lake's surface, a consequent shrinking of the lake and increasing dust emissions and air quality issues in the region. Past variability in the Colorado River allocations has reduced agricultural inflows to the Salton Sea, resulting in an increase in the lake salinity of 60 ppm (CH2M Hill, 2018a), about twice as saline as ocean water. A continued increase in salinity could cause irreversible damage to the lake's ecology by creating inhospitable breeding and habitat conditions for tilapia and other essential species in the Salton Sea food web (Cohen & Hyun, 2006). Therefore, quantifying inflows to the Salton Sea is crucial to inform any management plans in the SSW.

Modelling the Salton Sea presents the following challenges:

- The endorheic nature of the watershed makes automated watershed delineation difficult.
- The lack of publicly available field specific irrigation data impacts accuracy of water budget calculations.
- The presence of extensive canals and drainage network with no publicly available information about their distribution, properties, and management operations makes water budget calculations difficult.

The SWAT model was selected for this project because of its demonstrated application in systems with similar characteristics and challenges. In the following sections, summary of previous research as it relates to simulating water balance of irrigated agriculture is discussed.

Quantifying Inflows to Lakes

SWAT has been used to quantify inflows to lakes. Bosch et al. (2011) created SWAT models for six watersheds that generated streamflow to Lake Erie and evaluated model performance for

predicting discharge and sediment loading to Lake Erie. They found that SWAT simulations of stream discharge for all 6 watersheds varied from 'good' to 'very good' based on the Nash-Sutcliffe Efficiency (NSE) of 0.70-0.92 (Bosch et al., 2011). Bucak et al. (2017) utilized SWAT in conjunction with a Regression Model to assess the impacts of climate change and land use changes on water levels in Lake Beysehir, Turkey. This 650 km^2 lake is situated in a 4,704 km^2 large watershed with mean annual precipitation of 490±94 mm. SWAT simulated inflows to the lake along with SWAT generated potential evapotranspiration (PET) were input to the regression model to calculate changes in lake levels with different climate change and land use change scenarios. The authors demonstrated that the SWAT model could be used successfully to simulate inflows to the lake ($NSE \geq 0.5$) (Bucak et al., 2017). Finally, Shabani et al. (2017) setup a SWAT model for the endorheic Devil's Lake watershed (10,187 km^2) in North Dakota, to evaluate the water balance and Sulfur concentrations in the lake. They found that SWAT performed well ($NSE \geq 0.5$) in simulating daily flow in tributaries (Shabani et al., 2017). Therefore, previous studies have demonstrated that SWAT can be used with success to model surface inflows to lakes.

The endorheic nature of the Salton Sea poses a challenge in the physical representation of lake boundary within the SWAT delineation of the watershed. While previous studies have successfully modelled lake inflows (Bosch et al., 2011; Bucak et al., 2017; Shabani et al., 2017), simulating lake evaporation requires an accurate representation of the lake's surface area within the model. SWAT allows lakes and reservoirs to be represented as a discrete point on the stream network that receives flow from the upstream watershed, regardless of the size of the waterbody. While this representation works for lakes that also serve as outlet of the watershed, it could reduce accuracy of water balance predictions in watersheds with large lake to watershed ratios, or lakes that receive inflows from multiple streams (Molina-Navarro et al., 2018). Molina-Navarro and others (2018) outlined a methodology to accurately represent lakes in SWAT watershed delineation. This method

utilizes GIS techniques that incorporates the lake's shapefile as a subbasin within the watershed's delineated subbasins. We utilized this technique to incorporate the Salton Sea as a subbasin within the model.

Incorporating Irrigation Practices in Agricultural Watersheds

Intensively irrigated watersheds in arid and semi-arid regions, where rainfall is not enough to support plant growth, can have elevated evapotranspiration (ET) rates due to a combination of irrigation enhanced soil moisture and variability in climatological forcings (Wei et al., 2018). Irrigation inputs such as the amount and timing of irrigation application influence crop ET as well as irrigation-based surface runoff. Groundwater recharge from irrigated versus non-irrigated catchments has been observed to be significantly different, especially in arid regions (Githui et al., 2012). Therefore, accounting for irrigation is extremely important in establishing regional water budgets in irrigated catchments. Incorporating irrigation in large scale studies is often hindered by the lack of information on crop specific irrigation demand and application practices. Studies have represented irrigation in large scale models such as the Variable Infiltration Capacity (VIC) model where irrigation demand was calculated as the difference between current soil moisture, and minimum of crop specific evapotranspiration or soil moisture at field capacity while operating at a 1 km resolution (Nazemi & Wheater, 2015). Another study used the difference between current soil moisture content and soil moisture at field capacity in the NICE model to calculate irrigation demand (Nazemi & Wheater, 2015). However, both of these studies calculated irrigation demand at large coarse scales (1-10 km), which presents a challenge in identifying field scale water budgets. SWAT has been widely used for a variety of applications in irrigated catchments, including the transport and mitigation of agricultural pollutants (Dechmi & Skhiri, 2013; Luo et al., 2008), estimating irrigation-based groundwater recharge (Awan & Ismaeel, 2014) or crop water demand for different management scenarios (Ficklin et al., 2009; Marek et al., 2017). Xie and Cui (2011)

modified SWAT by incorporating new processes for irrigation and drainage of rice paddy fields in a 1,100 km^2 catchment. Results showed improvement in simulated runoff and crop yields (Xie & Cui, 2011). In SWAT2009, applied irrigation water in excess of field capacity would return to the source and was not included in the soil water balance calculations. Dechmi et al. (2012) modified the SWAT2009 source code to better incorporate water applied in excess of crop consumption in the hydrologic balance (Dechmi et al., 2012). Modifications included – 1) changing the amount of applied irrigation water to a user defined value as opposed to the amount of water held at field capacity, 2) adding irrigation excess water to percolation out of the soil profile, and 3) modifying the subbasin routine chronology to calculate soil water balance after irrigation operations. The updated SWAT2012 model (used in this project) handles soil water balance in irrigated subbasins in a manner similar to that of Dechmi et al. (2012).

The amount and timing of irrigation influences the partitioning of irrigation water into crop ET, surface runoff and percolation. If users have data on irrigation amounts and timing, they can utilize the "manual irrigation" option to schedule realistic irrigation options in SWAT management files. McInerney et al. (2018) demonstrated a method to capture the spatial and temporal variation in irrigation application that stems from field scale differences in farmer's irrigation practices. They utilized field-scale daily irrigation input data, and irrigation depth for crop types to create a spatially variable, event-based irrigation schedule for SWAT model of the Barr Creek Catchment, Australia. These modifications significantly improved model simulations where NSE improved from 0.15 to 0.56 and bias reduced from ~40% to ~2% (McInerney et al., 2018).

While the previously mentioned studies improved the representation of hydrologic processes within agricultural areas, they all utilized observed irrigation inputs. The limited availability of data on timing and depth of irrigation is a major obstacle to create accurate hydrologic models of irrigated areas. This is also true for the SSW, where irrigation forms a significant portion of the regional

water budget; however, the lack of field specific irrigation input poses a great challenge to incorporate irrigation practices in the model.

An alternative to the manual irrigation option in the SWAT model is "automatic irrigation" scheduling. Automatic scheduling of irrigation is based on a user defined threshold that triggers the application of irrigation. This threshold can be defined based on either Plant Water Stress (PWS) or Soil Water Deficit (SWD). Plant water stress is a constraint on optimal plant growth that is calculated as a fraction of actual plant transpiration to potential plant transpiration. This water stress factor varies between 0 (under optimal conditions) to 1. Soil water deficit threshold is the maximum allowable depletion of the soil water (mm H_2O) below field capacity, after which irrigation is triggered. This SWAT methodology is similar to the irrigation practice of Management Allowable Depletion (MAD) of soil water. MAD is defined as the optimal soil-water deficit at the time of irrigation, such that providing irrigation at this threshold reduces crop water stress (NRCS, 2005). Uniyal et al. (2019) utilized both PWS and SWD based automatic irrigation techniques to estimate irrigation requirements for four catchments across the globe. They assessed irrigation as simulated by both PWS and SWD, and found that PWS consistently underestimated the applied irrigation amount, and SWD auto-irrigation simulated more realistic irrigation application (Uniyal et al., 2019). In 2017, Chen and others utilized observed ET and crop yield data to test the efficacy of different SWAT methods for simulating irrigation management in the Texas High Plains. They utilized SWD based auto-irrigation as one of their method, as this option is reflective of actual field irrigation practices being commonly scheduled in response to changes in root zone soil water content (Chen et al., 2017). While their study demonstrated reasonable performance for simulating crop ET ($NSE \geq 0.80$) and streamflow ($NSE \geq 0.50$), it also highlighted a deficiency of the SWAT auto-irrigation option, wherein irrigation was applied even after the harvest and overestimated applied irrigation. This limitation of the SWAT model has been highlighted in previous papers and

is addressed in the Methods section of this thesis. SWAT model only represents applied irrigation depths and does not distinguish between types of irrigation such as sprinkler, furrow, or flood irrigation. This was a major limitation of the study.

Water Balance of Irrigation Canals

In addition to the field scale application of irrigation, it is essential to consider the system of canals that distribute water within agricultural regions. Crop growth in arid and semi-arid regions is limited by water availability. In such areas, irrigation compensates for limited water availability by transferring water from streams, aquifers, and reservoirs through a series of lined or unlined canals. Seepage losses from earthen canals can constitute a significant portion of water loss in irrigated areas (Swamee et al., 2000). The Imperial Irrigation District (IID) in the southern portion of the Salton Sea watershed services its farms through a network of 2,500 km of canals. Additionally, 330 km of major canals transfer water from the Colorado River at the Imperial Dam to its main agricultural areas in the U.S. Wei et al. (2018) modified and utilized SWAT to simulate management practices, including canal seepage, in a 732 km^2 watershed in the Lower Arkansas River Valley, Colorado. They found that out of all management practices, canal seepage was essential to modeling and capturing streamflow in irrigated areas as seepage raised shallow groundwater tables and increased streamflow (Wei et al., 2018). Xiong et al. (2019) improved the physical representation of canals in an intensively irrigated area in the Yellow River basin by using the canals as subbasin boundaries, hence enabling more realistic application of irrigation water from a canal to its recipient agricultural field (Xiong et al., 2019). Both of these studies incorporated canals in their models as drainage features and were able to successfully capture the hydrologic processes associated with them, thus demonstrating that canals and their associated hydrologic processes can be represented in a SWAT model. However, the challenge remains in delineating canals in automated watershed delineation algorithms where land surface elevation from a Digital

Elevation Model (DEM) is used to delineate streams and subbasins based on flow accumulation grids.

Model Calibration

Model calibration is an essential step in improving hydrologic model performance. During calibration model parameters are adjusted until model outputs such as streamflow or evapotranspiration match observed data. The process of calibration in models with high spatial and temporal heterogeneity can be complex and cumbersome particularly in spatially distributed, process-based models that rely on multiple parameters to simulate hydrologic processes. Successful model calibration depends on availability of observations, mathematical representation of hydrologic processes in the model, knowledge of watershed characteristics (Immerzeel & Droogers, 2008), and the number of calibrating parameters. Furthermore, a large number of model simulations is often required to find optimum model parameters. Automatic calibration approaches can help overcome some of these difficulties by implementing computationally efficient optimization algorithms. While some parameters can be measured or obtained from datasets (soil hydraulic conductivity, rooting depth, etc.), others are empirical parameters (such as lag coefficients) that are intrinsic to the model's representation of a physical process and need to be estimated during model calibration. Estimating physically based parameters for large scale model application is challenging due to the limited availability of observations.

SWAT Calibration and Uncertainty Program (SWAT-CUP) is a widely used computer program that couples the SWAT model with multiple optimization algorithms, including Sequential Uncertainty Fitting (SUFI-2), Particle Swarm Optimization (PSO), Generalized Likelihood Uncertainty Estimation (GLUE) and Parameter Solution (ParaSol) (Abbaspour, 2015). Khoi and Thom (2015), compared the 4 methods for calibrating a SWAT model in a large (12,000 km^2) watershed in Vietnam (Khoi & Thom, 2015). They found that while the NSE values were

comparable across the 4 methods, SUFI-2 had the least bias and least uncertainty in model simulations. SUFI-2 was also found to be the most computationally efficient method for parameter estimation as it required the least number of model simulations (1000 compared to 4000-10,000). Zhang and others (2019) compared the performance of SUFI-2 and GLUE in two catchments with different characteristics (topography and size), and found that SUFI-2 performed better than GLUE in the mountainous, semi-arid catchment (Zhang et al., 2019).

Application of SWAT in the Salton Sea Watershed

The Salton Sea Watershed is surrounded by mountain ranges on the northeastern and northwestern boundaries. Subbasins in these mountain ranges are headwaters to the Whitewater River, which is one of the major streams in the northern portion of the watershed. While Alamo and New River south of the Salton Sea contribute larger flows to the lake, it is important to account for inflows from the Whitewater River as well. Previous studies have demonstrated application of SWAT in mountainous watersheds in arid climates. Koycegiz and Buyukyildiz (2019) applied the SWAT model in a ~154 km^2 headwater catchment in the semi-arid/arid Carsamba River Basin in Turkey. They calibrated the model against observed streamflow using SUFI-2 optimization algorithm and found that the model performance was satisfactory with NSE of 0.78 and R^2 of 0.79 during calibration (2006 – 2011) and NSE of 0.50 and R^2 of 0.51 during validation (2012 - 2015) period (Koycegiz & Buyukyildiz, 2019).

The SWAT model has also been used in a range of applications including conservation practices, land use and climate change impact assessment, and estimating pollutant load for a wide range of environmental conditions and spatial scales (Gassman et al., 2007). A study in 2019 demonstrated the applicability of SWAT model for estimating nitrogen loadings from agriculture in the San Joaquin watershed in California (Wang et al., 2019). They found that SWAT model performance in simulating nitrogen loads during calibration was satisfactory (NSE = 0.45) at the watershed outlet

but was unsatisfactory at the outlet of an upstream sub-watershed (NSE = -0.11). However, model performance during the validation time frame was unsatisfactory at both outlets. Paul and Nagahban-Azar (2018), evaluated model calibration performance and parameter sensitivities using three optimization algorithms for a SWAT model setup for the large (15,358 km^2) semi-arid, agricultural San Joaquin Watershed in California (Paul & Negahban-Azar, 2018). They found that the best model performance metrics were obtained by SUFI-2 while using NSE as an objective function (NSE = 0.76 – 0.91). While this study demonstrated the feasibility of utilizing SWAT in a large, semi-arid watershed, this model did not incorporate irrigation operations and did not target headwater subbasins for calibration.

This study is focused on the Salton Sea Watershed (SSW), a large irrigated agricultural catchment in southern California and northern Mexico (Kannan et al., 2019). The main goal of this project is to quantify long term water balance of the SSW and capture streamflow generation processes in two hydrologically distinct systems in the watershed – undisturbed headwater subbasins in the mountain ranges, and irrigated agricultural subbasins in the southern part of the watershed. Specifically, we focus on answering three main research questions:

1) How to optimize spatial discretization of hydrologic response units (HRUs) to capture spatial variability of hydrologic fluxes while reducing computational time?
2) How spatial and temporal variability of hydrologic fluxes vary across the watershed as a function of climate variability and Colorado River inflows?
3) What are the implications of changes in Colorado River inflows and their impact on lake inflows and irrigation?

2. METHODS

2.1 Site Description

The Salton Sea watershed (SSW) is a 21,801 km^2 transboundary arid watershed located in southeastern California, and about 15% of its area is in northern Mexico. The watershed spans Riverside, San Bernardino, San Diego, and Imperial counties in the U.S., and extends across the international border into the Mexicali Valley of Baja California, Mexico. Elevation in the SSW ranges from -87m below sea level to 3498 m above sea level, with a mean elevation of 1705 m (Figure 1). The topographically closed watershed is bounded by the San Jacinto and Santa Rosa

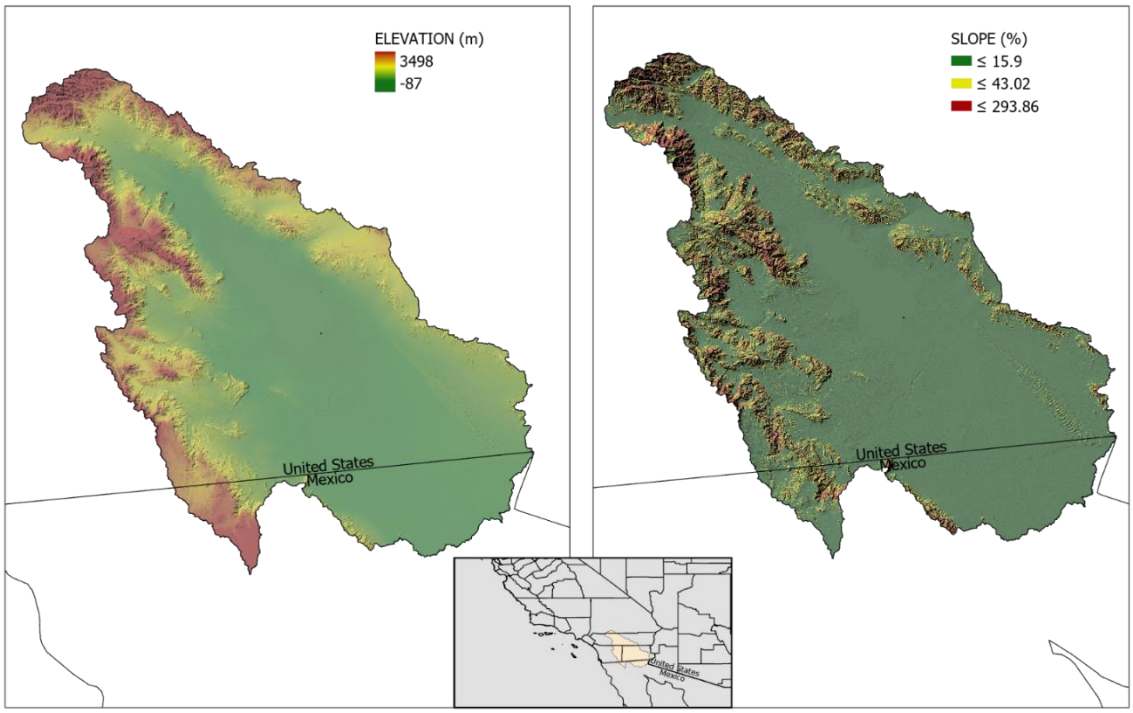

Figure 1. Land surface elevation (m) and slope (%) of the Salton Sea Watershed obtained from a 30 m Digital Elevation Model. The inset map shows watershed location on the west coast of the United States.

Mountain ranges in the northwest, that extend into the Peninsular Mountain ranges of Baja California to the southwest. On the eastern edge, the watershed is bounded by the San Bernardino mountain ranges in the northeast, extending to Orocopia and Chocolate mountain ranges to the east.

The Salton Sea is a terminal lake with an area of 888 km^2 located in the lowest portion of a rift valley called the Salton Trough.

2.1.1 Climate

The SSW is in an arid climate zone and experiences significant interannual variability in precipitation. Much of the precipitation falls in the winter months of November through March (Figure 2) particularly in the northern and northwestern mountain ranges (Figure 3). Between 1980 and 2018, the SSW experienced an average annual precipitation of 148±78.9 mm and average annual Potential Evapotranspiration (PET) of 2,719±456 mm (Thornton et al., 2016). During the same time period, the average daily temperature was 21±0.65 (Thornton et al., 2016).

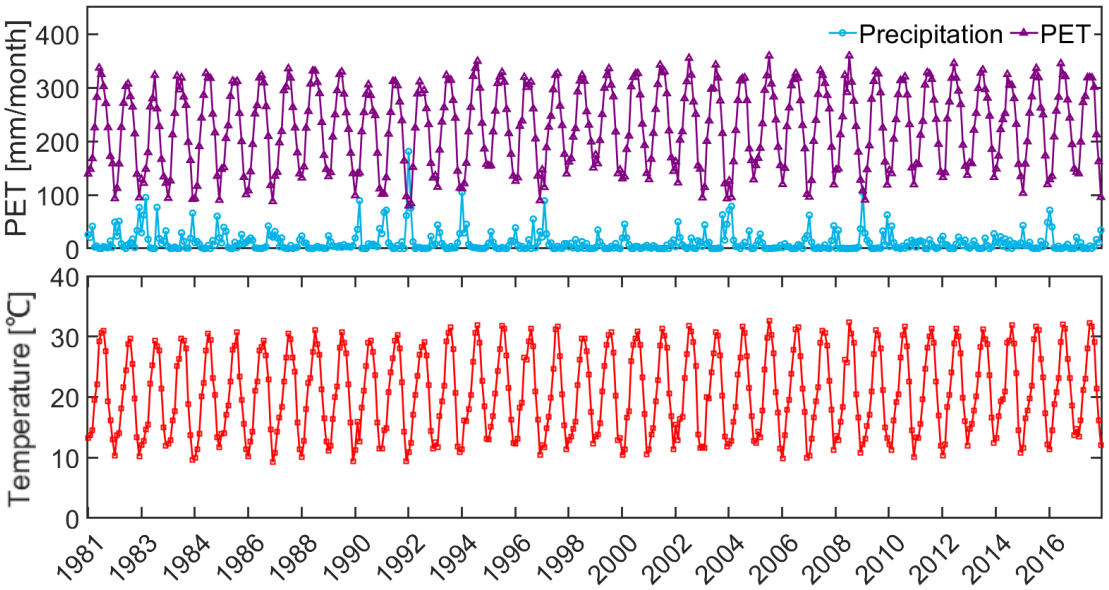

Figure 2. Monthly watershed average PET, precipitation, and mean temperature between 1980 and 2018 (Thornton et al. 2016).

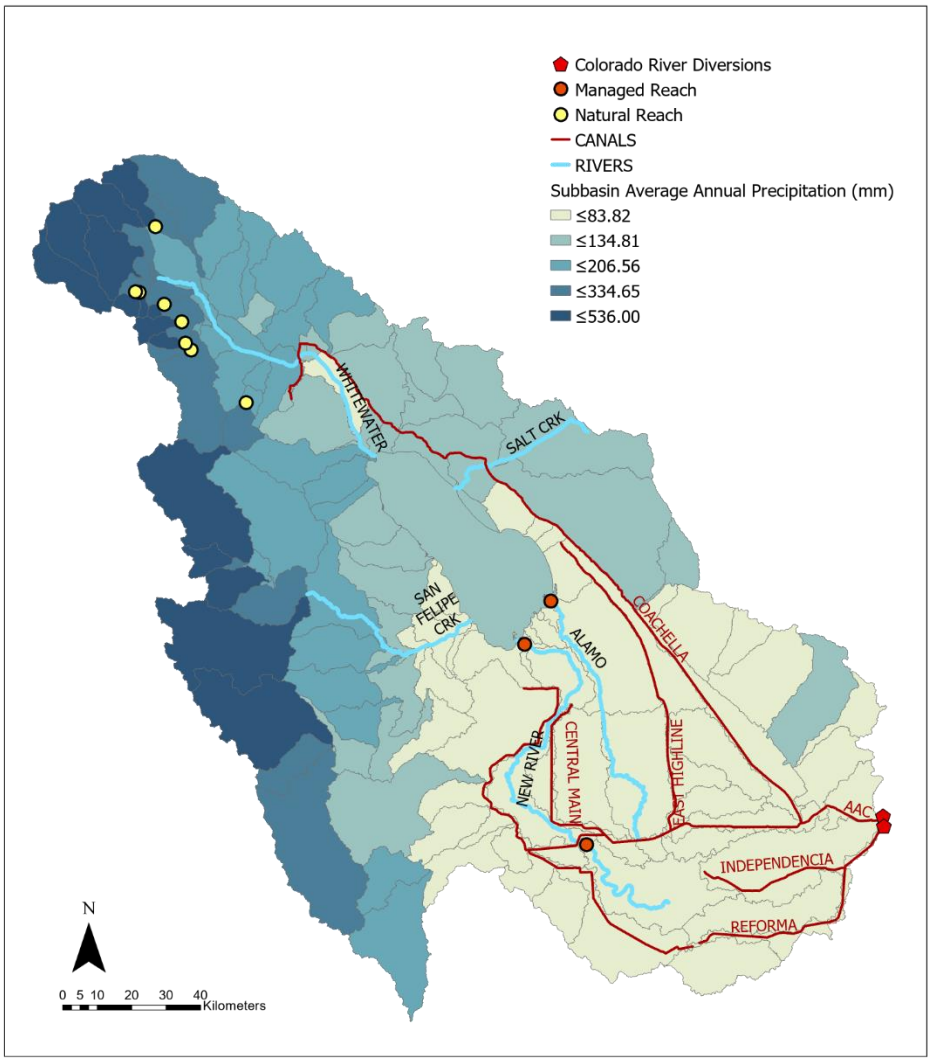

Figure 3. Spatial variability of mean annual precipitation (1980-2018) in the Salton Sea Watershed.

2.1.2 Land Cover/Land Use

According to the 2001 National Land Cover Database (NLCD), 70.9% of the watershed is covered by perennial grasses or arid rangelands typical of South Western United States (Figure 4). Forests cover 3.3% of the watershed area, mainly in the higher elevation mountains bordering the northern and northwestern edge of the watershed, and urban areas cover 4.7% of the watershed. According to NLCD 2001, about 15.3% of the watershed is agriculture, located in three major agricultural regions: Coachella Valley in the north, and the Imperial Valley Irrigation District (IID) and

Mexicali Valley in the south. Due to lack of publicly available data, only general information about agriculture in the Mexicali Valley is incorporated in this project. According to the land use dataset from the National Commission for Knowledge and Use of Biodiversity (CONABIO), agriculture covers an area of 1221 km^2 in the Mexicali Valley portion of the SSW.

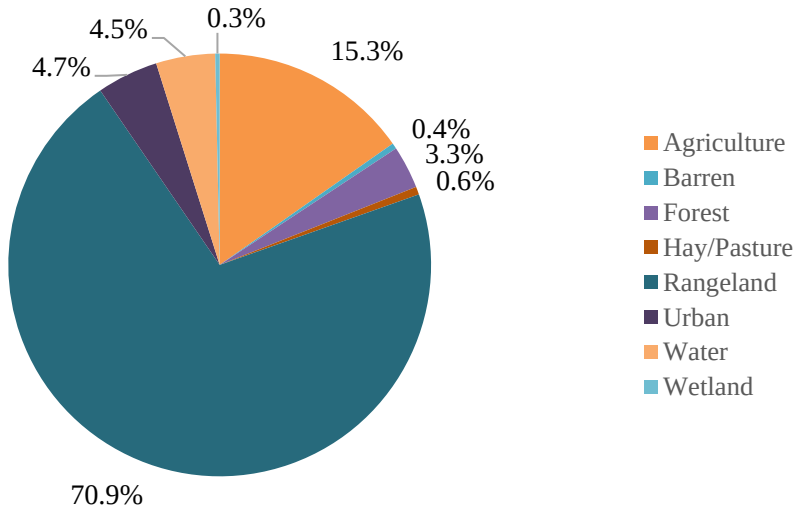

Figure 4. The percent area (%) occupied by various land use/land cover categories within the Salton Sea Watershed in 2001 (NLCD).

Table 1. Area of various land use categories within the Salton Sea Watershed (NLCD 2001). Forest land cover consists of 91% Evergreen forest, 7% Mixed forest and 3% Deciduous forest.

Land Use	Area (km^2)	Area (%)
Rangeland	15448	70.9
Agriculture	3329.3	15.3
Urban	1024.5	4.7
Water	985.4	4.5
Forest	713.8	3.3
Hay/Pasture	131.4	0.6
Barren	95.4	0.4
Wetland	73.6	0.3

Majority of the agriculture lands in the watershed are in the Imperial Irrigation District (IID), which is one of the most productive agricultural regions in the United States. IID produces more than two-thirds of winter vegetables consumed in the US, and about three-quarters of summer hay and other field crops in southern California (Medellín-Azuara et al., 2012). While the net farmed area within IID varies annually, according to the 2001 National Land Cover Database (NLCD) , about 1,861 km^2 of agricultural area (Homer et al., 2020; Jin et al., 2019; Yang et al., 2018) is irrigated with Colorado River waters delivered through the All-American Canal. Irrigation practices in the IID include – flood (>60% of area), row (> 25% of area), followed by sprinkler and drip irrigation (Imperial Irrigation District, 2018).

According to the 2001 NLCD data, agriculture in the Coachella Valley occupies about 152 km^2. Typical irrigation methods in the Coachella Valley depend on the crop type and include furrow irrigation, border strip irrigation, micro-sprinkler irrigation, drip irrigation, and sprinkler irrigation (Natural Resources Conservation Service, 2006). Majority of the agricultural area is irrigated with Colorado River water, though groundwater is also used for irrigation. In 2004, Colorado River provided 290 million m^3 (235,842 acre-feet) of irrigation water in the Coachella Valley, and groundwater supplied 76 million m^3 (61,600 acre-feet) (Natural Resources Conservation Service, 2006).

2.1.3 Soil

Soil dataset for the US and Mexican portions of the watershed were obtained from different sources and combined to create a cohesive spatial dataset (Section 2.3.3). According to the combined spatial soil dataset of the Salton Sea watershed, bedrock dominates 26% of the watershed, followed by Sandy Loam (19%), and Sandy soils (15%) (Table 2). Sandy Loam soil underlies agricultural regions of the Coachella Valley, and Silty Clay Loam and Clay Loam are in the IID and Mexicali Valley agricultural fields, respectively (Figure 14).

Table 2. Soil texture classes in the Salton Sea Watershed. This data does not include soil texture for approximately 5% of the watershed area underlying the Salton Sea.

Soil texture	Area (km^2)	Area (%)
Bedrock	5745.24	26.39
Sandy Loam	4135.44	19
Sand	3294.85	15.13
Loamy Sand	2306.38	10.59
Silty Clay Loam	2202.73	10.12
Clay Loam	1746.23	8.02
Sandy Clay Loam	1223.96	5.62
Sandy Clay	140.98	0.65
Silt Loam	33.06	0.15
Loam	24.62	0.11

2.2. Major Hydrologic Features

2.2.1 Salton Sea

The Salton Sea is a shallow endorheic lake located centrally within the Salton Sea Watershed (SSW). It is California's largest inland lake with a surface area of 888 km^2 and an average depth of 8.8 m (29 feet) that can reach up to 15.5 m (51 feet) (Salton Sea Authority, 2017). The Salton Sea is also a federally designated agricultural sump (Cohen, 2014) that acts as a drainage reservoir for agricultural runoff from farms in the Coachella Valley in the north and Imperial and Mexicali regions in the South. There is no surface drainage out of the Salton Sea, and the lake exists in a balance between inflows to the lake and lake surface evaporation.

Lake inflows are primarily from the Alamo River (732±52 million m^3/year) and New River (543±51 million m^3/year) in the south, Whitewater River (69±22 million m^3/year) in the north, and Salt Creek in the east (2.6±3.9 million m^3/year) as measured by the USGS gages (Figure 5). Agricultural drainage, groundwater discharge and ephemeral washes also contribute to the lake inflows, however, exact percentages are not quantified due to lack of data. Alamo River and New River flows are largely comprised of agricultural runoff and other wastewaters originally derived

from the Colorado River inflows to the Imperial Irrigation District and Mexicali Valley (Tompson et al., 2008). Agricultural and municipal runoff in Mexicali Valley drain to the New River with mean annual flow of 173±72 million m^3/year, measured by a USGS Gage at the international border, and comprises 31.9% of the New River inflow to the Salton Sea. The Whitewater River in the North contributes about 5% of the Salton Sea inflows and the remaining inflows come from agricultural drains in the Imperial Irrigation District, rainfall derived flows from Salt and San Felipe Creeks and groundwater inflows.

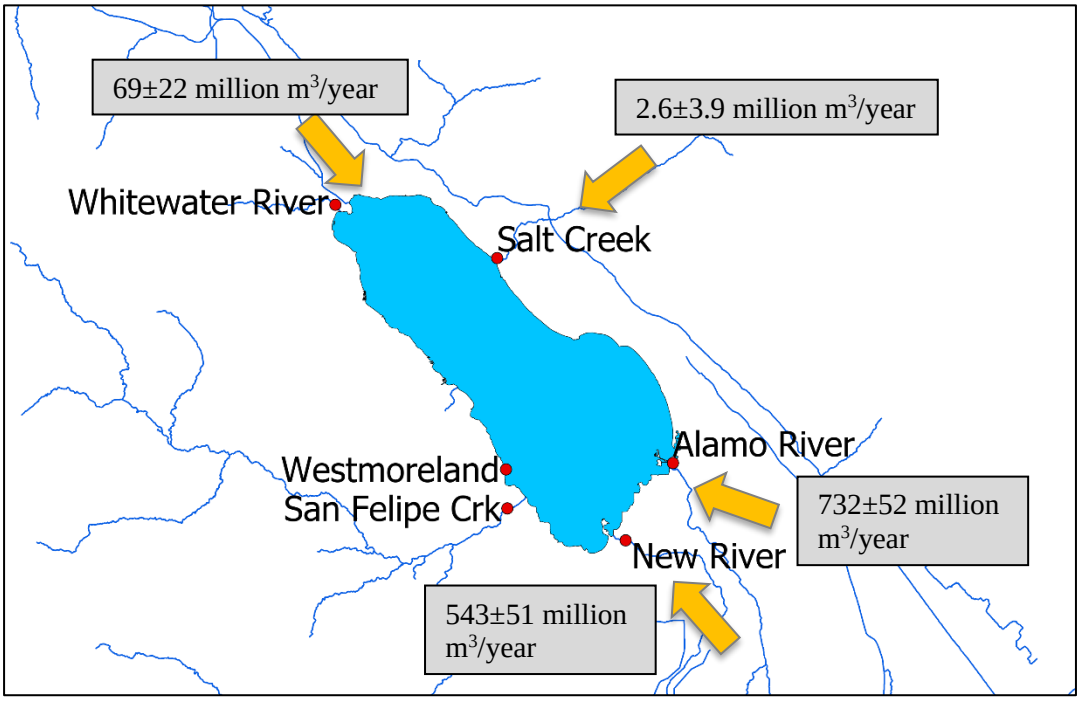

Figure 5. Mean annual inflows as measured at USGS Gages at Westmoreland (gage: 10254005), Alamo River (gage: 10254730), New River (gage: 10255550), Whitewater River (gage: 10259540) and Salt Creek (gage: 10254050).

There are seasonal fluctuations in lake levels, with the lake area shrinking during the summer months and reaching its annual minimum in the fall. Lake area expands through the winter months and reaches its peak in spring (Figure 7). Between 1988 and 2018, the average maximum annual

change in lake level was about 0.40 m; however, maximum changes in annual lake water levels has increased to 0.45 – 0.55 m since 2005 (Figure 6).

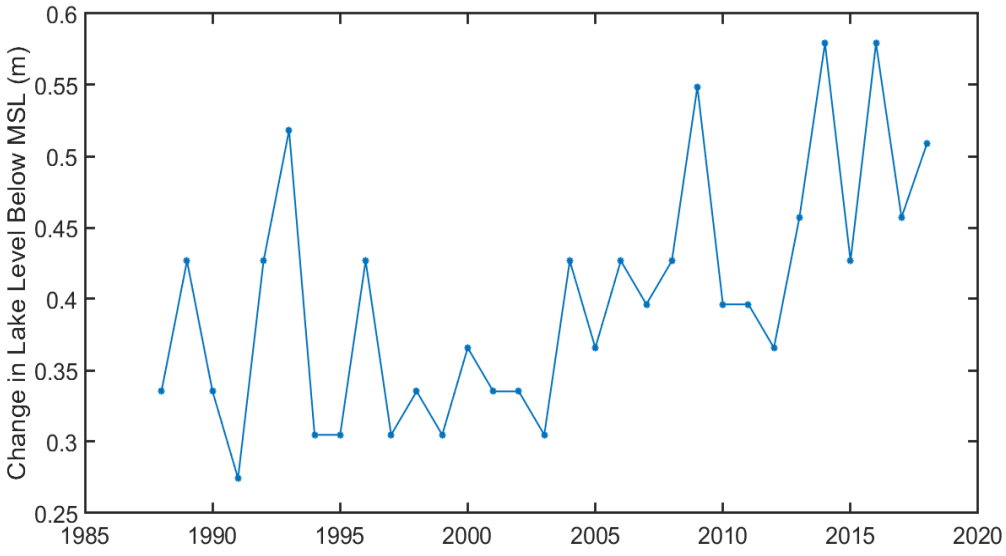

Figure 6. Maximum annual changes in the Salton Sea Lake Levels at Westmoreland between 1988 and 2018. The maximum annual change in lake level has increased since 2005. Maximum annual change is calculated as the difference between the maximum and minimum lake level for the year.

Lake surface water elevation data from the USGS Gage 10254005 at Westmoreland indicates that the Salton Sea level has been gradually declining since 1988 from -69.22 m (below MSL) to -71.84 m (below MSL) in 2018 (Figure 7). A comparison of inflows to the lake from the major rivers (Alamo River, New River, Whitewater River and Salt Creek), shows no declining trend in the lake inflows (Figure 8). The next section describes the major surface water features in detail.

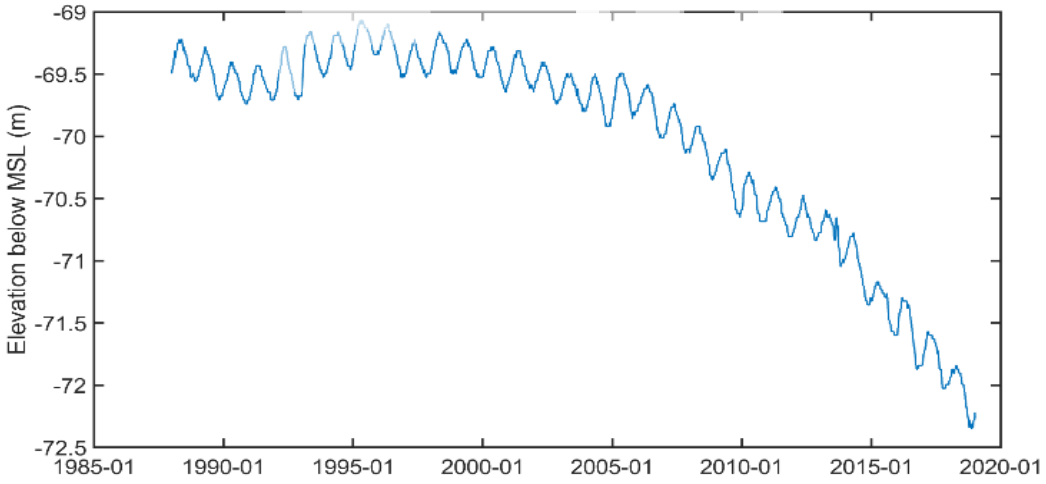

Figure 7. Salton Sea lake levels measured by the USGS gage 10254005 at Westmoreland.

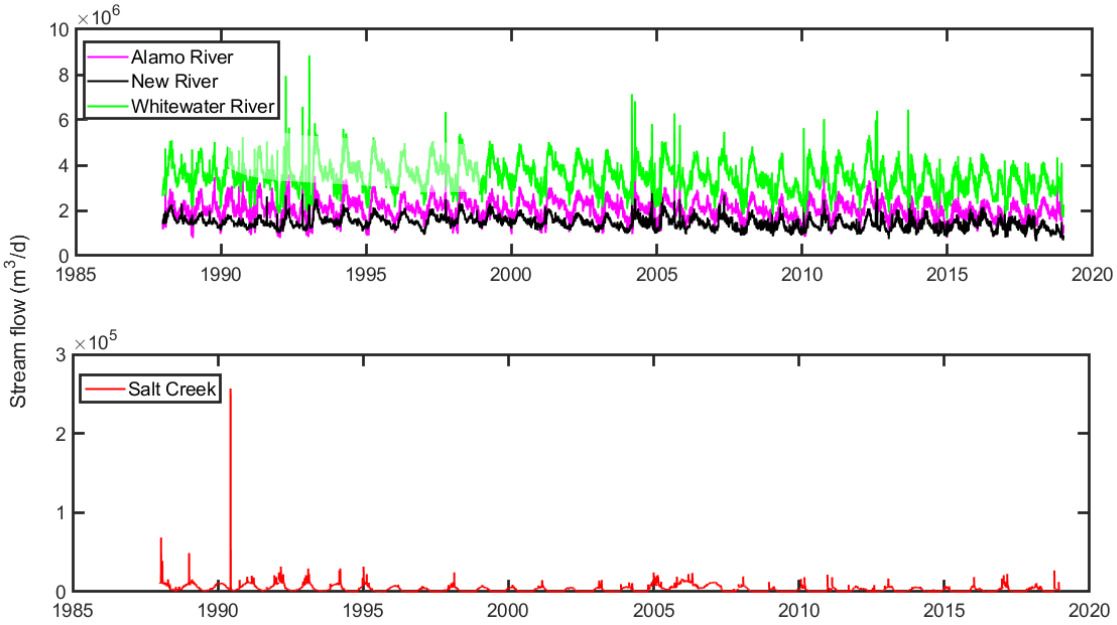

Figure 8. Inflows to the Salton Sea as measured by USGS gages at the mouth of Whitewater, New and Alamo Rivers and Salt Creek at the Salton Sea.

2.2.2 Major Streams

The Whitewater River is 86.7 km (53.9 mile) long and originates in the San Gorgonio and San Jacinto mountain regions and drains urban and agricultural areas of the Coachella Valley before draining to the Salton Sea. The mean annual flow of Whitewater River between 1980 and 2018 (USGS Gage 10259540 at Mecca) near the mouth of the river is 69±21 million m^3/year. This river and its contributing tributaries are heavily managed for aquifer recharge and municipal water supply (MWH, 2012). Daily flows from eight headwater reaches in the San Jacinto mountain ranges are measured by USGS gages and contribute flow to the Whitewater River (Figure 9). Seven of these reaches drain the western edge of the watershed and include Snow, Falls, Chino Canyon, Tahquitz, Andreas, Palm Canyon Creek and Deep Creeks. The eight gage is on the Mission Creek in the northeast. Flow in these reaches is characteristic of streams in the arid Southwestern regions, with large peak flows generated during intense winter storms.

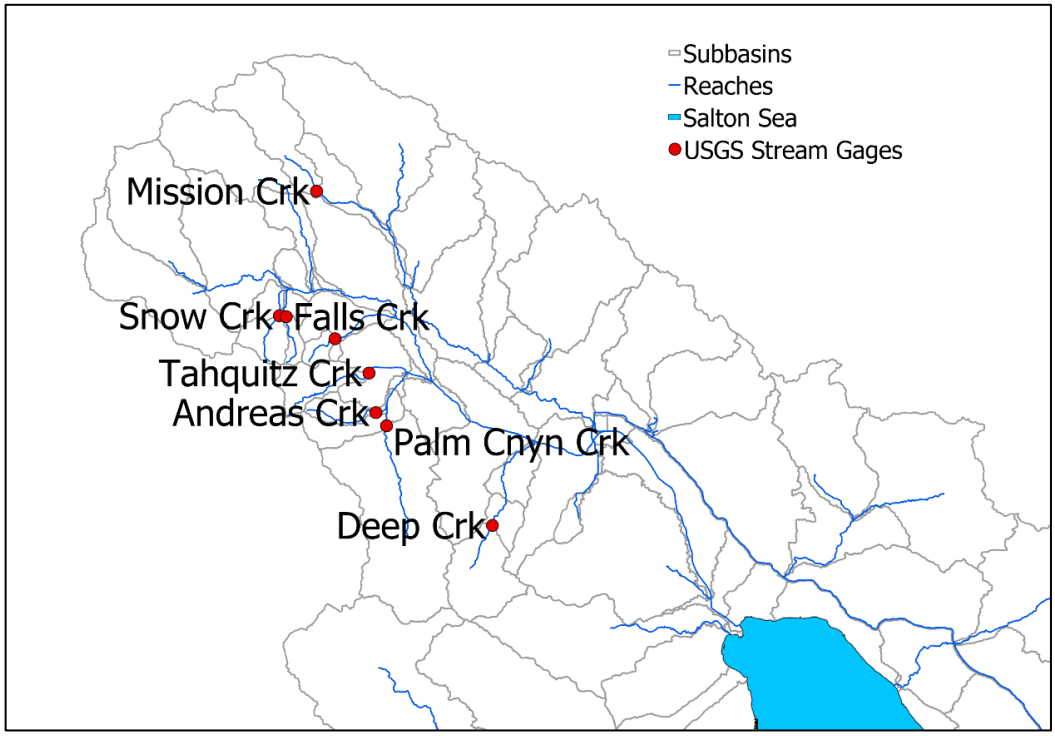

Figure 9. USGS stream gages located on the headwater subbasins draining to the Whitewater River.

Salt Creek is a 42 km (26 mile) long intermittent creek that originates in the Orocopia and Chocolate Mountains on the eastern border of the watershed (Figure 3). Salt Creek is intersected by the Coachella Canal, and there is evidence of increased baseflow from canal seepage in this creek (CH2M Hill, 2018b). USGS gage 10254050 at the mouth of the creek shows mean daily flow of 2±3.9 million m^3/year during 1980 and 2005.

San Felipe is a major natural creek that originates in the Santa Rosa mountains in the west (Figure 3), and travels east towards the Salton Sea. This creek is ephemeral in its upper reaches but is fed by perennial springs near its discharge point (Tompson et al., 2008). The USGS gage 10255885 measured San Felipe creek flows into the Salton Sea, and has limited data available from 1960 till 1991. As a result, this gage is not utilized in model calibration and validation here.

In the South, two major rivers – the New and Alamo Rivers drain to the Salton Sea. Much of the inflows to the Salton Sea from these rivers are comprised of agricultural and municipal runoff from the Imperial Irrigation District and Mexicali. The Alamo River is an 83.7 km long river that drains the eastern region of the Imperial Irrigation District. Flow records from the USGS Gage 10254730 at the mouth of the river indicates mean inflow of 733±52 million m^3/year between 1980 and 2005 (). The Alamo River constitutes the largest inflows to the Salton Sea. While the Alamo River originates in Mexicali, a weir was constructed in 1997 to prevent dry weather flows originating in Mexico to flow into the U.S. (CH2M Hill, 2018b).

The New River is a 125 km long river that originates in Mexico and flows north across the international border into the Imperial Irrigation District to drain to the Salton Sea. The mean annual New River flows at the USGS gage 10254970 at the international border is 173±72 million m^3/year and reaches 543±50 million m^3/year at the Salton Sea between 1980 and 2005 (USGS gage 1025550).

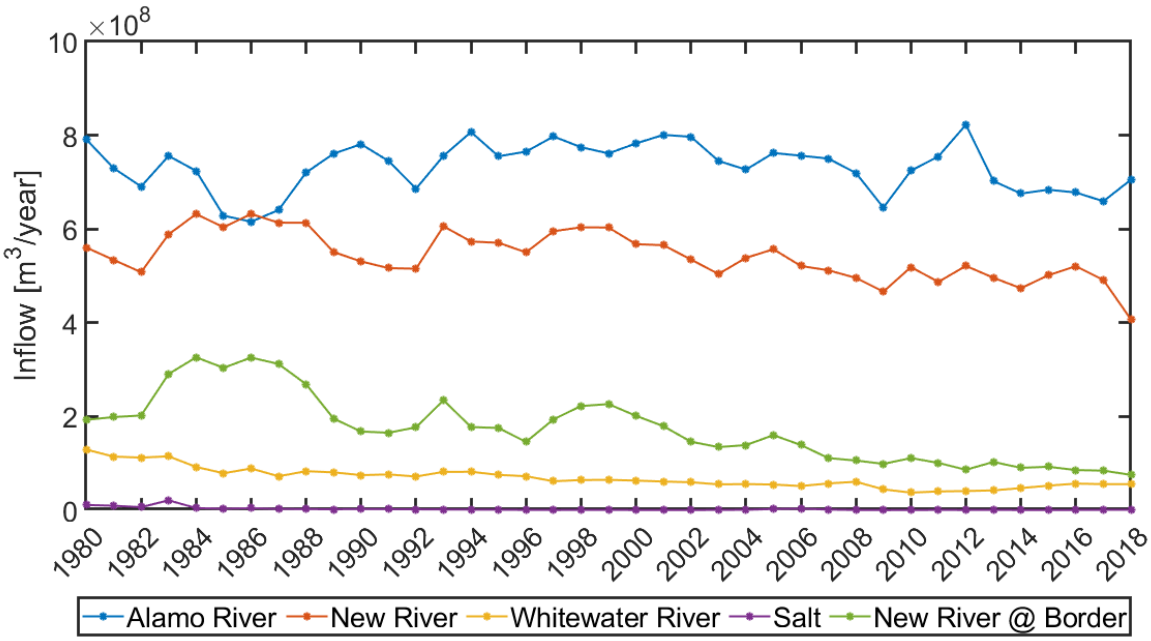

Figure 10. Annual inflows (1980 - 2018) of major reaches draining to the Salton Sea.

2.2.3 Imported Inflows to the Salton Sea Watershed

Despite its arid climate, the Salton Sea Watershed is home to one of the most productive agricultural regions in the United States. This is largely due to imported Colorado River inflows to the watershed. The Colorado River waters are diverted to the Salton Sea at the Pilot Knob Hydroelectric Plant and Morelos Dam in Mexico. Pilot Knob Hydroelectric Plant is located on the Southeastern edge of the watershed, near the California-Arizona and Mexican border. USGS Gage 09527500 on the All-American Canal below Pilot Knob measures daily flow from the Colorado River into the American portion of the watershed (**Error! Reference source not found.**). Gage records indicate a mean annual flow of 4±0.25km^3 (3,247,989.7±200,707 acre-feet), between 1980 and 2005.

Morelos Dam is located on the Mexico-Arizona border, about 1.6 km below the California border. This is the last dam on the Colorado River, and diverts water from the Colorado to the Mexican portion of the Salton Sea Watershed in Mexicali Valley. The dam is operated by the International Boundary and Water Commission (IBWC) which maintains gage 09522030 at the dam. This gage

provides daily flow records of Colorado River diversions into Mexicali Valley with mean annual flow of 2.3±0.62 km^3 (1,839,482±500,815.7 acre-feet) between 1980 and 2005. Inflows from this diversion point are not included in this study.

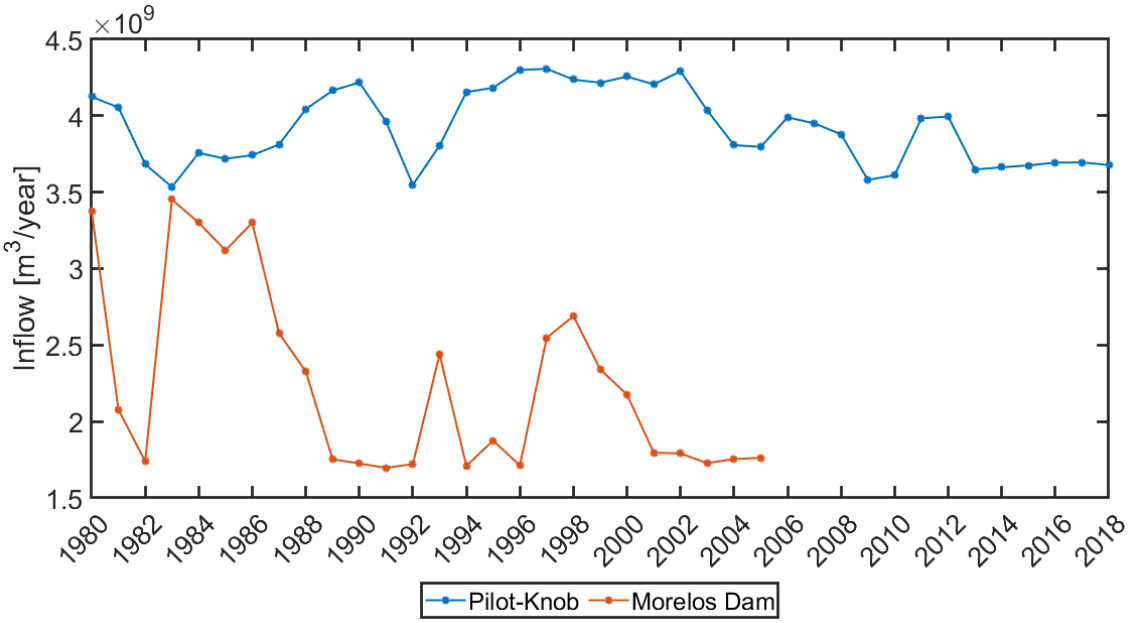

Figure 11. Annual inflows to the Salton Sea Watershed at Pilot Knob (USGS Gage: 09527500) and Morelos Dam (IBWC Gage: 09522030). Flow data for Morelos Dam was not easily available after 2005, and hence, is not included in this figure.

2.2.4 Water Infrastructure within the Watershed

The All-American Canal (AAC) is a 130 km (80 mile) long canal that diverts water from the Colorado River at Imperial Dam in Yuma, Arizona. The AAC enters the watershed at Pilot Knob hydroelectric plant, where mean annual flow has been recorded by the USGS Gage 09527500 (**Error! Reference source not found.**). The AAC runs parallel along the international border and s upplies water to the Imperial Irrigation District (IID). IID services its farms through an extensive system of 2,681 km (1,666 miles) main and lateral canals (Imperial Irrigation District 2016).

The Coachella Canal is 196 km long and diverts water from the AAC at the USGS gage 9527590. The canal traverses along the eastern foothills of the watershed (Chocolate and Orocopia

mountains) before veering west into the Coachella Valley. Flows at USGS gage 9527590 between 2003 and 2018 indicate a mean annual flow of 361±114 million m^3.

Mexicali Valley receives Colorado River waters through the Morelos Dam. In Mexicali, Colorado River waters are distributed through two major canals – Canal Reforma and Canal Independencia (Burt et al., 2012). Canal Reforma runs westward through the SSW and distributes water to irrigation and municipal users in the Mexicali Valley. Approximately 110 million m^3/year of water from the Reforma Canal is transmitted to the Tijuana Aqueduct at the western end of the canal (Burt et al., 2012). While these canals are incorporated into the model setup, Colorado River flows supplied and distributed through them are not simulated in this study. However, New River inflows at the international boundary are added as an internal boundary condition since measured flow is available at USGS gage 10254970.

2.3 Semi-Distributed Hydrologic Modeling Using SWAT

Soil and Water Assessment Tool (SWAT) is a semi-distributed, continuous in time, process-based watershed model (Neitsch et al., 2009). It is one of the most widely used hydrologic and water quality models in the world (Gassman et al., 2010). SWAT divides a watershed into smaller spatially connected subbasins. These subbasins are each drained by a major channel (reach) that transports water downstream. Each subbasin is further divided into smaller spatial units known as Hydrologic Response Units (HRUs). HRUs are the smallest spatial unit for hydrologic simulations by SWAT. The SWAT model simulates hydrology in two phases – land phase and routing phase. The land phase controls the amount of water, sediment, and pollutant loadings to the main reach draining a subbasin. The routing phase controls the movement of water, sediments, and pollutants to the outlet of the watershed. Water balance is the driving force behind all hydrologic process studied within a subbasin:

$$SW_t = SW_0 + \sum_{i=1}^{t}(R_{day} - Q_{surf} - E_a - W_{seep} - Q_{gw}) \quad \text{eq. 1}$$

Where (all units are mm H_2O)*:*

SW_t = Final Soil Water Content

SW_0 = Initial Soil Water Content on day i

R_{day} = Precipitation on day i

Q_{surf} = Amount of surface runoff on day i

E_a = Evapotranspiration on day i

W_{seep} = Water infiltration to the vadose zone on day i

Q_{gw} = Water return flow on day i

We utilized QSWAT, a QGIS interface for SWAT to set-up the watershed model (Dile et al., 2018). The following sections describe the model setup for the Salton Sea Watershed (SSW) with emphasis on the main equations used to capture rainfall-runoff processes in SWAT. Erosion and nutrient loading processes are not considered in this thesis.

2.3.1 Conceptual Model of the Salton Sea Watershed

The SWAT model for the Salton Sea utilizes a 30 m resolution DEM to delineate the main reaches within the watershed and drainage areas (subbasins). A subbasin is further delineated into smaller spatial units with similar hydrologic response, called Hydrologic Response Units (HRUs). HRUs are the basic spatial and computational units for simulating hydrologic processes in response to precipitation and irrigation, meteorological forcings (solar radiation, temperature, humidity, and wind), land use, and soil. Each HRU generates recharge to the underlying aquifer and streamflow to the main reach within a subbasin. The total streamflow contribution from a subbasin to its main reach is the area weighted average of the streamflow generated by the constituent HRUs within the subbasin. Flow in a reach contributes inflow to its downstream channel. The model generates HRU, subbasin and watershed level hydrologic fluxes (actual evapotranspiration, surface flow, lateral

flow, groundwater return flow, percolation, and recharge) and state variables (soil moisture). The model also generates reach level inflow and outflow as well as evaporative and transmission losses.

The SWAT model of the Salton Sea Watershed is run on a daily time step. The model includes the major surface drainage features in the watershed including streams and the major canals in the watershed (Figure 12). IID supplies water to its agricultural lands through an extensive water distribution system consisting of 2,681 km of canals. Since we do not have information on water diversions within this dynamic system of canals, we only incorporate the AAC, and three major canals that divert water from the AAC to the IID – East Highline, Central Main and Westside Main in the model. These canals are represented as reaches in SWAT. Coachella Canal is a major canal that moves large volumes of water from the south to the northern portion of the watershed. Therefore, the Coachella Canal was also incorporated in its entire length (196 km) as a reach. In Mexico, both Canal Reforma and Canal Independencia were incorporated as reaches as well. However, flow into and out of the Mexican canals was not considered in this study. This section describes major processes used to simulate the daily water balance and inflows to the Salton Sea.

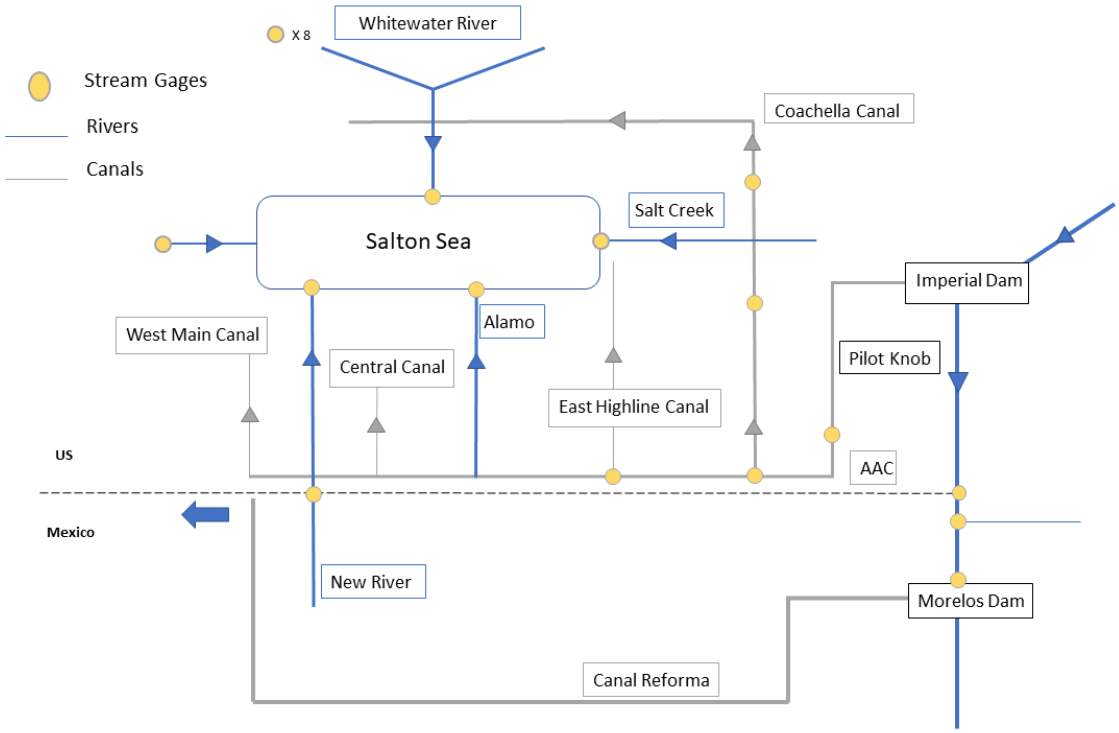

Figure 12. Water distribution system within the Salton Sea Watershed as represented in the SWAT model.

Land Phase: Precipitation is initially intercepted by vegetation canopy or held in depressions on the soil surface. Water at the soil surface may infiltrate the soil or become runoff and contribute to streamflow. We utilized the SCS Curve Number method to calculate surface runoff on a daily time step as hourly rainfall data is not available for implementing the Green-Ampt infiltration model in SWAT. Initial abstractions from canopy storage are taken into consideration while calculating surface runoff using the SCS Curve Number Method. Infiltration into soil profile is calculated as the difference between precipitation and surface runoff. The amount of surface runoff is dependent on the rate of water application (through rainfall or irrigation), slope, antecedent soil moisture conditions and vegetation. The SCS Curve Number is a function of antecedent moisture conditions, soil permeability and land use. It is an empirical value that drops as soil approaches wilting point and increases to about 100 as soil approaches saturation. The larger the Curve Number, the higher

the fraction of precipitation that becomes runoff. The amount of runoff generated (Q_{surf}) is calculated as:

$$Q_{surf} = \frac{(R_{day} - I_a)^2}{(R_{day} - I_a + S)} \quad \text{eq. 2}$$

Where, R_{day} is daily rainfall depth (mm H_2O), I_a is initial abstractions (approximated as 0.2S), which includes surface storage, initial interception, and infiltration prior to runoff, and S is retention parameter, calculated as a function of Curve Number (CN):

$$S = 25.4\ (\frac{1000}{CN} - 10) \quad \text{eq.3}$$

Surface runoff generated using the SCS curve number method contributes to peak flow within the subbasin channel. Peak flow occurs when the furthest part of a watershed from the channel is contributing flow to the channel. This relationship is captured by the time of concentration (t_{conc}) which is the time from the beginning of a rainfall event to when the entire subbasin is contributing flow to the channel outlet. Time of concentration is calculated as the sum of the time of concentration of overland flow (t_{ov}, time for surface runoff from most remote part of subbasin to reach outlet) and time of concentration of channel flow (t_{ch}, time from most upstream channel to reach outlet).

$$t_{conc} = t_{ov} + t_{ch} \quad \text{eq. 4}$$

Time of concentration of overland flow (t_{ov}), is calculated as:

$$t_{ov} = \frac{L_{slp}^{0.6} * n^{0.6}}{18 * slp^{0.3}} \quad \text{eq. 5}$$

Where, L_{slp} is subbasin slope length (m), n is Manning's roughness coefficient, and *slp* is subbasin slope. Time of concentration of channel flow (t_{ch}), is calculated as:

$$t_{ch} = \frac{0.62 * L * n^{0.75}}{Area^{0.125} * slp_{ch}^{0.375}} \quad \text{eq. 6}$$

Where, L is channel length from a most distant point to a subbasin outlet (m), n is Manning's roughness coefficient for channel bed, Area is subbasin area (km^2), and slp_{ch} is channel slope (m m^{-1}). Finally, the peak runoff rate (q_{peak}) is calculated as:

$$q_{peak} = \frac{\alpha_{tc} * Q_{surf} * Area}{3.6 * t_{conc}} \quad \text{eq. 7}$$

Where, q_{peak} is Peak runoff rate (m^3 s^{-1}), α_{tc} is fraction of daily rainfall that occurs during the time of concentration, Q_{surf} is surface Runoff (mm H_2O), Area is area of subbasin (km^2), and t_{conc} is time of concentration in the subbasin (hr).

Water that does not leave as surface runoff, percolates through the soil, and the amount of infiltration is calculated as the difference between precipitation and surface runoff. Soil water is available for evapotranspiration or for redistribution through the subsurface. Evapotranspiration (ET) is the major source of water loss from precipitation and applied irrigation. Intensively irrigated watersheds in arid regions where rainfall is not enough to support plant growth, can have elevated ET rates due to a combination of irrigation enhanced soil moisture and natural climatological forcings (Wei et al., 2018). Potential Evapotranspiration (PET) is the "amount of water transpired by a short green crop, completely shading the ground, of uniform height and never short of water". Therefore, PET represents the maximum water that can be lost through evaporation and transpiration from a landscape. SWAT has three widely accepted numerical methods – Penman-Monteith, Priestley-Taylor and Hargreaves for PET calculation. We used the Penman-Monteith method to calculate PET for SSW SWAT model. The Penman-Monteith method requires 4 climatic inputs on a daily time step to calculate PET - solar radiation, relative humidity, air temperature and wind speed.

$$\lambda E = \frac{\Delta.(H_{net} - G) + \rho_{air} * c_p * [e_z^0 - e_z]/r_a}{\Delta + \gamma * (1 + r_c/r_a)} \quad \text{eq. 8}$$

Where λE is the latent heat flux density (MJ m^{-2} d^{-1}), E is the depth rate of evaporation (mm d^{-1}), Δ is the slope of the saturation vapor pressure-temperature curve de/dT (kPa ◦C^{-1}), H_{net} is the net radiation (MJ m^{-2} d^{-1}), G is the heat flux density to the ground (MJ m^{-2} d^{-1}), ρ_{air} is the density of air (kg m^{-3}), c_p is the specific heat at constant pressure (MJ kg^{-1} ◦C^{-1}), e_z^o is the saturation vapor pressure of the air at height z (kPa), e_z is the water vapor pressure of air at height z (kPa), γ is the psychometric constant (kPa ◦C^{-1}), r_c is the plant canopy resistance (s m^{-1}), and r_a is the diffusion resistance of the air layer (aerodynamic resistance) (s m^{-1}).

SWAT discretizes the soil profile within the root zone into multiple layers (up to 10) and simulates percolation or downward movement of soil moisture using a storage routing technique. Percolation occurs when field capacity of a soil layer is exceeded, and the layer below is not saturated. The rate of percolation is governed by the saturated hydraulic conductivity of soil.

$$w_{perc,ly} = SW_{ly,excess} * (1 - \exp[\frac{-\Delta t}{TT_{perc}}]) \quad \text{eq. 9}$$

Where, $W_{perc,ly}$ is amount of water percolating out of the soil layer (mm H_2O), $SW_{ly,excess}$ is drainable amount of water in a soil layer on a day (mm H_2O), Δt is length of time step (hrs), and TT_{perc} is travel time for percolation through a layer (hrs).

The travel time for percolation is unique for each layer and is calculated as:

$$TT_{perc} = \frac{SAT_{ly} - FC_{ly}}{K_{sat}} \quad \text{eq. 10}$$

Where TT_{perc} is travel time for percolation through a layer (hrs), SAT_{ly} is saturated water content of layer (mm H_2O), FC_{ly} is water content of layer at field capacity (mm H_2O), K_{sat} is saturated hydraulic conductivity of layer (mm hr^{-1}).

In areas where a relatively impermeable zone occurs within 2 m of the soil profile, water can accumulate above the impermeable layer and result in lateral flow (or interflow) that contributes to streamflow. A kinematic storage model is used to predict lateral flow in each soil layer.

$$Q_{lat} = 0.024 * (\frac{2 * SW_{ly,excess} * K_{sat} * slp}{\phi_d * L_{hill}})$$ eq. 11

Where, Q_{lat} is lateral flow discharge (mm H_2O/day), Slp is slope (m m^{-1}), L_{hill} is average length hillslope (m), and Φ_d is drainable porosity of soil layer (mm/mm).

Once water exits the bottom of the root zone, it is partitioned into recharge to groundwater. In reality, water flows through the vadose zone that lies above the saturated zone before reaching the aquifer. Movement through the vadose zone is not directly modeled by SWAT, and the model incorporates a time lag in water exiting the soil profile to become aquifer recharge. The empirical function calculates recharge to aquifers as a function of delay time or drainage time of the overlaying geologic formations.

$$w_{rchrg,i} = \left(1 - \exp\left[-1/\delta_{gw}\right]\right) * w_{seep} + \exp\left[-1/\delta_{gw}\right] * w_{rchrg,i-1}$$ eq. 12

Where, $w_{rchrg,i}$ is the amount of recharge on a day i (mm H_2O), $w_{rchrg,i-1}$ is recharge entering aquifer on day i-1 (mm H_2O), w_{seep} is the amount of water percolating past the bottom of the soil profile (mm H_2O) and δ_{gw} is the delay or drainage time for overlaying geologic formation (days).

Groundwater systems in SWAT are discretized into shallow and deep aquifers. The shallow aquifer is an unconfined aquifer that contributes flow to the main channel within a subbasins, replenishes soil moisture or is accessed by plants for transpiration. Baseflow occurs only when the amount of water in the shallow aquifer exceeds a threshold defined by the user. The steady state response of groundwater flow to recharge is calculated as:

$$Q_{gw} = \frac{8000 * K_{sat}}{L_{gw}^2} * h_{wtbl}$$ eq. 13

Where, Q_{gw} is the baseflow into a reach on a given day (mm H_2O), K_{sat} is the hydraulic conductivity of aquifer (mm/day), L_{gw} is the distance from the ridge or subbasin divide to the main channel (m) and h_{wtbl} is water table height (m). The deep aquifer is a confined aquifer that contributes flow to

streams or channels outside the watershed. Therefore, any recharge to the deep aquifer is considered to be lost from the watershed.

Routing Phase: The total inflow (water yield) to a reach from its contributing subbasin is calculated as the sum of the surface runoff (Q_{surf}), lateral runoff (Q_{lat}), and groundwater discharge (Q_{gw}) generated within the subbasin, minus any transmission losses (t_{loss}) from reaches.

$$\textit{Water Yield} = Q_{surf} + Q_{lat} + Q_{gw} - t_{loss} - \textit{pond abstractions} \quad \text{eq. 14}$$

Once in a channel, flow is subject to losses from evaporation, transmission, and potential diversions from the reach. The remaining flow is routed from a channel to its downstream channel using a variable storage routing method.

2.3.2 Watershed Delineation

QSWAT uses a Digital Elevation Model (DEM) and the Terrain Analysis Using Digital Elevation Model (TauDEM), an automatic watershed delineation algorithm, to delineate a watershed (Tarboton, 2008). We utilized a 1 arc-second, approximately 28-meter DEM available from the USGS's National Map Viewer (USGS, 2019). We resampled the DEM to a 30-meter resolution using the Resample tool in ArcGIS Pro 2.4.0. The 30 m DEM was further processed before delineating the watershed using TAUDEM. These processing steps include:

1) Incorporating main canals as drainage features within the watershed
2) Incorporating the Salton Sea as a subbasin

The SSW is a highly managed watershed where large volumes of water are transported within the watershed through 667 km of major canals. It is important to incorporate these canals in the hydrologic model to capture seepage and evaporation losses from canals. The DEM Reconditioning methodology in ArcHydro geoprocessing tools incorporates drainage features (such as streams, ditches, canals, etc.) into a DEM, by subtracting the elevation of grid cells in the DEM along a pre-defined reach layer. The DEM Reconditioning methodology was used in ArcGIS Pro 2.4.0 to

incorporate these manmade features and 658 km of major natural drainage features from the National Hydrology Dataset, as channels into the DEM (AGREEDEM).

AGREEDEM output from ArcHydro was used in QSWAT to delineate the watershed. The Salton Sea Watershed (SSW) is an endorheic watershed, such that all drainage within the watershed terminates at the centrally located Salton Sea. TauDEM was unable to incorporate the large shallow area of the Salton Sea as the terminus for all the subbasins. Instead, it routed all reaches to an artificial outlet on the southern border of the watershed. To correct for this error, we created an artificial outlet in AGREEDEM by cutting out a centrally located pixel within the Salton Sea. This resulted in the routing of all subbasins to the Salton Sea, however, the lake boundary was not delineated correctly as a subbasin. We utilized SWAT2Lake, a QGIS plugin (Molina-Navarro et al., 2018) to incorporate the Salton Sea as a distinct subbasin and a single HRU defined as water (Figure 13).

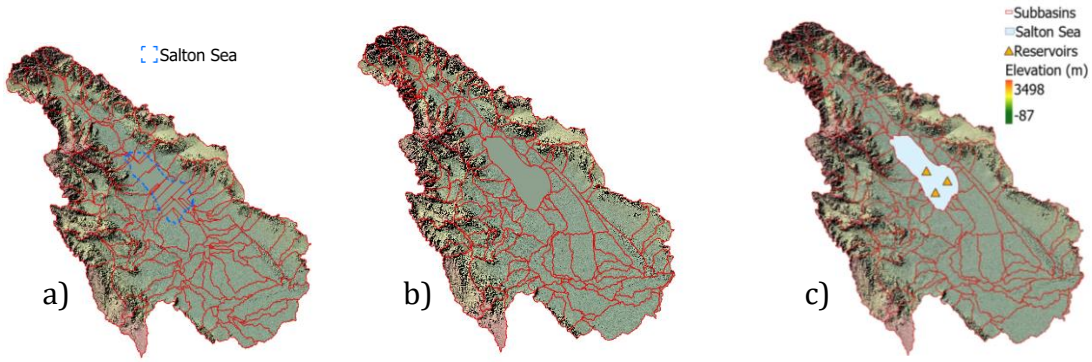

Figure 13. Delineation of subbasins within the Salton Sea Watershed: a) Original TAUDEM delineation of subbasins across the Salton Sea; b) Inclusion of Salton Sea as a subbasin using the stream reconditioning method of ArcHydro and SWAT2Lake lake delineation tools, and c) Reservoir features used to capture the changes in Salton Sea area.

The SWAT2Lake tool created a subbasin conforming to the shape of the Salton Sea. However, this is a static representation of the Salton Sea that does not capture changes in lake surface area. Lakes and reservoirs can be incorporated in SWAT by – 1) the use of 'Water' HRU or, 2) the use of

impoundment features such as reservoirs. We utilized both options to represent hydrologic processes of the Salton Sea. The model simulates 'WATR' as 'no crops' and calculates evaporation at a constant flux from the subbasin (Jalowska & Yuan, 2019). In addition to designating land use as 'Water', we also incorporated reservoir at the end of the main reaches terminating at the Salton Sea (Figure 13). These reaches are the most downstream reaches in the drainage network before the outlet at the Salton Sea, and hence, represent the accumulated inflows from the watershed to the Salton Sea.

While the steps above resulted in the correct routing of all drainage features to the Salton Sea, the intersections of manmade canals and natural channels were incorrectly delineated. These were manually corrected in ArcGIS Pro 2.4.0. This resulted in the delineation of final watershed boundary with a total area of 21,801 km^2, and 155 subbasins ranging in area from 1 to 943 km^2.

2.3.3 Datasets for Definition of Hydrologic Response Units

A Hydrologic Response Unit (HRU) is the smallest spatial unit on which SWAT performs hydrologic simulations. SWAT creates HRU's within a subbasin based on unique combinations of land use, soil, and slope. The SSW is a transboundary watershed that lies within Southern California and Mexicali Valley in Mexico. One of the biggest challenges of this project was to generate consistent land use and soil data across the American and Mexican portions of the watershed. Datasets in Table 3 were compiled in ArcGIS Pro to obtain consistent land use and soil datasets for the watershed.

Table 3. Datasets utilized in creation of HRUs in the Salton Sea Watershed.

Data	**US**	**Mexico**
DEM	National Elevation Dataset (NED)	
Soil	STATSGO2	SoilGrid250m
Land Use	NLCD/CDL/BOR	CONABIO

Soils: The National Resource Conservation Service's (NRCS) State Soil Geographic Database (STATSGO2) was used for the American portion of the watershed. STATSGO2 is a spatial dataset that contains soil parameters such as texture, soil depth, hydraulic conductivity, etc. that are required for SWAT hydrology simulation. This database had a total of 39 soil polygons within the US portion of the Salton Sea Watershed. While NRCS's Soil Survey Geographic Database (SSURGO) is a newer, updated and more detailed version of the STATSGO2 database; it is incomplete for the SSW and was not used. STATSGO2 provided information on all key soil parameters required for SWAT, except for the topsoil layer albedo, for which it only had information for 17 out of 39 soil polygons. Soil albedo for the rest of the polygons are from the soil albedo dataset by NRCS (Table 4).

Two soil datasets were considered for use in the Mexican portion of the watershed – 1) a 7 km resolution Digital Soil Map of the world provided by the Food and Agriculture Organization (FAO), and 2) a 250 m resolution spatial dataset provided by the International Soil Reference and Information Center (ISRIC). ISRIC's SoilGrid250m is a global soil dataset created using machine learning algorithms and local soil datasets (Figure 14). It estimates soil properties at 6 standard depths of 0, 15, 30, 60, 100 and 200 cm (Hengl et al., 2017). This dataset was chosen over the FAO data because of its finer spatial resolution. SoilGrid250m contained detailed information of soil parameters in the Mexican portion of the watershed for 9 out of the 13 key soil parameters (Table 4).

Table 4. Soil parameters required for simulating soil hydrological processes in SWAT, and source datasets used to calculate the parameters.

SWAT Parameter	Definition	US	MEXICO
HYDGRP	Soil Hydro group	STATSGO	HYSOGs250m[1]
SOL_ZMX	Max Soil Depth	STATSGO	SoilGrid250
SOL_Z (layer #)	Soil Depth	STATSGO	SoilGrid250
SOL_BD (layer #)	Soil Wet Bulk Density	STATSGO	SoilGrid250 - derived
SOL_AWC (layer #)	Soil Available Water Capacity	STATSGO	SoilGrid250
SOL_K (layer#)	Saturated Hydraulic Conductivity	STATSGO	SoilGrid250 + SPAW
SOL_CBN (layer #)	Soil Carbon	STATSGO	SoilGrid250
SOL_CLAY (layer #)	Clay	STATSGO	SoilGrid250
SOL_SILT (layer #):	Silt	STATSGO	SoilGrid250
SOL_SAND (layer #)	Sand	STATSGO	SoilGrid250
SOL_ROCK (layer #)	Rock	STATSGO	SoilGrid250
SOL_ALB (top layer)	Albedo	NRCS	SOTERLAC[2]

[1](Ross et al., 2018)
[2](ISRIC, 2005)

SWAT requires moist bulk density **(**BD_{WET}**)** in Mg/m^3, while SoilGrid250m reports dry bulk density (BD_{DRY}) in kg/m^3. SoilGrid250m also reports saturated volumetric water content (θ) of soils. To calculate moist bulk density, dry bulk density and saturated volumetric water content (θ) and density of water (997 kg/m^3) are used as follows:

$$BD_{WET} = \frac{BD_{DRY} + (\theta * 997)}{1000000} \quad \text{eq. 15}$$

SWAT also requires the saturated hydraulic conductivity of soil layers. We utilized the NRCS's SPAW Hydrology and Water Budgeting software (Saxton & Willey, 2006) along with soil texture classes (% sand, silt and clay) and organic carbon content from SoilGrid250m to calculate the saturated hydraulic conductivity of all seven soil layers in Mexico.

Soil albedo (α) values were calculated using Chroma Meter Munsell color values (Col_{val}) from ISRIC's Soil and Terrain Database (SOTER), and using the following regression equation (Post et al., 2000):

$$\alpha = 0.0069 \times Col_{val} - 0.114 \quad \text{eq. 16}$$

The final soil raster dataset used in the SWAT model consists of 54 unique soil polygons with 39 from STATSGO2 in the American portion of the watershed, and 15 from SoilGrid250m in the Mexican portion of the watershed.

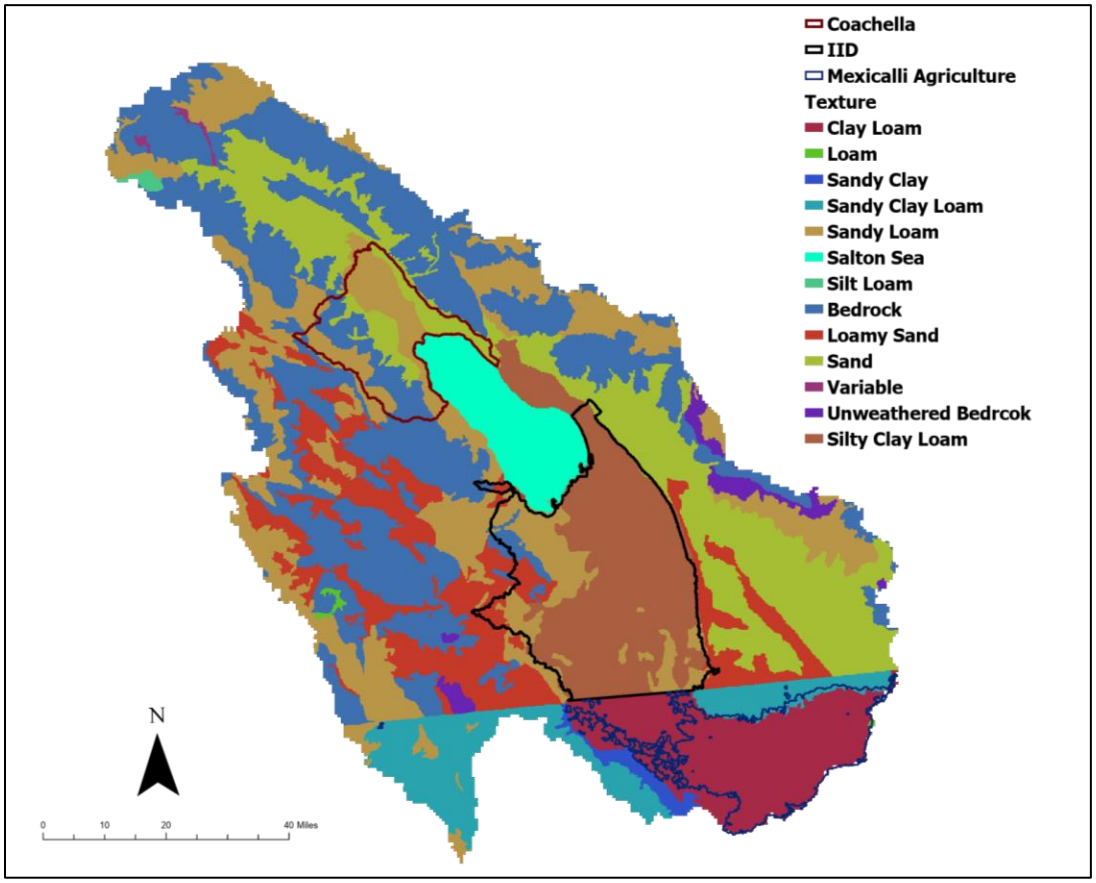

Figure 14. Spatial distribution of soil textural classes within the Salton Sea Watershed. The major agricultural regions are outlined as IID (black), Coachella (red) and Mexicali Valley (blue).

Land use: The National Land Cover Database (NLCD) provides national land cover on a 30 m resolution every 2 years from 2001 to 2016. An analysis of the NLCD datasets revealed that areas under land uses in the US portion of watershed did not change significantly between 2001 and 2007. Therefore, NLCD 2001 was chosen to represent the spatial distribution of land use during the calibration time frame of 1995-2005 (Figure 15), instead of NLCD 2007. NLCD describes a

generic agricultural land use and does not include spatial boundaries for specific crop types. Specific crops types are incorporated into the land use layer using steps described in Section 2.4.1. For Mexico, 2007 land Cover dataset from National Commission for the Knowledge and Use of Biodiversity (CONABIO) was used. This spatial dataset provided information on generic land cover classes at 250 m resolution. The landcover classes were reclassified to categories in the SWAT land use database (Table 5). The two spatial datasets (NLCD01 and CONABIO07) were merged using ArcGIS Pro 2.4.0.

Table 5. Reclassification of land use categories in Mexico to create consistent land cover classes with SWAT land use database.

CONABIO LU	**SWAT LU**
Temperate or sub-polar needleleaf forest	Evergreen Forest
Tropical or sub-tropical shrubland	Shrubland
Temperate or sub-polar shrubland	Shrubland
Tropical or sub-tropical grassland	Grass/Pasture
Wetland	Wetland Mixed
Cropland	Agricultural land – generic
Barren land	Barren
Urban and built-up	Developed/Med Intensity
Water	Open Water

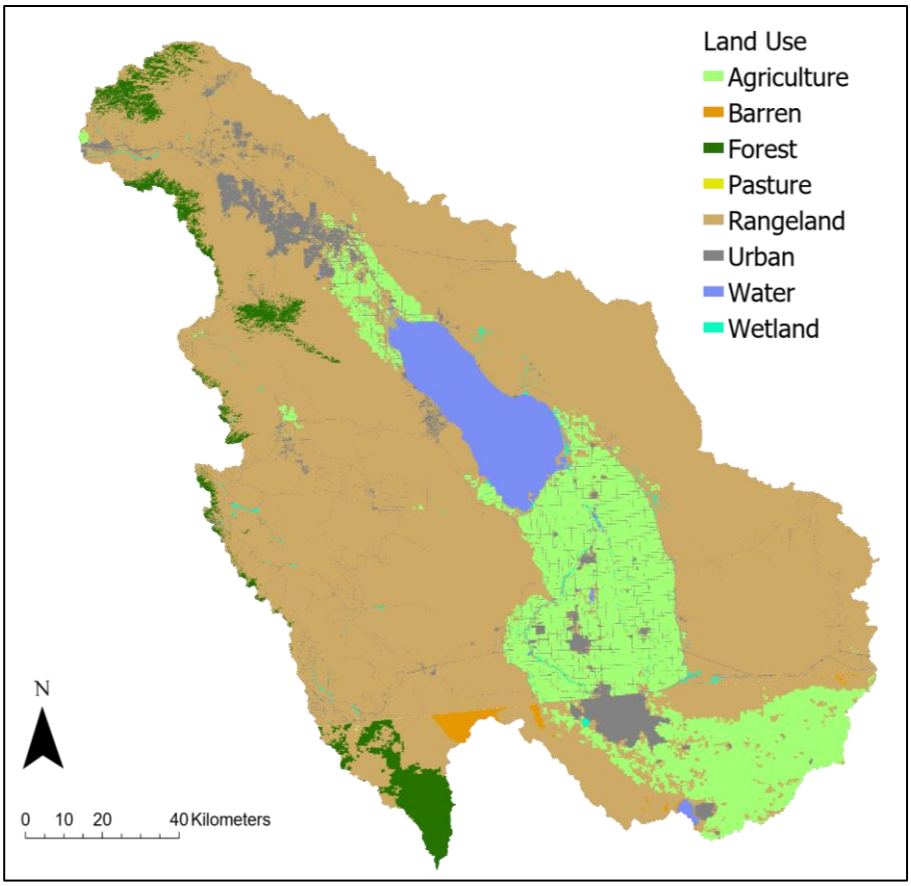

Figure 15. Spatial distribution of land use within the Salton Sea Watershed. Datasets used: NLCD 2001 (US) and CONABIO 2007 (Mexico).

2.3.4 Optimal Spatial Discretization of Hydrologic Response Units

HRUs are the basic computational units in SWAT created based on unique combinations of land use, soil type, and slope, and a set of user defined thresholds for slope classes and area. Ideally, HRUs would be created for every unique combination of land use, soil, and slope without qualifying any area thresholds to capture the maximum heterogeneity within the watershed. However, since HRUs are the basic computational unit on which hydrologic simulations are performed, the processing time increases proportionally with the number of HRUs. Therefore, it is important to determine the optimum number of HRUs using sensitivity analysis to capture maximum heterogeneity in hydrologic responses while reducing computational time.

Optimal Number of Slope Classes: There is a high variability in slope within the watershed as the topography varies from relatively flat (<9% slope) in the valley floor to high elevation areas in the northern mountain regions. In order to account for slope variability, we delineated HRUs based on different number of slope classes and tested watershed scale fluxes by performing SWAT model simulations (Table 6). Slope classes were defined based on Natural Jenks Classification by classifying the 30 m slope map to 2, 3 and 4 classes and then delineating HRUs in QSWAT. We used 1991 and 1992 forcing data with similar annual precipitation (213.4 mm/year and 292.6 mm/year, respectively) to run the model. To reduce the impact of initial conditions, 2 years of warmup period (1989-90) is considered. Results indicate that while 4 slope classes best captures HRUs heterogeneity, it also discretizes 9027 HRUs, and increases model run time. An analysis of watershed scale fluxes revealed that using 3 slope classes reduced the number of HRUs to 7387 from 9027, while maintaining similar watershed scale fluxes of lateral runoff, groundwater return flow and evapotranspiration (Figure 16). Therefore, we chose 3 slope classes as the optimal number of slope classes to define HRUs.

Table 6. The effect of slope classes on number of discretized HRUs.

Scenario	Name	# Slope Classes	Slope Breaks	# HRU'S
1	Slope0	0	None	3807
2	Slope2	2	4.5 (median)	7005
3	Slope3	3	15.9; 43.02	7386
4	Slope4	4	11.32; 30.6; 55.5	9027

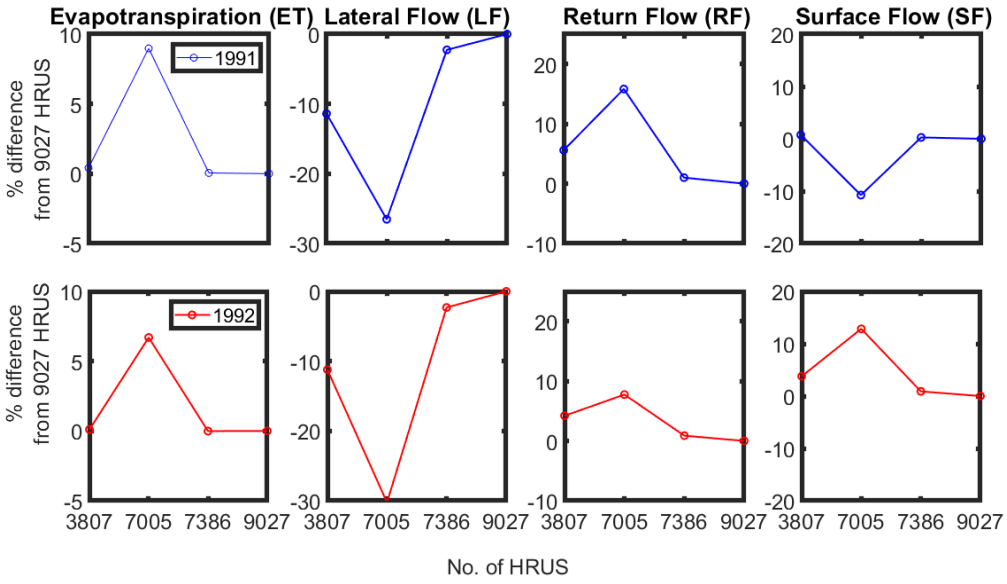

Figure 16. Impact of number of slope classes on HRU discretization. This figure shows the difference between watershed scale hydrologic fluxes (evapotranspiration, lateral flow, groundwater return flow, and surface flow) from HRUs created using zero, two, three, and four slope classes.

Optimal Area Threshold: To further reduce the number of discretized HRUs with three slope classes, we performed another sensitivity analysis to define area thresholds for defining HRUs. Two types of area thresholds were analyzed – variable area and constant area. Variable area threshold is a function of percent area of a subbasin and can result in different area thresholds for different subbasins. A constant area threshold is defined uniformly across all subbasins.

Table 7. Impact of area thresholds on the number of discretized HRUs.

Scenario	Threshold	Threshold Type	# HRU'S
1	1%	Variable	1763
2	2%	Variable	1321
3	90,000 m^2	Constant	3616
4	None	-	7386

Variable area thresholds of 1% and 2% reduced the number of HRUs drastically (Table 7), but resulted in large differences in watershed scale surface runoff, lateral runoff, groundwater return flow (baseflow) and evapotranspiration (Figure 17). A constant area threshold of 90,000 m^2 reduced the number of HRUs from no area threshold by about half, while generating similar watershed scale responses to no area thresholds scenario (Figure 17). Therefore, an area threshold of 90,000 m^2 with 3 slope classes (defined at 15.9% and 43.02%) resulted in optimal HRU discretization for the study watershed.

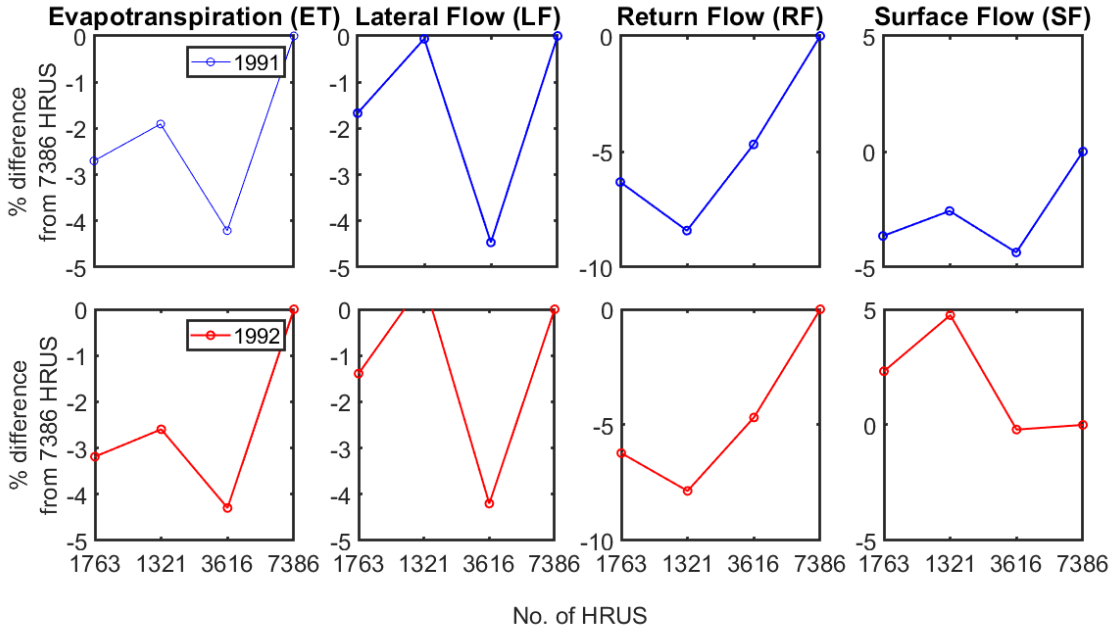

Figure 17. Impact of area thresholds definitions on HRU discretization and flux simulation. This figure shows the difference between watershed scale hydrologic fluxes (evapotranspiration, lateral flow, groundwater return flow, and surface flow) from HRUs created using 1%, 2% area and 90,000m^2 area thresholds, from no area thresholds.

2.4 Irrigation Application

Irrigation is a major input in the Imperial and Coachella Valleys and agriculture-based runoff constitutes a significant component of inflows to the Salton Sea. Quantifying the impacts of crop types and irrigation practices are essential to understand the water budget of the Salton Sea Watershed. Irrigation practices were incorporated into the model using management (.mgt) files.

Management operation such as planting and harvesting dates as well as applied irrigation are set up on an HRU level via modifying the management file parameters. In the SSW model set up, automatic irrigation is chosen. To schedule automatic irrigation of crops, the management files require information on the following operations:

1) Plant Growth Operation: This operation initiates plant growth
    a. MONTH/DAY: Timing of planting crops
    b. PHU_PLT: Number of heat units to bring crop to maturity
2) Harvest/ Harvest and Kill Operation: This operation kills and harvest the plant
    a. MONTH/DAY: Timing of harvest/kill operation of crop
3) Auto-Irrigation Operation**:**
    a. AUTO_WSTR: Water stress that triggers irrigation
    b. IRR_MAX: Max irrigation amount applied, default = 25.4 mm
    c. IRR_EFF: Irrigation efficiency (0-100)
    d. IRR_ASQ: Irrigation surface runoff ratio (0-1)

2.4.1 Defining Crop Functional Types

The Salton Sea Watershed has 3 major agricultural areas in Coachella Valley, IID and Mexicali Valley. The CONABIO land use dataset discretizes generic cropland area in Mexicali Valley. Due to lack of data on specific crop types and crop growing seasons, a generic agriculture land use is defined in the Mexicali Region. The United States Department of Agriculture, National Agricultural Statistics Service's (USDA-NASS), provides high resolution (30 m x 30 m) Cropland Data Layer (CDL) spatial datasets for the American portion of the watershed between 2008 and 2018. While this dataset delineates field scale boundaries of crops grown within the watershed, it does not contain datasets for the calibration time frame of 1995-2005 (specified in Section 2.6). Therefore, CDL 2008 was chosen to delineate crop areas as this dataset is chronologically closest

to the calibration time frame of 1995-2005. The CDL2008 dataset was incorporated into the land use layer for the Salton Sea Watershed. This was done in ArcGIS Pro2.4.0, using the Raster Calculator Tool, where a raster consisting of only agricultural cells in CDL2008 (CDL_AG), was added to the generic "Agriculture" land use in the NLCD land use map. As site specific parameters are not available from all the crop types, we used information on agricultural practices in the Salton Sea Watershed from the University of California, Agriculture and Natural Resources (UC-ANR) (Dr. Aliasghar Montazar, personal communication, 2020) and Bureau of Reclamation (BOR) annual reports on agriculture in the Lower Colorado River Basin (including IID and Coachella Valley) to classify the list of CDL crops to 16 Crop Functional Types (Table 8).

Table 8. Crop Functional Types (CFTs) within the Salton Sea Watershed. These groups were created by first identifying the crops grown in the area (Dr. Aliasghar Montazar, personal communication, 2020) and then classifying them into CFTs.

Crop Functional Type	Crops
Alfalfa	Alfalfa
Bermuda	Bermuda, Klein Grass
Cabbage	Cauliflower, Cabbage
Citrus	Citrus
Crucifers	Broccoli
Deciduous Orchards	Dates
Field Grain	Corn, Sorghum
Grapes	Table Grapes
Herbs	Herbs
Legume/Solanum Vegetables	Beans, Bell Peppers
Lettuce	Lettuce
Melons	Watermelon, Cantaloupe
Small Grains	Oats, Wheat
Small Vegetables	Carrots, Onions
Sugar Beets	Sugar Beets
Sweet Corn	Sweet Corn

A plant growth database (crop.dat) in SWAT contains plant growth parameters for all crops in the CDL database. For each CFT, area-weighted, average crop parameters for simulating plant growth were calculated. These parameters are: base and optimum temperature for plant growth, leaf area index, canopy height, maximum rooting depth, radiation use efficiency, maximum stomatal conductance, parameters to capture effect of vapor pressure deficit on stomatal conductance, and parameters pertaining to plant nutrient uptake and yield. Planting and harvesting dates for the 16 CFT's within the watershed were assigned after consultation with the cooperative extension specialist in the region (Dr. Aliasghar Montazar, personal communication, 2020) (Table 9).

Table 9. CFT growth operations and Potential Heat Units (PHUs).

CFT	Planting	Harvest	Harvest & Kill	PHUS
Alfalfa	1st September	31st October, 31st December, 28th February, 31st March, 30th April, 31st May, 30th June, 31st July	31st August	7086.2
Bermuda	1st September	1st November, 1st January, 1st March, 1st May, 1st June	31st August	7086.2
Cabbage	15th October		31st March	2185.2
Citrus	Grown year around, with harvests between October and March			6014.4
Crucifers	15th October		31st March	2185.2
Deciduous Orchards	Grown all year, with one harvest in November			5546.6
Field Grain	13th February		22nd July	2642.0
Grapes	Grown all year, with one harvest in October			3634.0
Herbs	1st January		15th July	3634.0
Legume/Solanum	31st October		15th March	1272.0
Lettuce	15th October		15th March	1470.5
Melons	1st February		1st July	1086.0
Small Grains	15th November		15th June	4030.2
Small Vegetables	15th October		31st March	1614.0
Sugar Beets	30th September		1st July	4489.4
Sweet Corn	30th September		10th June	2002.8

2.4.2 CFT Parameters - Potential Heat Units

Crop growth in SWAT is simulated based on the heat unit theory, which quantifies a crop's heat requirements for growth till maturity (Neitsch et al., 2009). Crop growth occurs above a minimum, or a base temperature, up until a maximum temperature, after which growth ceases. The only portion of the mean daily temperature that contributes to crop growth is the temperature that exceeds the crop's base temperature (Neitsch et al., 2009). Temperature contribution to crop growth is measured in heat units, where 1 heat unit (HU) = 1°C. Potential Heat Units (PHUs) are the total number of heat units required for a crop to reach maturity. Crop growth is simulated till the PHUs required for the crop to reach maturity are achieved.

The base temperature for crop growth and days to maturity for the crop are required to calculate the PHU for a crop. SWAT plant growth database provides the base temperature for each crop in the CDL database. Crop growing seasons from Table 9 were used to determine the number of days to maturity for each CFT class. The average daily temperatures in the agricultural subbasins were extracted for every day during the growing season for the years 1995 and 2005. The heat units for a day within the growing season were calculated as:

$$HU = T_{avg} - T_{base} \quad \text{when, } T_{avg} > T_{base} \qquad \text{eq. 17}$$

Where, T_{avg} is the mean daily temperature (°C) and T_{base} is the base temperature for the CFT (°C).

The total number of heat units for a crop to reach maturity (PHUs) were calculated as:

$$PHU = \sum_{d=1}^{m} HU \qquad \text{eq. 18}$$

Where HU is the number of heat units acquired on day, d = 1, on the day of planting up until the day of maturity, m. PHUs were calculated for 1995 to 2005. These annual PHUs were averaged to obtain an average annual PHU for the SWAT management files (Table 9).

2.4.3 CFT Parameters - Soil Water Deficit

Auto-irrigation is triggered when the water content in a soil layer falls below the field capacity (FC, mm H_2O) by a user defined Soil Water Deficit (SWD) water stress threshold (mm H_2O). SWD is the maximum amount of depletion allowed below field capacity of a soil layer before a crop experiences water stress and potentially reduces growth and yield. Therefore, irrigation is triggered when:

$$SW\ (mm\ H_2O) < FC\ (mm\ H_2O) - SWD\ (mm\ H_2O) \quad \text{eq. 19}$$

To calculate SWD, first plant available water capacity (AWC_d) depth for each soil layer in agricultural subbasins was calculated using the soil's volumetric fraction plant available water capacity (AWC_v) and soil depth (D_{soil}, mm) parameters in the SWAT project database:

$$AWC_d\ (mm\ H_2O) = AWC_v * D_{soil} \quad \text{eq. 20}$$

Management Allowable Depletion (MAD) values of 11 out of 16 CFTs were obtained (Table 10) from Oklahoma State University (OSU) to calculate the SWD thresholds (Allan et a (1998). The average of these MAD values (0.49) were used as MAD values for the remaining 9 CFTs and the generic agriculture crop type in Mexico. The following steps were used to calculate the SWD thresholds to be used in the SWAT management files:

1) Underlying soil layers were identified for each CFT, resulting in the identification of 71 unique CFT-soil combinations
2) Maximum rooting depth was determined for each CFT-soil combination, where maximum rooting depth was defined as the shallower depth between crop rooting depth (RD_{max}) and the rooting depth defined for the soil (Z_{max}) in the soil database.
3) The AWC of each soil layer within the maximum rooting depth was used to calculate the SWD for the soil-crop combination:

   $$SWD = AWC_d * MAD \quad \text{eq. 21}$$

These SWD values were incorporated in crop specific auto-irrigation operation (operation number 10).

2.4.4 Auto-Irrigation Operation

Irrigation depth (mm/event), frequency of irrigation events and seasonal timing of irrigation were obtained from the Cooperative extension specialist in the region (Dr. Aliasghar Montazar, personal communication, 2020). Irrigation depth was used for IRR_MX parameter in the auto-irrigation operation (Table 10). Auto-irrigation operations were written for each CFT based on this data. For example, Broccoli (CFT = Crucifer), is irrigated using the sprinkler irrigation (228.8 mm/event) between October and December, after which it is irrigated using furrow irrigation (101.6 mm/event) till harvest. This variability in irrigation was incorporated by writing two auto-irrigation operations, one in October and one in December to reflect the sprinkler (October) and furrow (December) irrigation amounts. The "Harvest and Kill" operation stops crop growth (operation number = 5). Previous studies have reported over application of irrigation because auto-irrigation operation continues to apply irrigation even after the harvest and kill operation has been used to stop plant growth (Chen et al., 2017). This was remedied by applying an auto-irrigation operation on the day of harvest and kill, where the SWD value was set to field capacity of the soil. Therefore, irrigation would only be applied when soil water content is less than (FC – SWD).

Table 10. CFT irrigation depths and Management Allowed Depletion (MAD) values.

CFT	Irrigation (mm)/event	Irrigation Type	MAD
Alfalfa	114.3	Flood (2-3 times/month)	0.55
Bermuda	114.3	Flood (2-3 times/month)	0.55
Cabbage	88.9	Every other week	0.49
Citrus	25.4	Summer (2 times/week) Spring & Fall (1 time/week) Winter (every other week)	0.5
Crucifers	228.6	Sprinkle (every other day between October and December)	0.49
	101.6	Furrow (every 2 weeks)	
Deciduous Orchards	165.1	Flood (1/month)	0.5
	16.51	Drip (every other day)	
Field Grain	101.6	Every 2 weeks	0.53
Grapes	25.4	Every 2 weeks	0.49
Herbs	85.98	No information	0.49
Legume/Solanum	17.78	Drip (weekly)	0.475
Lettuce	31.75	Sprinkler Every week	0.3
Melons	107.95	Flood Every other week	0.43
Small Grains	101.6	Every 2 weeks	0.49
Small Vegetables	228.6	Sprinkle (every other day)	0.49
	101.6	Furrow (every 2 weeks)	
Sugar Beets	114.3	Flood (every 2 weeks)	0.49
Sweet Corn	76.2	Flood (every 2 weeks)	0.49

Irrigation Efficiency (IRR_EFF): Irrigation efficiency parameter accounts for loss of water from the source (canal) to soil because of conveyance and evaporative loss. Irrigation efficiency was calculated using volumetric estimates from IID water Transfer EIR 2002 (CH2M Hill, 2002) (Table11). This information was used to calculate IRR_EFF as:

$$\frac{\text{Colorado River diversion to IID canals - Water Lost to Evaporation and Conveyance loss}}{\text{Colorado River diversion to IID canals}} \quad \text{eq. 22}$$

Table 11. Irrigation efficiency calculations using volumetric estimates from IID EIR (CH2M Hill, 2002).

	In (ac-ft)	Loss (ac-ft)	Efficiency
IRR_EFF	2859	231	0.92 = (2859 – 231)/2859

Irrigation surface runoff ratio (IRR_ASQ): This is the fraction of water applied to the field that leaves as surface runoff. This parameter was manually calibrated.

2.5 Climate Datasets

Precipitation is the major climatological input. In addition to daily precipitation, the model also requires daily input of temperature (minimum and maximum), relative humidity, solar radiation, and wind speed to calculate energy demand based on the Penman Monteith equation.

We used the Daily Surface Weather and Climatological Summaries (DAYMET) dataset created by Oak Ridge National Laboratory (ORNL) for daily precipitation, temperature, relative humidity, and solar radiation data (Thornton et al., 2016). DAYMET dataset provides climate data for the North American continent at a 1 km resolution (Table 12). This dataset was chosen because:

1) It provides climatological forcing data on a daily time step
2) It provides daily data at a finer spatial resolution of (1 km x 1 km), as compared to other daily gridded datasets like the Variable Infiltration Capacity model dataset (6 km x 6 km) (Livneh et al., 2015) and PRISM (4 km x 4 km) (Daly et al., 1997).
3) It provides data for the North American continent as compared to the PRISM dataset which only provides data for the continental US.

DAYMET shortwave solar radiation and actual vapor pressure data was processed to create climate inputs of daily solar radiation and relative humidity, respectively:

1. DAYMET shortwave solar radiation (Slr, MJ/m^2), was converted to daily solar radiation (H_{net}, MJ/m^2), using day length ($Dlen$, seconds/day) and the following equation:

   $$H_{net} = \frac{Slr \times Dlen}{1000000} \quad \text{eq. 23}$$

2. Relative humidity was calculated using DAYMET actual water vapor pressure and temperature using the following steps:

a. Mean Daily Temperature (T_{avg}), is calculated using minimum (T_{min}) and maximum temperature (T_{max}).

$$T_{avg} = \frac{T_{min} + T_{max}}{2} \quad \text{eq. 24}$$

b. Daily Saturation Vapor Pressure (Sat_{VP}), is calculated as a function of mean daily temperature (T_{avg}).

$$Sat_{vp} = exp\left(\frac{(16.78 \times T_{avg}) - 116.9}{T_{avg} + 237.3}\right) \quad \text{eq. 25}$$

c. Daily Relative Humidity, ($Relh$) was calculated as a function of actual vapor pressure (VP_{act}) and saturated vapor pressure (Sat_{vp}).

$$Relh = \frac{VP_{act}}{Sat_{vp}} \quad \text{eq. 26}$$

The North American Regional Reanalysis (NARR) from NOAA's National Center for Atmospheric Prediction (NCEP) was used for wind data (Mesinger et al., 2006). The NARR dataset provides gridded wind data at a 32 km resolution.

Table 12. Climate variables used in SWAT model and their associated source datasets.

Variable	Dataset
Precipitation	Daily Surface Weather and Climatological Summaries (DAYMET)
Minimum Temperature	
Maximum Temperature	
Relative Humidity	
Solar Radiation	
Wind	North American Regional Reanalysis (NARR)

The gridded datasets were used to create climate files for each subbasin in the watershed for the time period 1980 – 2018. A subbasin average climate file was created for each of the 5 climatic inputs by taking the area weighted average of the climate input within the subbasin. This resulted in a total of 5 climate files for each of the 155 subbasins or a total of 775 climate input files.

2.6 Model Calibration and Validation

The SSW model was calibrated using a combination of automatic and manual calibration approaches. This approach was applied in two phases. The first phase targeted natural hydrologic processes that generate streamflow in 8 gaged headwater subbasins of the Whitewater River in the north. The second phase targeted hydrologic processes within agricultural subbasins that generate discharge to the Alamo and New Rivers in the southern part of the Salton Sea Watershed. The second phase of the calibration approach did not include gaged agricultural subbasins within the Whitewater River drainage area, as groundwater is another source of irrigation in this region and no information on pumping rates is available. Additionally, this calibration approach does not include the gaged Salt Creek subbasin as seepage losses from the Coachella Canal impact streamflow at the Salt Creek (CH2M Hill 2018b) .

Calibration and validation time frames for the headwater subbasins were selected to maintain interannual variability in precipitation within the two-time periods, i.e., both periods had similar mean precipitation, and consisted of dry and wet years (Figure 18). It was found that the time periods of 1995-2005 and 2008-2018 fulfilled these criteria and were respectively chosen as calibration and validation time periods (Table 13). Five years of warm up period were chosen for the calibration (1990-1994) and validation (2003-2008) time frames to reduce the impact of initial condition on model simulations. The same time periods were also used to calibrate (1995 – 2005) and validate (2008 - 2018) the agricultural subbasins.

Table 13. Calibration and validation time periods for headwater and agricultural subbasins.

Phase	Time Period	Years	Precipitation	
			Total (mm)	Mean (mm/year)
Calibration	1995 - 2005	11	3668.4	333.5
Validation	2008 - 2018	11	3483.3	316.7

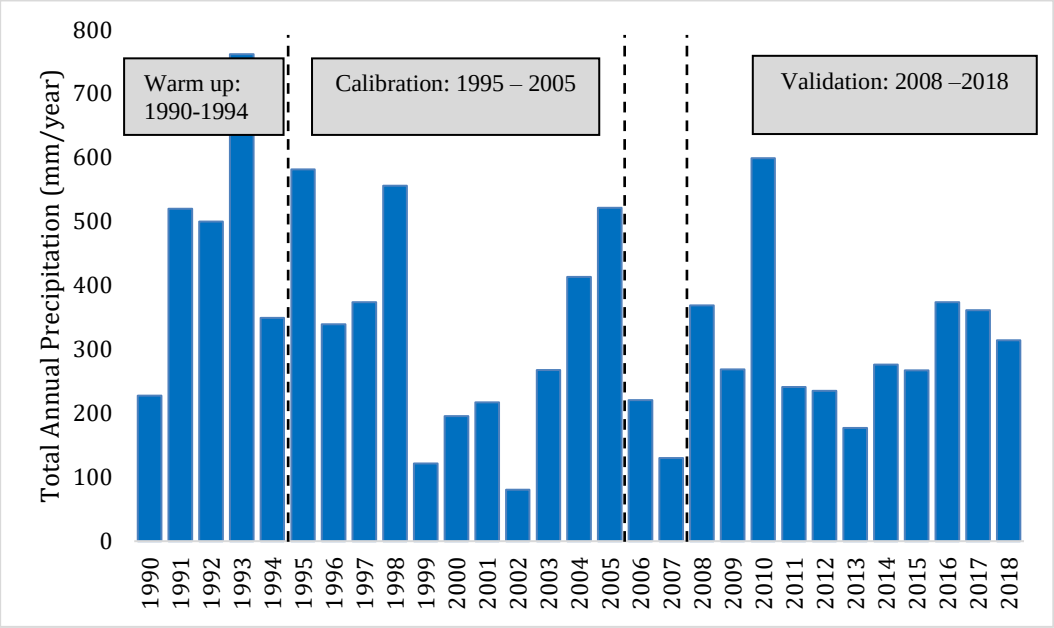

Figure 18. Area weighted annual precipitation for 8 headwater subbasins.

2.6.1 Phase 1: Automatic Calibration of Headwater Subbasins

The USGS has streamflow gages on 8 major headwater reaches that contribute flow to the Whitewater River (Section 2.2.2). Mean annual flows from the USGS gages are reported in (Table 14). Flows in these reaches are typical of ephemeral streams in the arid regions of the American Southwest, with low or no baseflows and large peak flows after extreme rain events. Headwater subbasins are dominated by range-brush or forest land cover types, with 6 out of 8 subbasins having more than half of their area covered by rangeland and 2 subbasins having more than half their area covered by forests (Table 15). Five of the 8 subbasins are largely composed of bedrock and have high runoff potential (soil hydrologic group C & D). Soil hydrologic groups are a Natural Resource Conservation Service (NRCS) soil classification system that groups soils based on infiltration characteristics. A soil hydrologic group is a group of soils that has similar runoff potential under similar storm and land use conditions. Runoff potential increases from hydrologic group A to D, with hydrologic group A having low runoff potential and hydrologic group D having high runoff potential.

Table 14. Mean annual precipitation, potential evapotranspiration and observed streamflow at 8 headwater reaches of the Whitewater River during calibration time frame (1995 - 2005).

Subbasin	Elevation (m)	Area (km^2)	Precipitation (mm/year)	PET (mm/year)	Annual Mean flow ± Standard Deviation (mm/year)
3	1225.9	252.5	273.2	2674.2	15.0 ± 24.7
16	1744.1	93.2	436.0	1797.6	8.9 ± 15.1
143	1370.1	22.6	382.5	2650.1	99.1 ± 74.6
145	2085.0	43.6	490.4	2171.7	92.6 ± 132.6
146	1535.9	12.6	400.9	2471.8	41.7 ± 46.8
149	1863.6	27.7	527.0	2203.3	221.1 ±148.2
150	1800.6	11.1	484.0	2271.4	73.2 ± 68.7
154	1414.7	79.4	236.0	1942.9	13.8 ± 24.4

Table 15. Land use and soil texture classes in the Whitewater River headwater subbasins.

Subbasin	Land use (% subbasin area)					Soil (% subbasin area)				
	Range land	Forest	Pasture	Urban	Barren	Sand	Silty loam	Loamy sand	Fine silty loam	Bed-rock
3	79.0	14.0	6.0	1.0	0.0		12.4	5.8	32.1	49.7
16	65.5	26.6	7.1	0.3	0.5				62.3	37.7
143	63.0	15.1	19.9	0.0	1.9				8.5	91.5
145	41.2	49.6	8.6	0.0	0.4					100.0
146	60.2	26.2	11.0	0.4	1.7	0.6				99.4
149	39.8	53.4	5.2	0.4	1.2	0.1				99.9
150	58.3	40.5	0.8	0.1	0.3					100.0
154	61.4	34.2	1.7	1.9	0.6		4.9	0.0	59.4	35.7

2.6.2 Description of SUFI-2 Algorithm

SWAT Calibration and Uncertainty Program (SWAT-CUP) is a standalone computer software used for sensitivity analysis (local and global), calibration, validation, and uncertainty analysis of SWAT models. SWAT-CUP is linked to multiple optimization algorithms – SUFI-2 (Abbaspour et al., 2004), ParaSol (van Griensven & Meixner, 2007), MCMC (Kuczera & Parent, 1998), GLUE (Beven & Binley, 1992) and PSO (Kennedy & Eberhart, 1995).

This project utilized the SWAT-CUP interface with SUFI-2 optimization algorithm to calibrate monthly streamflow at multiple gaging stations across the SSW. SUFI-2 is a stochastic uncertainty analysis routine that accounts for uncertainties in model simulations arising from uncertainty in model inputs (in our case - soil, land use, topography and climate), parameters (various empirical and non-empirical parameters), and the model itself (mismatch between physical processes that occur in the watershed and their representation in the model). SUFI-2 captures these uncertainties in the 95PPU or 95% probability distribution, captured within 2.5% and 97.5% of the cumulative distribution of the model output variable generated using a range of parameter values. Parameter values are generated using the Latin Hypercube sampling methodology and a set of user defined parameter ranges to create a randomized selection of parameter combinations and avoid bias in parameter selection. Model outputs are assessed on the basis of user selected objective functions such as the Nash Sutcliffe Efficiency (NSE), Mean Squared Error (MSE), Percent Bias (PBIAS), etc., or a combination of multiple objective functions. The 95PPU represents an envelope of "good solutions" or optimal parameter ranges that simulate streamflow (or other model outputs) similar to observed streamflow.

SUFI-2 quantifies the fit between model output (95PPU) and observed variable using two factors – P-factor and R-factor. The P-factor is the percentage of observed variable captured within the 95PPU. R-factor is the thickness of the 95PPU. Optimal results would be 100% inclusion of observed variable within the 95PPU (P-factor =1) and an extremely small R-factor. For streamflow, reasonable values of P-factor and R-factor are > 70% and 1, respectively (Abbaspour, 2015).

SUFI-2 operates by performing multiple successive iterations, and each iteration consists of multiple SWAT model runs defined by the user. As iterations proceed parameter ranges are narrowed to reduce the uncertainty of model predictions and improve the objective function (i.e., the similarity between observed and simulated output).

Parameter Selection : The most commonly used parameters for calibrating streamflow generation in undisturbed subbasins were identified through literature review. We identified 15 most commonly used parameters, and defined initial parameter ranges from literature review and general knowledge of the watershed (

Table ***16***). This range was further refined using a one at a time sensitivity (OAT) analysis to assess parameter ranges across which model performance was sensitive (

Table ***16***).

Table 16. Parameter ranges for headwater subbasins streamflow calibration. Initial ranges are from literature review. Refined ranges indicate parameter ranges obtained from a one at a time sensitivity analysis.

Process	Parameter	Description	Initial	Refined
Evapotranspiration	ESCO []	Soil Evaporation Compensation Factor	0-1	0.1 – 0.7
Evapotranspiration	EPCO []	Plant Uptake Compensation Factor	0-1	0.1 – 1
Groundwater	ALPHA_BF []	Baseflow recession constant	0-1	0.1 – 1
Groundwater	GWQMN (mm H_2O)	Threshold water level in shallow aquifer for baseflow	10 - 2000	200 – 2000
Groundwater	GW_DELAY (days)	Delay time for recharge to reach aquifer from the soil zone	0.5 - 500	100 – 500
Groundwater	RCHRG_DP []	Aquifer percolation coefficient	0-1	0.15 – 0.8
Groundwater	REVAPMN (mm H_2O)	Threshold water level in shallow aquifer for revap[1] to occur	0.1 - 3600	200 – 3600
Groundwater	GW_SPYLD (m/m)	Specific yield of Shallow Aquifer	0.01-0.35	0.02 – 0.3
Main Channel Routing	CH_K1 (mm/hr)	Effective hydraulic K in main channel alluvium	0.025 - 1000	50 – 470
Main Channel Routing	CH_N1 []	Manning's N Value for the main Channel	0.016 - 0.15	0.02 – 0.11
Percolation	SOL_K (mm/hr)	Saturated Hydraulic Conductivity	1.512 - 750	3 – 500
Surface Runoff	CN2 []	Moisture condition II CN	30 - 90	30 – 90
Surface Runoff	SURLAG (days)	Surface runoff lag coefficient	0.05 - 31	0.1 – 25
Tributary Chanel Routing	CH_N2 []	Manning's N Value for the tributary Channel	0.016 - 0.15	0.02 – 0.15
Tributary Chanel Routing	CH_K2 (mm/hr)	Effective hydraulic K in tributary channel alluvium	0.025 - 1000	140 - 470

[1] *Revap is the process by which water from the shallow aquifer returns to the root zone in response to moisture deficit in the soil profile.*

Objective functions: Nash Sutcliffe Efficiency (NSE) was used as the objective function for the calibration of headwater subbasins. NSE was selected as it is one of the most commonly used objective functions in hydrologic modelling (Moriasi et al., 2007). NSE is calculated as:

$$\text{NSE} = 1 - [\frac{\sum_{i=1}^{n}(Y_i^{obs} - Y_i^{sim})^2}{\sum_{i=1}^{n}(Y_i^{obs} - Y^{mean})^2}] \quad \text{eq. 27}$$

Where, Y_i^{obs} and Y_i^{sim} are the observed and simulated streamflow on day i, respectively, Y^{mean} is the mean observed flow and n is the total number of days in the simulation.

As the NSE metric is particularly sensitive to high flow events by using the squared deviations (Muleta, 2012), other objective functions were utilized to assess model performance – percent bias (PBIAS), root mean squared error (RMSE), and the Kling-Gupta Efficiency (KGE).

PBIAS: Percent bias metric reports whether the model over or under predicts observations.

$$PBIAS = [\frac{\sum_{i=1}^{n}\left(Y_i^{obs} - Y_i^{sim}\right)*100}{\sum_{i=1}^{n}(Y_i^{obs})}] \quad \text{eq. 28}$$

RMSE: The root mean squared error metric assesses the error in model simulations in units of the constituent of interest (streamflow).

$$RMSE = \sqrt{\sum_{i=1}^{n}(Y_i^{obs} - Y_i^{sim})} \quad \text{eq. 29}$$

KGE: The Kling Gupta Efficiency metric has been suggested as an alternative to the NSE metric, because of its ability to consider multiple model errors – error in variance, error in mean, and error in temporal dynamics. The KGE metric is calculated using linear correlation (R), variance bias (RELVAR), and mean bias (BIAS) (Gupta et al., 2009):

$$KGE = 1 - \sqrt{(r-1)^2 + (\frac{\sigma_{sim}}{\sigma_{obs}} - 1)^2 + (\frac{\mu_{sim}}{\mu_{obs}} - 1)^2} \quad \text{eq. 30}$$

Where, r is the linear correlation, σ_{sim} and σ_{obs} are the standard deviation of the simulated and observed data, respectively, and μ_{sim} and μ_{obs} area the mean of the simulated and observed data, respectively.

2.6.3 Calibration Approach of Headwater Subbasins

Two different calibration approaches were tested for the headwater subbasins. The first approach applies a constant factor to each parameter value and maintains spatial distribution of input parameters (Curve Number, Alpha Baseflow, Soil Hydraulic Conductivity, Soil Available Water Capacity). The second approach replaces all 15 input parameters with a value within a given range. While the second approach can result in significantly different values than the initial parameter values and may lead to a generalization of spatially distributed values; this approach is beneficial in remote catchments with lower-quality input data.

Approach1: Change Value Relative to Initial Value

In this approach, three parameters (Curve Number, Alpha Baseflow, Soil Hydraulic Conductivity) were changed on a relative basis and the remaining 11 parameters were replaced by values within a specified range (

Table ***16***). An additional sixteenth parameter, not identified in initial parameter selection was included in this approach – Soil Available Water Capacity (SOLAWC). This parameter was also changed relative to its initial parameter value. This approach was applied as follows:

1) Iteration 1: The first calibration iteration was run on a monthly time step for 400 model runs.

2) Iteration 2: New parameter ranges from iteration1 were used to initialize calibration on a monthly timestep, with 400 model runs. Global sensitivity analysis was used to identify the most sensitive parameters.

3) Iterations 3-6: New parameter ranges from iteration 2 were used to initialize calibration of most sensitive parameters on a monthly timestep (iteration 3). This was process was repeated for 5 more calibration iterations, resulting in a total of 6 monthly calibration iterations (iteration 1 – 6).

Table 17. Input parameters ranges used in each iteration in approach 1: relative change. The prefix "R_" indicates parameters that were changed relatively by a factor = 1+(value indicated in table). The prefix "V_" indicates that the parameter value was replaced by a value within a specified range.

Parameter	Iter1	Iter2	Iter3	Iter4	Iter5	Iter6
R_CN2	-0.5 - 0.5	-0.1 - 0	-0.2 - 0.1	-0.2 - 0.1	-0.2 - -0.1	-0.3 - -0.2
R_ALPHABF	-0.5 - 0.8	0.1 -0.8	-0.6	-0.5 - -0.2	-0.7 - -0.3	-0.9 - -0.5
V_GWDELAY	100.0 - 500.0	238.2 - 514.8	- - -	- - -	- - -	- - -
V_GWQMN	200.0 - 2000.0	974.9 - 2525.6	2257.8 - 3280.2	2759.3 - 3762.8	2929.1 - 3485.1	3023.2 - 3331.2
V_RCHRGDP	0.2 - 0.8	0.0 -0.5	0.0 - 0.2	0.0 - 0.1	0.0 - 0.1	0.0 - 0.1
V_GWSPYLD	0.0 - 0.3	0.1 -0.4	- - -	- - -	- - -	- - -
V_REVAPMN	200.0 - 3600.0	150.7 - 2450.9	726.8 - 2181.2	73.0 - 1478.8	405.8 - 1121.4	575.2 - 939.5
V_ESCO	0.1 - 1.0	0.1 -0.5	0.1 - 0.3	0.1 - 0.2	0.0 - 0.2	0.0 - 0.1
V_EPCO	0.1 - 1.0	0.5 -1.4	- - -	- - -	- - -	- - -
V_SOLK	-0.5 - 0.5	-0.2 - 0	-0.2 - 0.0	-0.3 - -0.1	-0.4 - -0.2	-0.5 - -0.3
V_CHN2	3.0 - 500.0	0.0 -0.1	- - -	- - -	- - -	- - -
V_CHK2	0.0 - 0.2	51.1 -330.4	- - -	- - -	- - -	- - -
V_CHK1	140.0 - 470.0	25.0 -321.8	226.3 - 364.1	276.9 - 378.0	243.5 - 333.2	214.0 - 293.5
V__CHN1	50.0 - 470.0	0.1 -0.1	0.1 - 0.2	0.1 - 0.2	0.1 - 0.2	0.2 - 0.2
V__SURLAG	0.0 - 0.1	1.1 -17.0	4.1 - 12.9	4.5 - 10.1	6.9 - 11.5	8.8 - 12.7
R__SOLAWC	-0.5 - 0.5	-0.1 - 0	0.2 - 0.5	0.3 - 0.4	0.2 - 0.3	0.2 - 0.27

Approach 2: Replace Value Within a Specified Range

The 15 parameters identified using literature review and their ranges determined from the OAT sensitivity analysis (

Table ***16***) were optimized through 7 successive iterations of monthly model simulations. Values of the 15 parameters were replaced with values from within a feasible input parameter range (Table 18). The first calibration iteration (iteration 1) was run on a monthly time step for 400 model runs. All parameters were replaced with values within a specified input range (Iter1, Table 18). New parameter ranges from Iteration 1 were used to initialize the next calibration iteration (Iteration 2) on a monthly timestep, with 400 model runs. This process was repeated for 5 more calibration iterations, resulting in a total of 7 monthly calibration iterations (Iter1 – Iter7).

Table 18. Input parameter ranges from successive iterations in approach 2. In this approach, values of a parameter were replaced from within the parameter ranges defined for that iteration.

Parameter	Iter1	Iter2	Iter3	Iter4	Iter5	Iter6	Iter7
V_CN2	30 - 90	30.00 - 60.57	42.43 - 67.32	30.69 - 55.11	30.68 - 43.13	31.63 - 39.30	32.21 - 36.94
V_ALPHABF	0.15 - 0.95	0.52 - 1.00	0.59 - 0.9	0.71 - 0.96	0.83 - 1	0.85 - 0.95	0.86 - 0.92
V_GWDELAY	100 - 500	238.19 - 514.81	346.5 - 563.32	421.48 - 571.45	473.29 - 577.01	506.27 - 572.29	527.26 - 569.29
V_GWQMN	200 - 2000	974.88 - 2525.62	1609. - 2879.32	2156.26 - 3250.48	2627.31 - 3570.00	3097.94 - 4039.70	3568.10 - 4508.95
V_RCHRGDP	0.15 - 0.8	0.01 - 0.52	0.20 - 0.60	0.09 - 0.42	0.01 - 0.28	0.01 - 0.14	0.01 - 0.08
V_GWSPYLD	0.02 - 0.3	0.13 - 0.36	0.17 - 0.30	0.22 - 0.33	0.26 - 0.35	0.30 - 0.37	0.33 - 0.39
V_REVAPMN	200 - 3600	150.65 - 2450.85	419.1 7- 1774.05	399.50 - 1316.12	386.20 - 1006.31	680.28 - 1268.78	959.37 - 1517.87
V_ESCO	0.1 - 0.7	0.10 - 0.50	0.23 - 0.49	0.23 - 0.40	0.23 - 0.34	0.20 - 0.29	0.18 - 0.26
V_EPCO	0.1 - 1	0.53 - 1.00	0.52 - 0.84	0.68 - 0.96	0.82 - 1.00	0.74 - 0.91	0.66 - 0.83
V_SOLK	3 - 500	3.00 - 253.22	3 - 129.7	3.00 - 66.89	3 - 35.22	3.00 - 19.44	3.00 - 11.39
V_CHN2	0.02 - 0.15	0.02 - 0.10	0.02 - 0.07	0.01 - 0.05	0.01 - 0.03	0.02 - 0.04	0.03 - 0.06
V_CHK2	140 - 470	51.06 - 330.41	3.00 - 213.30	3.00 - 124.35	3 - 73.02	36.73 - 104.23	69.25 - 134.32
V_CHK1	50 - 470	25.00 - 321.75	160.91 - 432.88	144.72 - 336.88	133.29 - 269.05	172.21 - 250.15	194.56 - 239.30
V_CHN1	0.02 - 0.11	0.06 - 0.13	0.08 - 0.12	0.09 - 0.12	0.11 - 0.13	0.11 - 0.12	0.11 - 0.12

V_SURLAG	0.1 - 25	1.05 - 17.02	7.16 - 19.41	7.63 - 15.48	7.93 - 12.97	9.08 - 11.67	9.68 - 11.01

The 8 headwater catchments were calibrated on a monthly basis using a total of 2800 model simulations (7 iterations with 400 simulations each). Two approaches were further used to improve results from these monthly iterations – 1) daily calibration and 2) relative change. These are discussed in the Results section.

2.6.4 Phase 2: Calibration of Agricultural Subbasins

Thirteen subbasins with agricultural HRUs were identified in the Imperial Irrigation District area, with agriculture occupying between 3.4% to 78.8% of the subbasin's area (Table 19). These subbasins covered a total of 2849.84 km^2, with agriculture occupying 1486.21 km^2 or 52.2% of the total area. Alfalfa, small grains (oats, wheat), Bermuda grass and field grains (corn, sorghum) cover more than 90% of the agricultural area within these 13 subbasins (Table 20). These subbasins were calibrated through a combination of manual and automated calibration techniques. Observed flow from USGS gages at New River (Gage 10255550) and Alamo River (Gage 10254730) were used to assess model performance on the basis of NSE and Kling-Gupta Efficiency (KGE) metrics.

Table 19. Total areas of subbasins & agricultural areas within drainage areas of New and Alamo Rivers.

Drainage Area (Reach #)	Agricultural subbasin	Total area (km^2)	Agriculture Area (km^2)	Agriculture Area (%)
Alamo River (98)	14	115.76	85.14	73.54
	20	230.44	12.15	5.27
	98	472.23	371.86	78.75
	99	351.77	237.95	67.64
	113	105.38	4.45	4.22
	114	444.22	343.44	77.31
	126	15.09	6.78	44.94
New River (133)	49	460.08	101.27	22.01
	122	21.34	16.22	76.04
	124	74.84	10.31	13.78
	129	102.46	3.49	3.40
	133	409.82	289.13	70.55

	135	46.40	4.01	8.64

Table 20. Total crop area (km^2) and portion of total IID agricultural area (%) covered by CFTs in the IID.

CFT	Area (km^2)	% Agricultural Area
Alfalfa	451.63	30.39
Small Grains	422.43	28.42
Bermuda	267.86	18.02
Field Grain	214.25	14.42
Small Vegetables	45.13	3.04
Sugar Beets	29.07	1.96
Citrus	18.86	1.27
Lettuce	15.64	1.05
Melons	9.06	0.61
Sweet Corn	7.31	0.49
Crucifers	3.10	0.21
Cabbage	1.19	0.08
Deciduous Orchards	0.46	0.03
Herbs	0.20	0.01

Manual Calibration: Simulated flows at these two gages using SWAT default parameter values were overestimated compared to observed flows. To identify major controls on simulated flows, a set of parameters were identified that control runoff from agricultural subbasins, and sensitivity of simulated flows to changes in these parameters were assessed. The surface runoff ratio (ASQ) parameter in the .mgt file governs the ratio at which applied irrigation is lost to surface runoff. Model sensitivity to surface runoff ratio (ASQ) was assessed to identify optimal parameter range for ASQ. East Highline, Central Main and Westside Main canals are the three major canals that branch off the AAC and supply agricultural water to the IID. However, no information is available

on how much water is transferred from the AAC to each of these canals. The sensitivity analysis helped to identify optimal transfer ratios from AAC to the canals. As large portions (~ 82%) of the three canals are unlined (IID, 2018), channel transmission losses can impact flows at New and Alamo Rivers. In SWAT, transmission loss (*tloss*, m^3 H_2O) from a reach is calculated as:

$$tloss = K_{ch} * TT * P_{ch} * L_{ch} \quad \text{eq. 31}$$

Where, K_{ch} is the channel bed hydraulic conductivity (mm/hr), TT is the flow travel time (hr), P_{ch} is the wetted perimeter (m), and L_{ch} is the channel length (km). Model performance was assessed against different values of K_{ch} – no loss (0 mm/hr), insignificant loss (1.24 mm/hr), moderate loss (9.5 mm/hr), moderately high loss (25.5 mm/hr) and high loss rate (38 mm/hr). Furthermore, SWAT simulated flows using default parameter values indicated a time lag between simulated and observed flows in New and Alamo Rivers. The surface runoff lag coefficient (SURLAG) influences the fraction of surface runoff reaching a reach. The baseflow recession constant (ALPHABF) is an index of groundwater flow (baseflow) response to recharge. Model sensitivity analysis to both of these parameters was performed to reduce the lag between simulated and observed flows in New and Alamo Rivers.

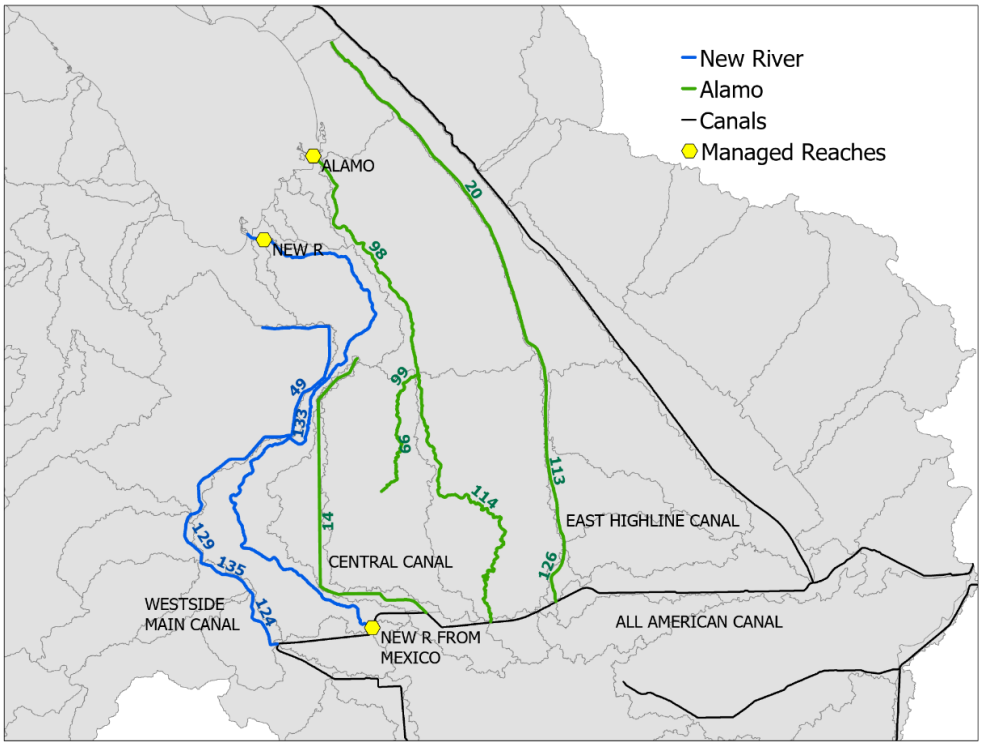

Figure 19. Subbasins with hydrologic connectivity within the drainage areas of New River (blue) and Alamo River (green).

Automatic Calibration: Results from the manual calibration were used to inform parameter selection and ranges for automatic calibration in SWAT-CUP using the SUFI-2 optimization algorithm. The 13 agricultural subbasins in IID were calibrated for 1 iteration consisting of 500 simulations. The subbasins were divided into two categories depending on whether they were hydrologically connected to or fell within drainage areas of Alamo River (reach 98) or New River (reach 133). The two categories were parameterized separately in the same calibration iteration. The drainage area of Alamo River (reach 98) consists of 7 subbasins (14, 20, 98, 99, 113, 114, 126), and the drainage area of the New River consists of 6 subbasins (49, 122, 124, 129, 133, 135) (Table 19, Figure 19).

2.6.5 Colorado River Inflow Scenarios

Optimal parameter sets resulting from the automatic calibration results were used to create the final model for agricultural subbasins in the IID. Inflows from the Colorado River through the AAC is the main source of water to the IID for agricultural irrigation. We designed two different scenarios to assess the impact of Colorado River inflows on the water budget of the IID. The years with maximum and minimum total annual flows from the Colorado River below Pilot Knob hydroelectric dam (USGS Gage 09527500) were identified during the time period 1980 – 2018 as 1997 and 1983, respectively. Daily flow data (m^3/d) was extracted for both years and used to create inputs for two scenarios:

- Scenario 1 (maximum annual flow): daily data from year 1997 was repeated for 18 years between 1990 and 2018.
- Scenario 2 (minimum annual flow): daily data from year 1983 was repeated for 18 years between 1990 and 2018.

These scenarios were compared to the baseline scenario with observed inflow data between 1990 and 2018.

3. RESULTS

A total of 8 headwater subbasins and 13 irrigated subbasins were calibrated through a combination of automatic and manual calibration approaches using streamflow observations. In total 3,386 km^2 of the Salton Sea Watershed was calibrated, with 546 km^2 in the headwater subbasins and 2,850 km^2 in the irrigated subbasins.

3.1 Calibration Phase 1: Headwater Subbasins

Two different approaches were examined for calibrating the 8 headwater subbasins. Originally 15 parameters had been identified for automatic calibration. In Approach 1, we considered an additional parameter – Soil Available Water Content for automatic calibration. In this approach,

the values of 4 parameters (Curve Number, Alpha Baseflow, Soil Hydraulic Conductivity, Soil Available Water Capacity) were changed relative to their initial values to maintain spatial heterogeneity of parameters across the calibrated subbasins. In Approach 2, the values of 15 parameters initially identified from literature review were replaced within a feasible parameter range determined from sensitivity analysis.

3.1.1 Approach 1: Relative Parameter Change Approach

Global Sensitivity Analysis: The 8 headwater subbasins were iteratively calibrated between 1995-2005 (with 5 year warm up between 1990 and 1995), on a monthly basis using 6 successive iterations, each consisting of 400 simulations. Global sensitivity analysis in SWAT-CUP develops a multiple regression model of Latin Hypercube generated parameter sets against the objective function (NSE) values of simulated streamflow to identify the most sensitive parameters. A t-test is used to identify the relative significance of each parameter, where parameter sensitivity is the average change in objective functions, relative to change in a parameter, while other parameters are also changing. The t-stat is computed to assess parameter sensitivity and is used to determine the p-value. A p-value < 0.05 was used to identify the most sensitive parameters (Abbaspour, 2015). Global sensitivity analysis results in Iteration 2 identified 11 most sensitive parameters, which were further calibrated in subsequent iterations (Table 21).

Table 21. Global sensitivity analysis of parameters in iteration 2 indicated that the model was most sensitive to 11 parameters (highlighted in green). Sensitive parameters are those parameters for which P-Value < 0.05. These 11 parameters were calibrated in subsequent iterations.

Parameter	t-Stat	p-Value
V_EPCO	0.04	0.97
V_CHK2	0.93	0.35
V_GWSPYLD	0.99	0.32
V_GWDELAY	1.11	0.27
V_CHN2	1.38	0.17
V_SURLAG	-2.25	0.03
V_RCHRGDP	2.46	0.01

R_ALPHABF	-2.69	0.01
R_SOLAWC	3.5	0
V_ESCO	-8.21	0
V_CHN1	8.7	0
R_SOLK	-14.26	0
V_REVAPMN	-14.63	0
R_CN2	-22.17	0
V_GWQMN	35.15	0
V_CHK1	54.01	0

Model Performance: The monthly NSEs for all headwater subbasins were significantly improved compared to the uncalibrated (default) model's NSE using default parameter values from soil and land cover databases in SWAT (Table 22). In all subbasins, NSEs were deteriorated from iteration 1 to iteration 2. However, NSE values in subbasins 3, 16, 143, 146, 150 and 154 were improved in subsequent iterations and the best NSE values were obtained at iteration 6 with the exception of two subbasins. The best NSE for subbasin 145 was achieved at iteration 5, and NSE of subbasin 149 did not improve beyond the first iteration.

Table 22. Monthly NSE values of 8 headwater subbasins using the relative parameter change approach, where values of 5 parameters were multiplied by a factor (1+ a value), to change it relative to the original input value. The Default column indicates model performance using SWAT default parameter values. Maximum NSE's across iterations are bolded.

Subbasin	Default	Iter1	Iter2	Iter3	Iter4	Iter5	Iter6
3	-16.46	-1.05	-2.43	-2.07	-1.40	-1.10	**-0.49**
16	-819.80	-294.91	-369.02	-335.62	-292.97	-263.55	**-213.14**
143	-7.55	0.01	-0.35	-0.08	-0.01	0.09	**0.36**
145	-4.39	0.08	-0.07	0.10	0.06	**0.23**	0.18
146	-35.83	-6.46	-8.43	-7.06	-5.31	-4.62	**-3.37**
149	-1.75	**0.56**	0.30	0.29	0.40	0.40	0.46
150	-16.78	-1.36	-1.83	-0.88	-1.09	-0.68	**-0.53**
154	-16.48	-1.87	-4.01	-3.50	-2.57	-2.16	**-1.31**

While the range of NSE values for all subbasins narrowed and improved through successive iterations (Figure 20) of the SUFI-2 optimization algorithm, the results are not satisfactory. Values of NSE between 0.0 and 1.0 are generally viewed as acceptable model performance; however, satisfactory model performance is achieved when NSE ≥ 0.5 (Moriasi et al., 2007). The relative

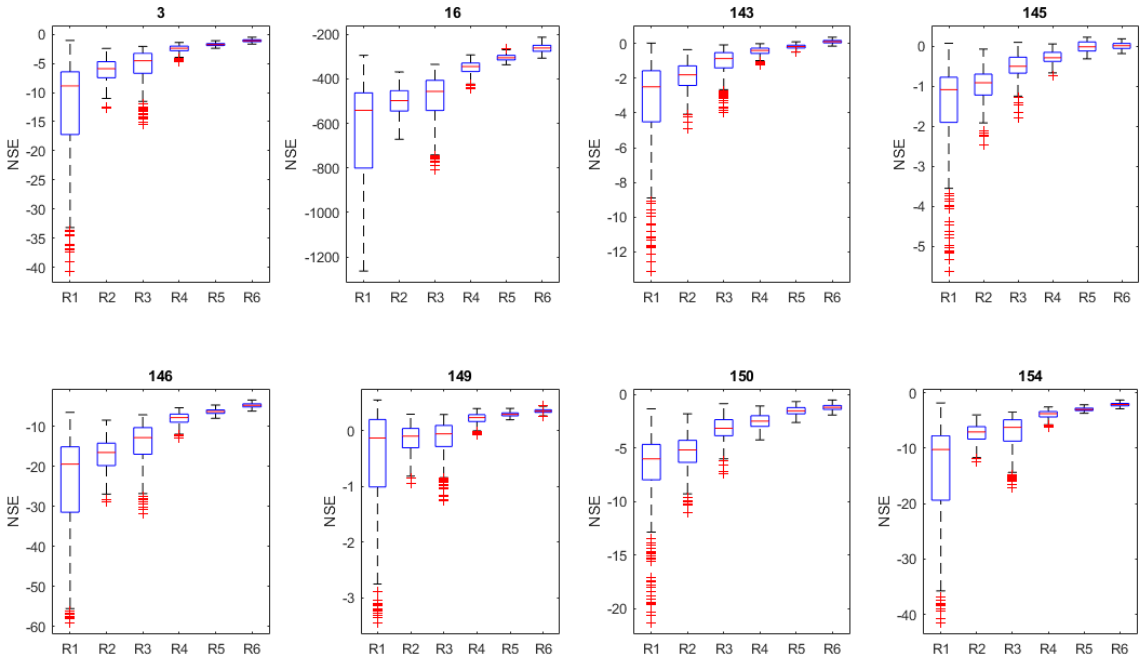

Figure 20. Ranges of NSE values for monthly streamflow in each of the 8 headwater subbasins obtained through iterations 1-6 using the relative parameter change approach.

parameter change approach resulted in acceptable model performance for 3 headwater subbasins (143,145,149), and in 5 headwater subbasins results were unacceptable since NSE < 0. This means that even after 2400 model simulations, the SUFI-2 optimization algorithm was unable to find optimum parameter sets for these 5 headwater subbasins (3,16,146,154) using the relative parameter change method. This result indicates that either more calibration iterations were required, or the initial input parameter values obtained from the national databases were incorrect.

Uncertainty Analysis: SUFI-2 optimization algorithm assesses the fit between model simulation (expressed as 95% probability distribution (95PPU) between 2.5% and 97.5% of the cumulative distribution of simulated output) and observed flow using two statistics: P-factor and R-factor. P-

factor is the percentage of observed data enveloped by the 95PPU and R-factor is the thickness of 95PPU. P-factor of >70% and a R-factor of ~ 1 are considered acceptable for discharge (Abbaspour, 2015). Results indicated that while R-factor and P-factor were decreased with successive iterations, these factors never reached their target thresholds mentioned above.

Best Parameter Values: The optimal parameter set for each subbasin was selected from the best performing simulation out of the 2400 simulations across the 6 iterations (Table 23).

Table 23. Range of parameter values for the default (uncalibrated model) and calibrated model. The calibrated model parameter values were derived from the best performing simulations for each subbasin (Table 22). The optimal parameter ranges reported here cover all 8 headwater subbasins.

Parameter	Default Model Values	Calibrated Model Values
R_CN2	39 – 89	20 – 73
R_APHABF	0.55 *	0.15 – 0.93
V_GWDELAY	31 *	167.5 – 376.5
V_GWQMN	1000 *	1750.25 – 3628.54
V_RCHRGDP	0.05 *	0.05 – 0.24
V_GWSPYLD	0.003 *	0.03 – 0.25
V_REVAPMN	750 *	576.64 – 1300.75
V_ESCO	0.95 *	0.02 – 0.30
V_EPCO	1 *	0.92 – 0.97
R_SOLK	2.52 – 330.28	1.55 – 202.66
V_CHN2	0.014 *	0.03 – 0.04
V_CHK2	0 *	190.74 – 212.19
V_CHK1	0 *	173.38 – 347.75
V_CHN1	0.014 *	0.09 – 0.16

V_SURLAG	2 *	8.93 – 11.06
R_SOLAWC	0 – 0.1	0.0 – 0.12

**These are default values from the model and were the same across all subbasins.*

Due to the overall poor performance of this calibration approach after 2400 model simulations, this approach was not considered further.

3.1.2 Approach 2: Replace Parameter Values Approach

Calibration on a Monthly Time Step: The second approach for calibrating the 8 headwater subbasins was to replace the values of 15 parameters within specified parameter ranges (Table 18). In this approach, calibration of monthly streamflow was performed using 7 successive iterations with 400 simulations each (2800 simulations). Overall, P-factor and R-factor decreased with successive iterations. This is expected, as the optimization algorithm narrows the range of parameter values, effectively reducing the variability of predicted stream flows within a given iteration, and results in a narrowed 95PPU envelope (smaller R-factor) of simulated flows. As the 95PPU envelope gets smaller, the percentage of observed data contained within the envelope also gets smaller, resulting in a reduced P-factor. The P-factor value for 5 out of the 8 subbasins did not reach the target of >70% during any of the monthly iterations. While P-value reached ~70% for 3 subbasins (143, 149 and 150), the maximum NSE for the subbasins were not included in the iteration with the best P and R factors.

Table 24. Monthly NSE values of 8 headwater subbasins calibrated using the replace parameter values approach. NSE values of simulated streamflow using SWAT default parameter values are shown in Default column. Bold numbers represent maximum NSE of each subbasin through successive iterations.

Subbasin	Default	Iter1	Iter2	Iter3	Iter4	Iter5	Iter6	Iter7
3	-16.46	0.28	0.72	0.71	**0.79**	0.76	0.75	0.73
16	-819.80	-147.96	-80.38	-41.76	-49.80	-17.61	-12.08	**-11.78**
143	-7.55	0.58	0.77	0.77	**0.81**	0.80	0.72	0.69
145	-4.39	0.02	0.18	0.38	0.43	0.43	**0.44**	0.43
146	-35.83	-3.23	-1.03	-0.61	-0.61	0.11	0.20	**0.26**
149	-1.75	**0.63**	0.59	0.59	0.56	0.51	0.46	0.39
150	-16.78	-1.25	-0.21	0.35	0.52	0.60	**0.61**	0.56

154	-16.48	-0.33	0.68	0.67	0.76	**0.76**	0.75	0.73

The best performing iterations (with the highest NSE) were identified for each of the 8 subbasins (Table 24). Five (3, 143, 149, 150 and 154) out of 8 subbasins had satisfactory model performance (NSE $\geq$ 0.5). According to performance ratings for NSEs (Moriasi et al., 2007), model performance was very good (NSE $\geq$ 0.65) for 3 subbasins – 3,143,154, and satisfactory (0.65 > NSE $\geq$0.50) for 2 subbasins (149 and 150). Even though model performance for subbasin 16 improved from the uncalibrated (default) model, none of the iterations achieved acceptable NSE for subbasin 16 which has the smallest mean annual flow among the headwater subbasins.

Table 25. Default and optimal parameter ranges in the 8 headwater subbasins calibrated using the replace parameter value approach. The optimal values were selected from the best performing iterations for each subbasin. Parameter values were obtained for subbasins 3 and 143 from iteration 4, for subbasin 16 and 146 from iteration 7, subbasins 145 and 150 from iteration 6 and subbasin 154 from iteration 5 (Table 24).

Parameter	Subbasin 3		Subbasin 16		Subbasin 143		Subbasin 145	
	Default	Calibrated	Default	Calibrated	Default	Calibrated	Default	Calibrated
CN2	70 - 84	53.01	70 - 80	34.02	70 - 84	48.98	77 - 89	40.82
ALPHA BF	0.55	0.92	0.55	0.88	0.55	0.91	0.55	0.90
GW DELAY	31	506.40	31	554.00	31	498.15	31	554.58
GWQMN	1000	3074.03	1000	4507.77	1000	2302.62	1000	3399.14
RCHRGDP	0.05	0.12	0.05	0.01	0.05	0.41	0.05	0.21
GW SPYLD	0.003	0.28	0.003	0.38	0.003	0.26	0.003	0.30
REVAPMN	750	448.77	750	1489.25	750	425.85	750	641.22
ESCO	0.95	0.40	0.95	0.19	0.95	0.26	0.95	0.30
EPCO	1	0.71	1	0.66	1	0.71	1	0.88
SOLK	2.52 - 330.28	7.55	2.52 - 101.62	3.16	2.52 - 101.62	3.08	27.72 -	3.36
CHN2	0.014	0.03	0.014	0.06	0.014	0.03	0.014	0.01
CHK2	0	6.19	0	131.96	0	121.46	0	14.29
CHK1	0	295.33	0	220.23	0	264.10	0	257.68
CHN1	0.014	0.10	0.014	0.11	0.014	0.12	0.014	0.12
SURLAG	2	13.88	2	10.32	2	8.03	2	11.79

Parameter	Subbasin 146		Subbasin 149		Subbasin 150		Subbasin 154	
	Default	Calibrated	Default	Calibrated	Default	Calibrated	Default	Calibrated
CN2	39 - 80	34.38	39 - 84	31.13	77 - 80	35.63	70 - 84	39.29
ALPHA BF	0.55	0.90	0.55	0.88	0.55	0.90	0.55	0.90
GW DELAY	31	550.22	31	376.50	31	553.23	31	474.72
GWQMN	1000	4122.03	1000	1750.25	1000	3388.71	1000	3488.69
RCHRGDP	0.05	0.04	0.05	0.24	0.05	0.14	0.05	0.01
GW SPYLD	0.003	0.33	0.003	0.25	0.003	0.37	0.003	0.34
REVAPMN	750	1059.20	750	1300.75	750	1215.08	750	884.62
ESCO	0.95	0.19	0.95	0.30	0.95	0.24	0.95	0.29
EPCO	1	0.82	1	0.97	1	0.87	1	0.88
SOLK	27.72 - 330.28	3.45	27.72 - 330.28	6.11	27.72 -	3.27	2.52 - 101.62	8.52
CHN2	0.014	0.05	0.014	0.04	0.014	0.03	0.014	0.01
CHK2	0	104.47	0	190.74	0	98.75	0	15.87
CHK1	0	236.33	0	173.38	0	215.37	0	167.06
CHN1	0.014	0.12	0.014	0.09	0.014	0.12	0.014	0.12
SURLAG	2	10.41	2	9.03	2	11.61	2	8.84

Exposed bedrock (where >90% of subbasin area is bedrock, Table 15) is the predominant landscape feature that significantly impacts subsurface flow processes in all headwater subbasins with the exception of subbasin 3, 16 and 154. Exposed bedrock was found in a cluster of 5 headwater subbasins (143, 145, 146, 149, and 150) in the northwestern edge of the watershed. This feature

consisted of 1-soil layer that was 1520 mm deep. It is interesting to note that model performance was satisfactory for all but 1 subbasin (subbasin 146) in the cluster of 5 subbasins. While topography, land use and soil were similar across the 5 subbasins, the factor that distinguished subbasin 146 from the rest was that it had low mean annual streamflow of ~ 42 mm/year as compared to subbasins 143, 145, 149 and 150 which have large mean annual flows (> 70 mm/year) (Table 14).

Table 26. Model evaluation criteria for 8 headwater subbasins during calibration (1995 -2005).

Subbasin	NSE	PBIAS (%)	RMSE (mm/d)	KGE	R	RELVAR	MEAN BIAS
3	0.79	-14.95	2.81	0.63	0.91	0.67	1.15
16	-11.78	-232.35	2.43	-6.90	0.47	7.92	4.77
143	0.81	22.76	0.55	0.73	0.89	0.90	0.77
145	0.44	12.39	3.03	0.43	0.67	0.55	0.88
146	0.26	-41.80	0.35	0.27	0.89	1.59	1.42
149	0.63	10.87	2.16	0.66	0.75	0.80	0.88
150	0.61	13.39	0.37	0.75	0.79	1.08	0.89
154	0.76	-96.70	0.81	0.01	0.91	0.81	1.97

While NSE is useful for assessing the overall fit of a simulated hydrograph to an observed one, it is also extremely sensitive to peak flows (due to squared deviations of mean flow residuals) (Moriasi et al., 2007). The KGE metric has been suggested as an alternative metric that addresses the shortcomings of NSE by combining the linear correlation, and errors due to bias in standard deviation (variability) and mean flow. A KGE value of > -0.41 has been suggested as the threshold above which model simulation is a better predictor of flow than the mean of observed flow. Using this threshold value, model simulations were acceptable for all subbasins, except subbasin 16 (KGE = -6.90). An analysis of the KGE components for subbasin 16 indicated that the model was unable to capture the timing of flows (low linear correlation of 0.47), high bias in simulated variance compared to observed variance (RELVAR = 7.92) and overprediction of mean monthly flow (BIAS = 4.77).

We applied two strategies to further improve model simulation of streamflow. In the first strategy, we changed parameter values relative to their optimal values identified in Table 25 in three successive iterations each consisting of 400 simulations (1200 simulations total). This strategy reduced NSE values and was not further pursued. In the second strategy, we used the best simulation from the monthly calibration to further calibrate the model at a daily time step (5 iterations each consisting of 400 simulations). This strategy also worsened NSE values of daily and monthly streamflow and was not pursued further. Therefore, parameter values of simulations with the highest NSEs are selected for each subbasin to validate the model for an independent period (identified in Table 24).

3.1.3 Validation

Model validation at a monthly timestep was performed using climate forcings from 2008 to 2018 period, with five years of warm up period between 2003 and 2008. Initial model performance was assessed using the NSE objective function. Model performance was significantly improved from the uncalibrated (default) model simulations during the validation timeframe of 2008 to 2018. During validation only two subbasins had satisfactory model performance (NSE $\geq$ 0.5) and only 4 headwater subbasins – 143, 145, 149, 150 had positive NSE values.

An analysis of percentage of months with zero mean monthly flow during the calibration and validation periods revealed that the three subbasins with acceptable model performance (subbasins 143, 149 and 150) had zero months of no flow during both time frames (Table 27). On the other hand, the 3 subbasins with poor model performance during validation (subbasins 3, 146 and 154) had larger number of months with no flow (Table 27) compared to the calibration period. Though subbasin 145 had 23% and 26% of months with no flow during calibration and validation, model performance for this subbasin was also acceptable (NSE = 0.37). A possible explanation for this could be that the mean annual flow generated from subbasin 145 was significantly larger than the

mean annual flow of subbasins 3, 16, 146 and 154 for which the model performed poorly. This result indicates that the model was a better predictor of streamflow in subbasins with – 1) perennial flows (143, 149, 150) and 2) large mean annual flows (> 60 mm/year).

Table 27. The percentage of months in observed and simulated monthly stream flow data that had no mean monthly flow during calibration (1995 - 2005) and validation (2008 - 2018) time frames. Monthly NSE and mean annual observed streamflow for calibration and validation time frames are also shown.

Subbasin	% of Months with Zero Mean Monthly Flow (Calibration)		% of Months with Zero Mean Monthly Flow (Validation)		NSE		Mean Annual Observed Flow (mm/year)	
	Observed	Simulated	Observed	Simulated	Cal	Val	Cal	Val
3	43%	0%	53%	0%	0.76	-0.17	15.0 + 24.7	5.6 + 8.8
16	32%	0%	14%	0%	-11.52	-29.57	8.9 + 15.1	12.1 + 13.3
143	0%	0%	0%	0%	0.77	0.49	99.0 + 74.6	71.5 + 34.6
145	23%	0%	26%	0%	0.43	0.37	92.6 + 132.6	60.7 + 68.2
146	8%	0%	50%	0%	0.24	-5.71	41.7 + 46.8	12.6 + 15.1
149	0%	0%	0%	0%	0.56	0.42	221.1 + 148.2	161.4 + 82.3
150	0%	0%	0%	0%	0.56	0.59	73.2 + 68.7	64.7 + 51.1
154	40%	0%	48%	0%	0.76	-0.38	13.8 + 24.4	7.0 + 11.4

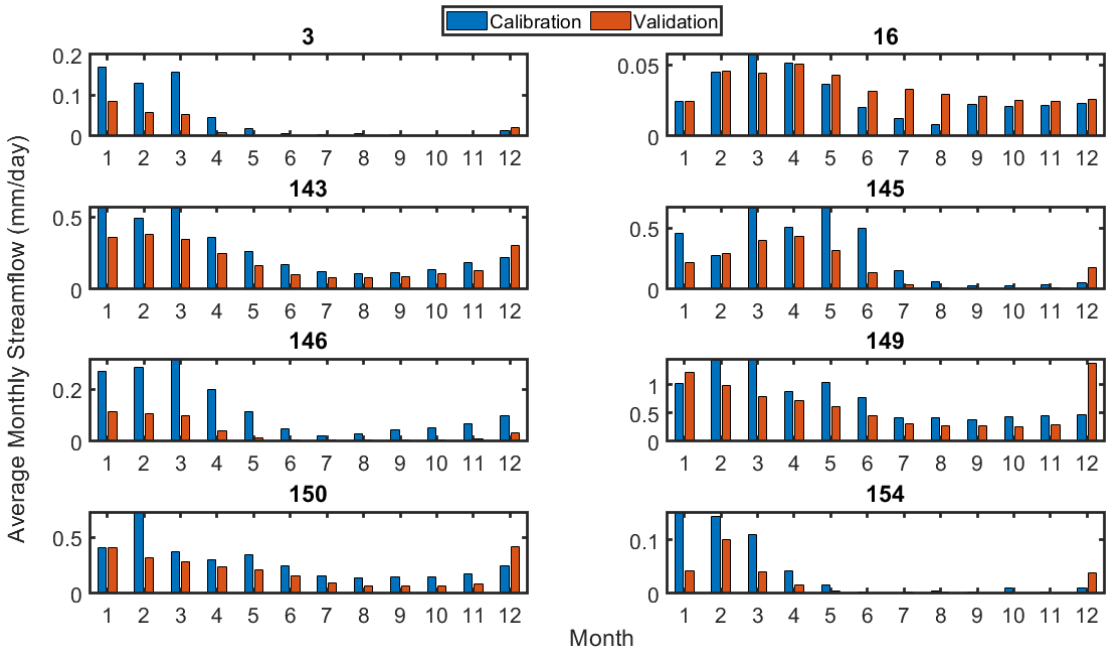

Figure 21.Observed mean monthly flows (mm/day) in 8 headwater subbasins for calibration and validation time frames. These values were obtained by averaging the mean monthly flow for a month across all years in the calibration or validation time frame.

Analysis of a subbasin's mean monthly flow computed across all simulation years for calibration and validation periods indicated that the model performed better when the mean monthly flows were comparable across calibration and validation time frames. In subbasins with poor model performance (3, 16, 146 and 150), large differences were observed between the mean monthly flows for the two time periods (Figure 21).

Model performance was further assessed using PBIAS, RMSE, and KGE (and its components R, RELVAR and BIAS) (Table 28). KGE values were greater than -0.41 for subbasins 143, 145, 149, and 150 indicating that the model was capturing the seasonality, timing, and magnitude of streamflow in these subbasins. In the rest of subbasins, poor performance is caused by large biases in mean and standard deviations of simulated flows.

The KGE value for subbasin 146 was -2.55 indicating poor model performance by overestimating peak and low flow conditions (Figure 27). Two questions arise with regard to model performance for subbasin 146 - 1) why model prediction failed for subbasin 146 which is clustered with subbasins 143, 145, 149 and 150 (Figure 22), and 2) why did the model perform better during calibration compared to validation? The mean annual flow generated in subbasin 146 (12.6 mm/year) is much lower than flow in subbasins 143, 145, 149 and 150 (60 – 161 mm/year). Additionally, 50% of mean monthly flow in the validation time frame was zero for subbasin 146, as compared to 0 months of no flow for subbasins 143, 149 and 150. The second question may be answered by noting the differences in the observed data between the calibration and validation periods for subbasin 146, where - 1) the number of months with no mean monthly flow during validation was 66 vs 10 during calibration (Table 27), and 2) there were large differences in flow magnitude during January-May of two time periods (Figure 21). The observed mean annual flow during calibration (42 mm/year) was also ~ 3 times larger than mean annual flow during validation (13 mm/year). However, the mean annual precipitation was comparable across the two time periods with 401 mm/year during calibration and 386 mm/year during validation. This discrepancy in mean annual streamflow during the two timeframes indicates the possibility of changes in hydrologic processes in the subbasin between calibration and validation time frames.

Table 28. Model evaluation criteria for 8 headwater subbasins during validation time frame (2008 - 2018).

SUBBASIN	NSE	PBIAS	RMSE	KGE	R	RELVAR	MEAN BIAS
3	-0.17	-175.47	2.38	-0.81	0.76	1.45	2.74
16	-29.57	-142.40	2.78	-3.82	0.23	5.54	2.42
143	0.49	24.26	0.43	0.66	0.81	1.15	0.76
145	0.37	11.02	1.55	0.47	0.61	0.66	0.89
146	-5.71	-302.26	0.38	-2.55	0.70	2.83	4.02
149	0.42	11.27	2.80	0.38	0.68	0.48	0.89
150	0.59	6.61	0.28	0.74	0.78	0.87	0.95

154	-0.38	-228.86	0.85	-1.33	0.61	1.15	3.29

Similar to the calibration period, a large bias in streamflow simulation was observed for subbasins 3, 154 and 16. The worst KGE of -3.82 was for subbasin 16. The model was unable to capture seasonality of flow (R = 0.23), overestimated the variance of simulated flow (RELVAR = 5.54) and overestimated the mean of simulated flow (BIAS = 2.42) for subbasin 16 (Figure 24).

The model often overestimated both peak flow and no-flow conditions in subbasin 3 (Figure 23). While it was able to capture the timing of peak flows for subbasin 3, it often simulated flow during no-flow months, resulting in a high RMSE value of 2.38 mm/day and overestimation of flows.

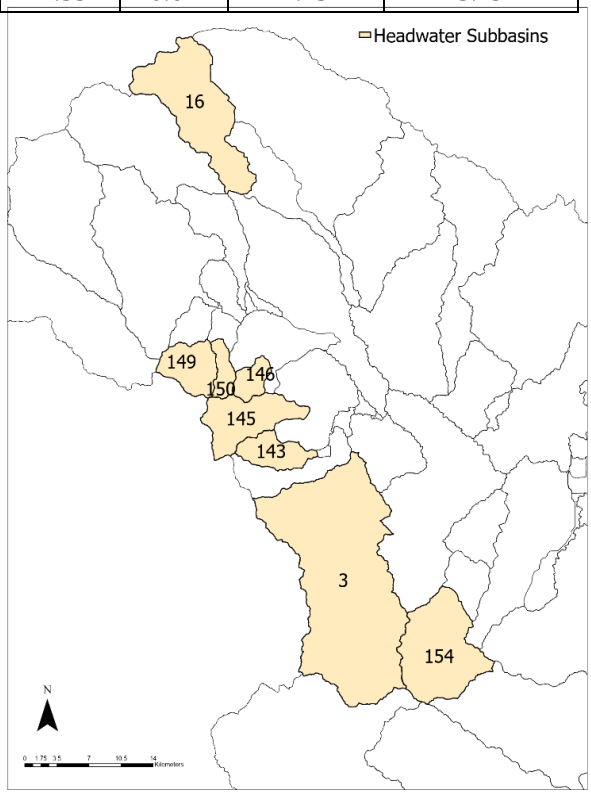

Figure 22. Location of the 8 headwater subbasins within the Salton Sea Watershed.

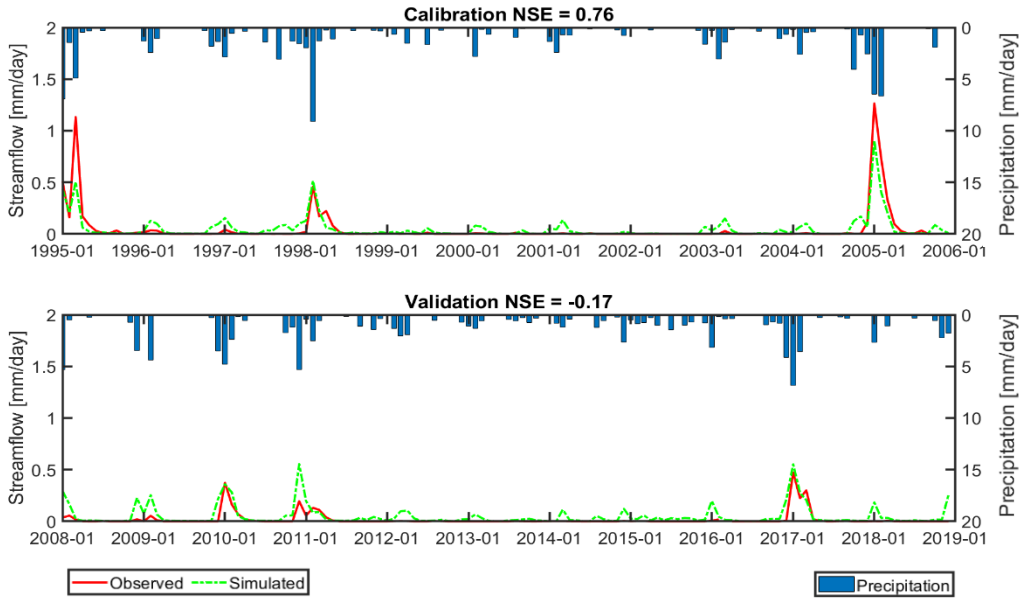

Figure 23. Subbasin 3 mean monthly streamflow (mm/day) – top: calibration (1995 - 2005) and bottom: validation (2008 - 2018).

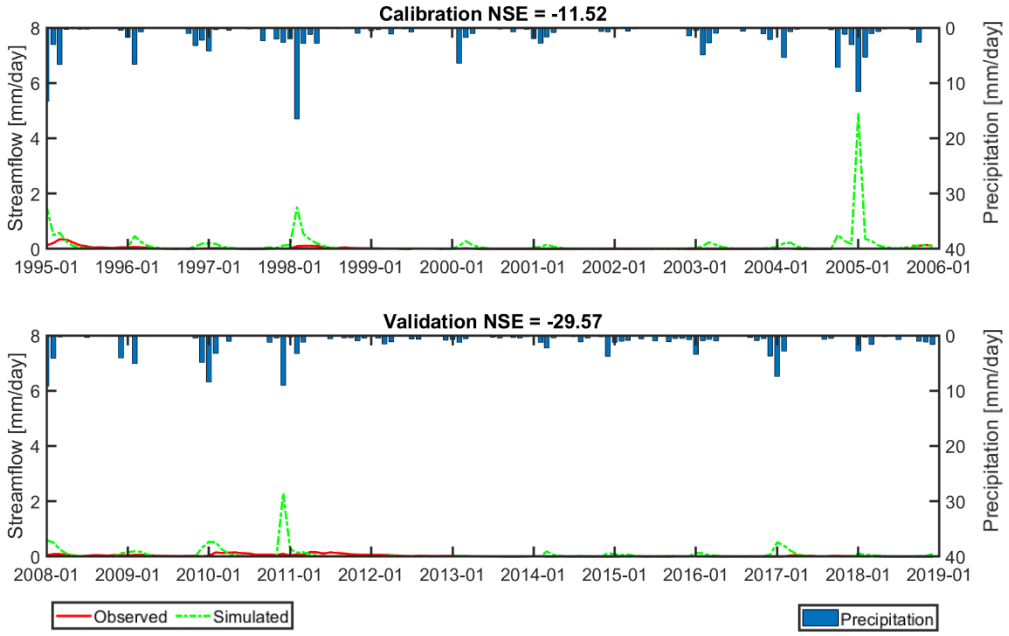

Figure 24. Subbasin 16 mean monthly streamflow (mm/day) – top: calibration (1995 - 2005) and bottom: validation (2008 - 2018).

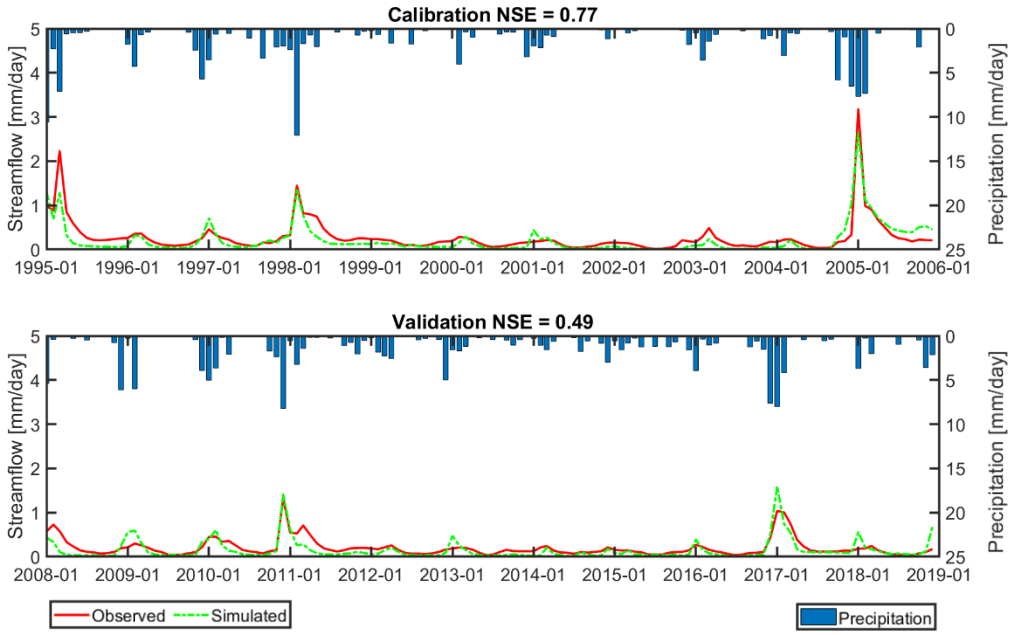

Figure 25. Subbasin 143 mean monthly streamflow (mm/day) – top: calibration (1995 - 2005) and bottom: validation (2008 - 2018).

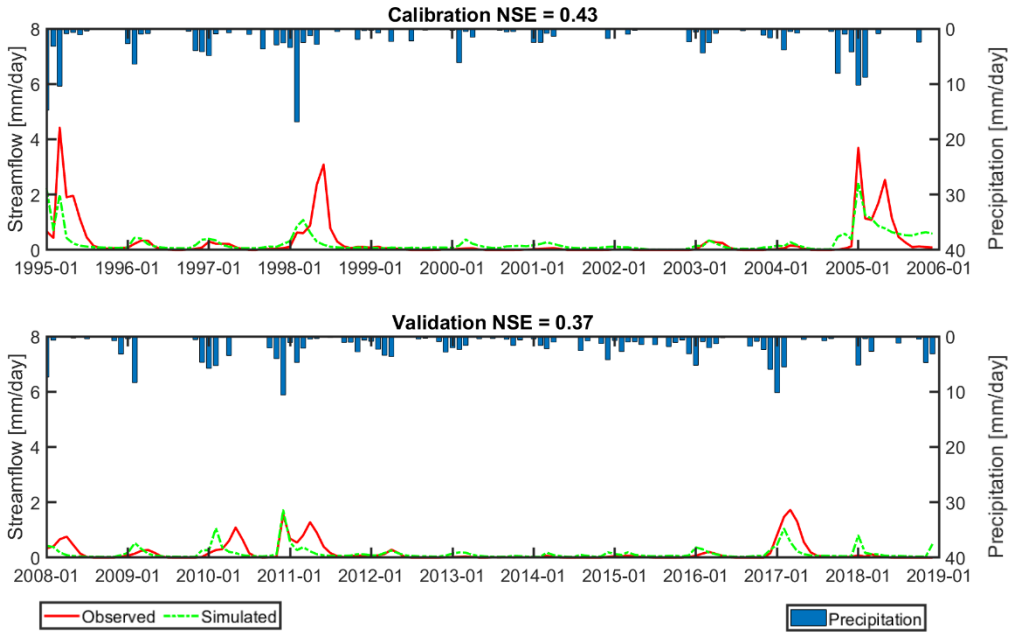

Figure 26. Subbasin 145 mean monthly streamflow (mm/day) – top: calibration (1995 - 2005) and bottom: validation (2008 - 2018).

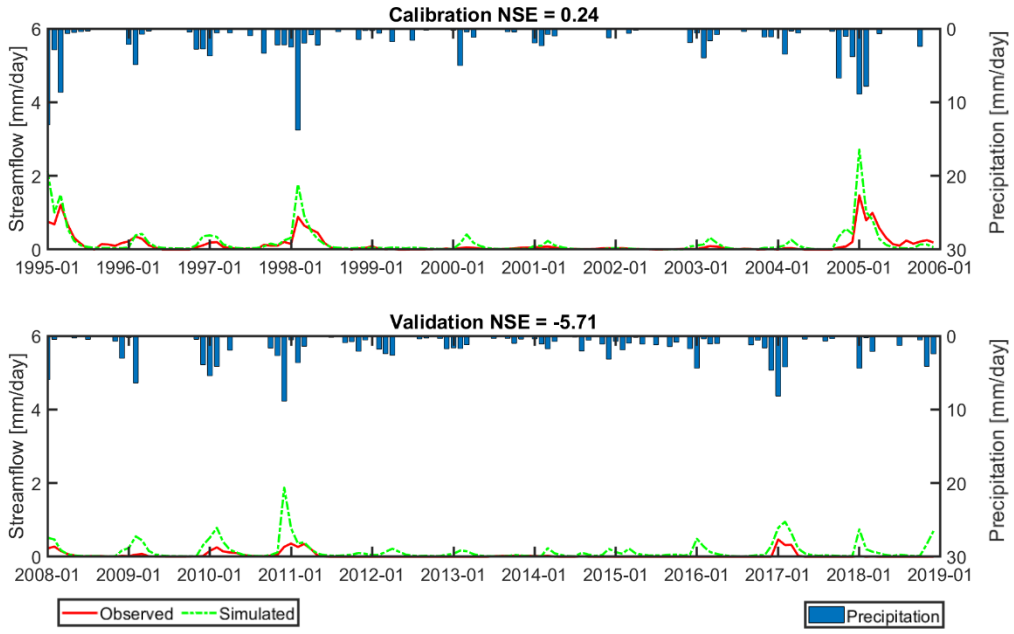

Figure 27. Subbasin 146 mean monthly streamflow (mm/day) – top: calibration (1995 - 2005) and bottom: validation (2008 - 2018).

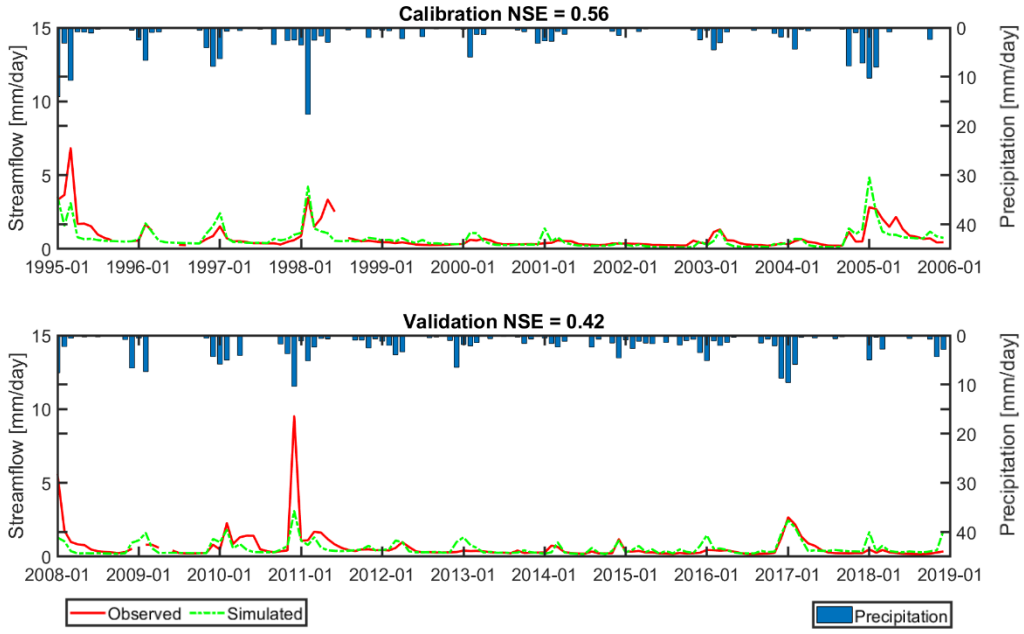

Figure 28. Subbasin 149 mean monthly streamflow (mm/day) – top: calibration (1995 - 2005) and bottom: validation (2008 - 2018).

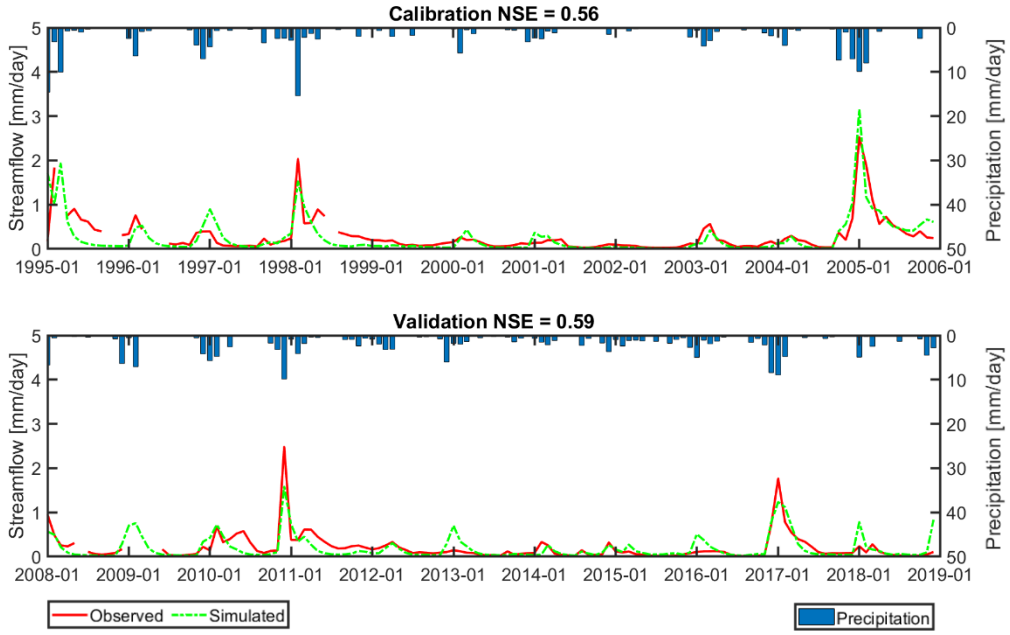

Figure 29. Subbasin 150 mean monthly streamflow (mm/day) – top: calibration (1995 - 2005) and bottom: validation (2008 - 2018).

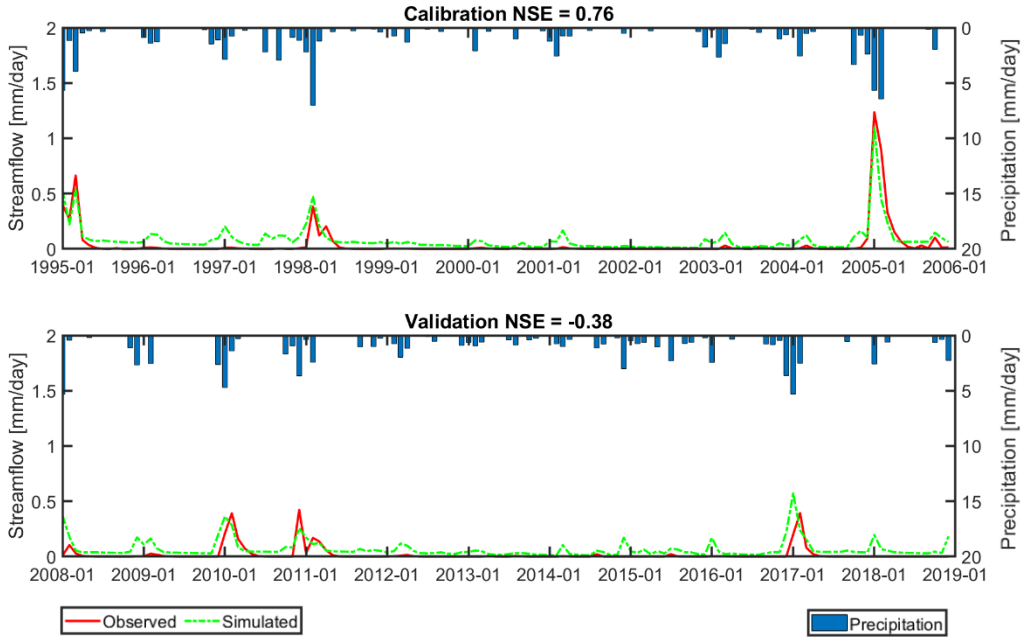

Figure 30. Subbasin 154 mean monthly streamflow (mm/day) – top: calibration (1995 - 2005) and bottom: validation (2008 - 2018).

3.1.4 Subbasins Water Balance

Precipitation is partitioned into three main fluxes – evapotranspiration, percolation from the bottom of root zone which eventually recharges the shallow aquifer, and water yield (streamflow) from the subbasin which is the sum of surface runoff, lateral runoff, and groundwater discharge to streams. Daily hydrologic fluxes were summed over the entire simulation period to obtain total hydrologic fluxes during calibration (1995 - 2005) and validation (2008 - 2018) periods. The percentage of total flux over total precipitation for calibration and validation time frames was quantified to understand flux partitioning in the headwater subbasins (**Error! Reference source not found.**). T he water balance of subbasin 3, 154, 145 and 16 is not discussed in this analysis due to poor model performance in these subbasins.

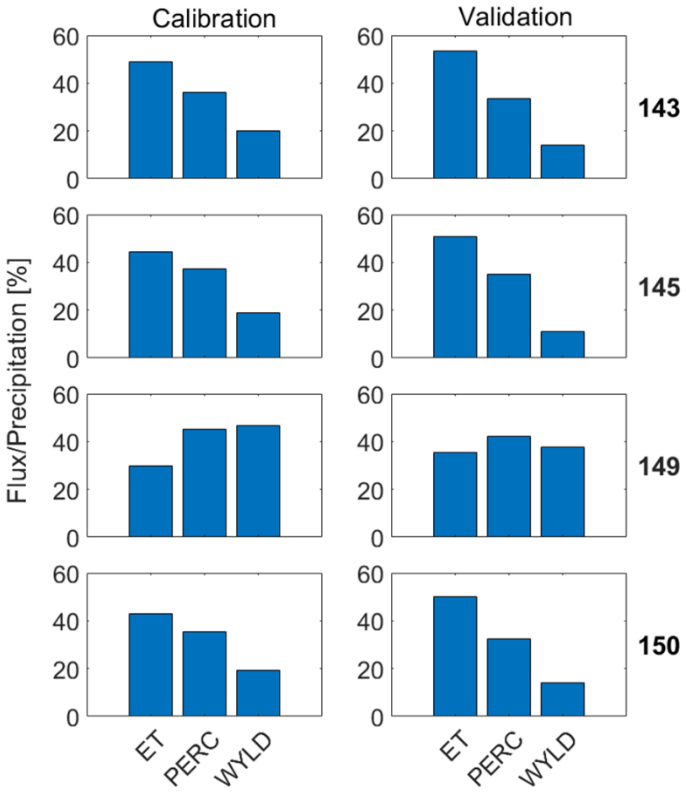

Figure 31. Flux partitioning during calibration and validation time frames in 4 headwater subbasins with acceptable model performance. Evapotranspiration (ET), Percolation (PERC) and Water Yield (WYLD) were calculated as a percentage of total precipitation in the subbasin.

The headwater subbasins considered in this analysis contribute flow to tributaries of the Whitewater River, and it is important to understand flow contribution from these subbasins to the Whitewater River and potentially to the Salton Sea. The calibrated model was used to identify streamflow generation or water yield (WYLD) from headwater subbasins. It was found that subbasin 149 generated maximum mean annual streamflow (WYLD) in both calibration and validation periods (Figure 32). This result is attributed to the fact that mean annual precipitation in subbasin 149 was the largest during both calibration and validation periods. An analysis of the percent total flux over total precipitation indicated that the dominant flux for subbasin 149 oscillated between water yield and percolation (**Error! Reference source not found.**).

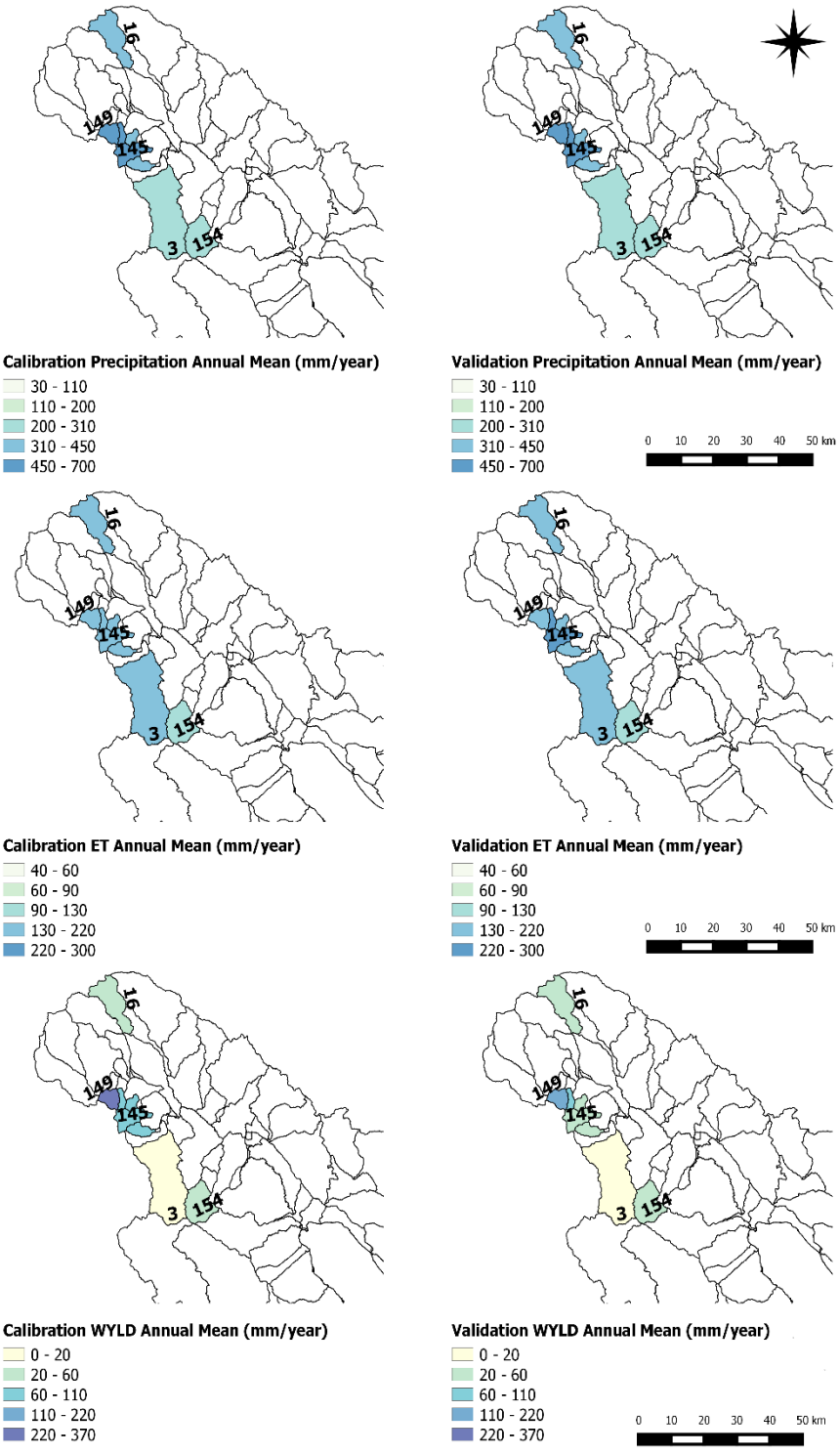

Figure 32. Mean annual precipitation (top panel), evapotranspiration (middle panel) and water yield (bottom panel) estimates from headwater subbasins during calibration (1995-2005) and validation (2008 - 2018) time periods.

Water budget partitioning indicated that subbasin 149 generated streamflow even during drier years (calibration: 1999 and 2002; validation: 2013). Total annual water yield (mm/year) for subbasin 149 was broken down to three main constituents – surface runoff (SURQ mm/year), lateral flow (mm/year) and groundwater discharge (mm/year) (**Error! Reference source not found.**). It was f ound that streamflow generation (water yield) was sustained primarily by lateral flow and groundwater discharge during calibration and by lateral flow during validation years. Subbasin 149 is spatially contiguous with subbasins 143, 146 and 150, all of which receive comparable mean annual precipitation to subbasin 149. Unlike subbasin 149, the dominant flux for subbasins 143, 146 and 150 were evapotranspiration (calibration: 43-53% and validation: 50-55%), followed by percolation (calibration: 32-47% and validation: 29-39%) during both calibration and validation periods. This result is expected for semi-arid watersheds. While flux partitioning in these 3 subbasins differed from subbasin 149, streamflow generation in these subbasins was similar to that of subbasin 149, with high lateral flow contribution to streamflow from subbasins 150, 146, and 143.

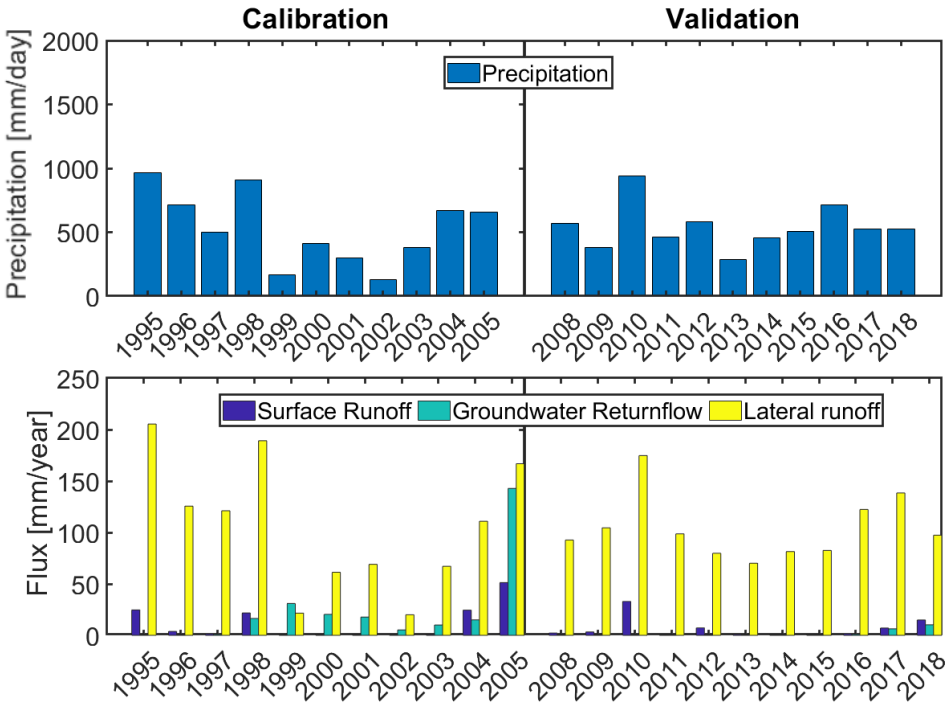

Figure 33. Streamflow generation in subbasin 149. Top Panel: total annual precipitation. Bottom Panel: total annual surface runoff, groundwater return flow and lateral runoff flow.

3.2 Calibration Phase 2: Agricultural Subbasins

3.2.1 Calibration

Thirteen subbasins with agriculture land cover were identified in the Imperial Irrigation District (IID) that drain to the Salton Sea. Observed streamflow from USGS Gages at New River (reach 133) and Alamo River (reach 98) were used to assess model performance for agricultural subbasins. Colorado River inflows were input to the system at the AAC (reach 86) and then transferred to East Highline (reach 126, 113 and 20), Central Main (reach 14) and Westside Main (reach 124, 135, 129, and 49) canals. As no data is available on cropping patterns and irrigation rates in Mexicali Valley, inflows to the New River from Mexico were specified as a boundary condition for the model at reach 87 using data from USGS gage 10254970. Reach 87 is the last section of the New River before it enters IID. Therefore, specifying inflows at reach 87 captured the inflows to New

River from Mexico. Initial manual calibration of the agricultural subbasins was conducted on a daily time step, followed by automatic calibration on a monthly time step. The uncalibrated model (default model) for these agricultural subbasins had unsatisfactory model performance with daily NSE of -612.52 and -131.60 for the New River (133) and Alamo River (98), respectively. It was observed that simulated flows were much larger than observed flows with a PBIAS of 405% and 197% for New River and Alamo River, respectively. High flows were attributed to the large value of the surface runoff ratio parameter (ASQ). ASQ is the ratio of applied irrigation water that leaves as surface runoff. Sensitivity analysis of model performance to the surface runoff parameter (ASQ) indicated that model performance improved significantly when ASQ was reduced from the default value (Table 30). Reducing ASQ reduced surface runoff losses from irrigation and reduced streamflow, respectively. While model performance continued to improve with a reduction of ASQ, it was decided that an ASQ value of 0.35 was reasonable and was selected as the calibrated ASQ value for 12 subbasins. The exception was for subbasin 14, where the ASQ value was lowered to 0.10 as this subbasin drains to Central Canal (reach 14) (Figure 19). This exception was made as the Central Canal is mainly used for distributing surface irrigation water rather than a drainage system for irrigated water.

Table 29. Model performance as indicated by the NSE of simulated flows at Alamo and New Rivers for different surface runoff ratio (ASQ) parameter values during the calibration time period (1995 - 2005).

Subbasin	**ASQ 0.86**	**ASQ 0.30**	**ASQ 0.20**	**ASQ 0.25**	**ASQ 0.30**	**ASQ 0.35**	**ASQ 0.40**
Alamo River (98)	-131.60	-9.78	-8.05	-6.34	-4.67	-3.12	-1.95
New River (133)	-612.52	-8.35	-7.61	-6.72	-5.54	-4.43	-3.20

We then conducted manual calibration to find the optimal transfer ratios to the Central Main canal (reach 14) by varying the transfer ratio from the AAC. It was found that the best model performance was achieved at 25% transfer rate (Table 30).

Table 30. Model performance as indicated by the NSE of simulated flows at Alamo and New Rivers with respect to different transfer ratios from the AAC to the Central Canal (reach 14).

Subbasin	15% transfer	20% transfer	25% transfer	30% transfer
Alamo River (98)	-3.12	-2.47	-2.08	-2.48
New River (133)	-4.43	-4.42	-4.54	-4.61

Drains from the West Main canal carry water from surrounding areas to the New River. We added a transfer function from the West Main canal (reach 49) to the New River (reach 133) to capture these drainage flows. We varied the transfer ratios between 0–30% and assessed model performance by calculating NSE at the New River and Alamo River gages. It was found that model performance improved with increasing transfers from West Canal (Table 31). However, we selected a 15% transfer ratio for the automatic calibration method, as New River has water through the entire reach, and we did not want to reduce streamflow contributions from irrigated subbasins during automatic calibration.

Table 31. Model performance as indicated by the NSE of simulated flows at Alamo and New Rivers with respect to transfer ratio from West Main Canal (reach 49) to New River (reach 133).

Subbasin	0% transfer	5% transfer	10% transfer	15% transfer
Alamo River (98)	-2.08	-2.08	-2.08	-2.08
New River (133)	-4.54	-3.30	-2.42	-1.40

After identifying transfer ratio of AAC to Central Canal, West Canal to New River and ASQ values for the subbasins; the model was automatically calibrated on a monthly basis using SWAT-CUP SUFI-2 software. Values for 4 parameters (surface runoff lag coefficient, baseflow recession constant, channel hydraulic conductivity and baseflow alpha factor for bank storage) were replaced by a value within a given parameter range. Values for soil hydraulic conductivity were changed relative to input value in the soil database. The model was calibrated for 1 iteration consisting of 500 simulations.

Table 32. Default and calibrated parameter values after automatic calibration in SWAT-CUP using SUFI-2 optimization algorithm. Alamo drainage area consists of subbasins - 14, 20, 98, 99, 113, 114, 126 and New River drainage area consists of - 49, 122, 124, 129, 133, 100 subbasins. The prefix "V_" indicates that the parameter values was replaced within a specified range. The prefix "R_" indicates that the parameter was changed relative to its initial value.

Parameter	Default Values	Calibrated Values	
		Alamo Drainage	New River Drainage
V_SURLAG	2	4.47	4.64
V_ALPHABF	0.048 (1/days)	0.65	0.44
V_CHK2	0 (mm/hr)	39.57	37.91
V_ALPHABNK	0 (days)	0.55	0.85
R_SOLK	3.3 – 331 (mm/hr)	0.46*	0.18*

***** *This value indicates the factor by which the initial parameter value was changed, with change factor = 1+value.*

Parameter values identified from automatic calibration resulted in a monthly NSE of -0.48 for Alamo River (reach 98) and -1.05 for New River (reach 133). Results from the calibrated model indicated a lag and underestimation of flow in both New and Alamo Rivers. Two potential causes for this were identified as:

1) Under application of irrigation in subbasins within the drainage area of Alamo River. There were days where flows out of Central Canal (reach 14) were zero, resulting in insufficient water for irrigation. Increasing the transfer from 25% to 30% increased the NSE for Alamo River to 0.03 by reducing the number of days that flow out of Central Canal was zero.
2) Underrepresentation of drainage flow from West Canal to New River. The transfer ratio was increased from 15% to 25% resulting in an increase of -1.05 to -0.19.

Table 33. Final model performance metrics for agricultural subbasins during calibration (1995-2005).

Subbasin	NSE	PBIAS	RMSE (m^3/s)	KGE	R	RELVAR	MEAN BIAS
Alamo River (98)	0.03	8.86	48.72	0.52	0.81	1.43	0.91
New River (133)	-0.19	13.95	32.91	0.77	0.88	1.14	0.86

Final model NSE for New River was unsatisfactory (monthly NSE < 0) and NSE for Alamo River was only slightly better (Table 33). The model underpredicted flow in both rivers with PBIAS of

9% for Alamo River and 14% for New River. Final model performance was also assessed using the KGE metric which evaluates model performance by accounting for linear correlation between observed and simulated data, variability bias and mean bias. The KGE metric for both reaches in the final model were acceptable. Correlation between observed and simulated data for both New and Alamo Rivers was high at 0.88 and 0.81, respectively. The bias in mean simulated and observed flow were relatively low for both reaches (MEAN BIAS of 0.86 and 0.91 for New River and Alamo River, respectively). However, the model overestimated variability in stream flow for both reaches with REL VAR of 1.14 for New River and REL VAR of 1.43 for Alamo River.

3.2.2 Validation

The calibrated model was run on a monthly time step for the Validation time frame between 2008 and 2018, with 5 years of warm up between 2003 and 2008. NSE for both New and Alamo Rivers was reduced from the calibration period. The percent bias in simulated flows for Alamo River was similar for calibration (8.9%) and validation (8.6%) periods (Figure 34). The bias in simulated New River flows increased significantly from calibration (14%) to validation period (25%). An assessment of the KGE metrics indicated that model performance improved for Alamo (reach 98) from the calibration (0.52) to validation time frame (0.60) (Figure 34), and for the New River decreased from the calibration (0.77) to validation time frame (0.52) (Figure 35).

Table 34. Model performance metrics for agricultural subbasins during validation (2008-2018).

Subbasin	NSE	PBIAS	RMSE	KGE	R	RELVAR	Mean BIAS
Alamo River (98)	0.00	8.57	46.29	0.60	0.73	1.29	0.91
New River (133)	-1.85	24.61	50.76	0.52	0.60	0.90	0.75

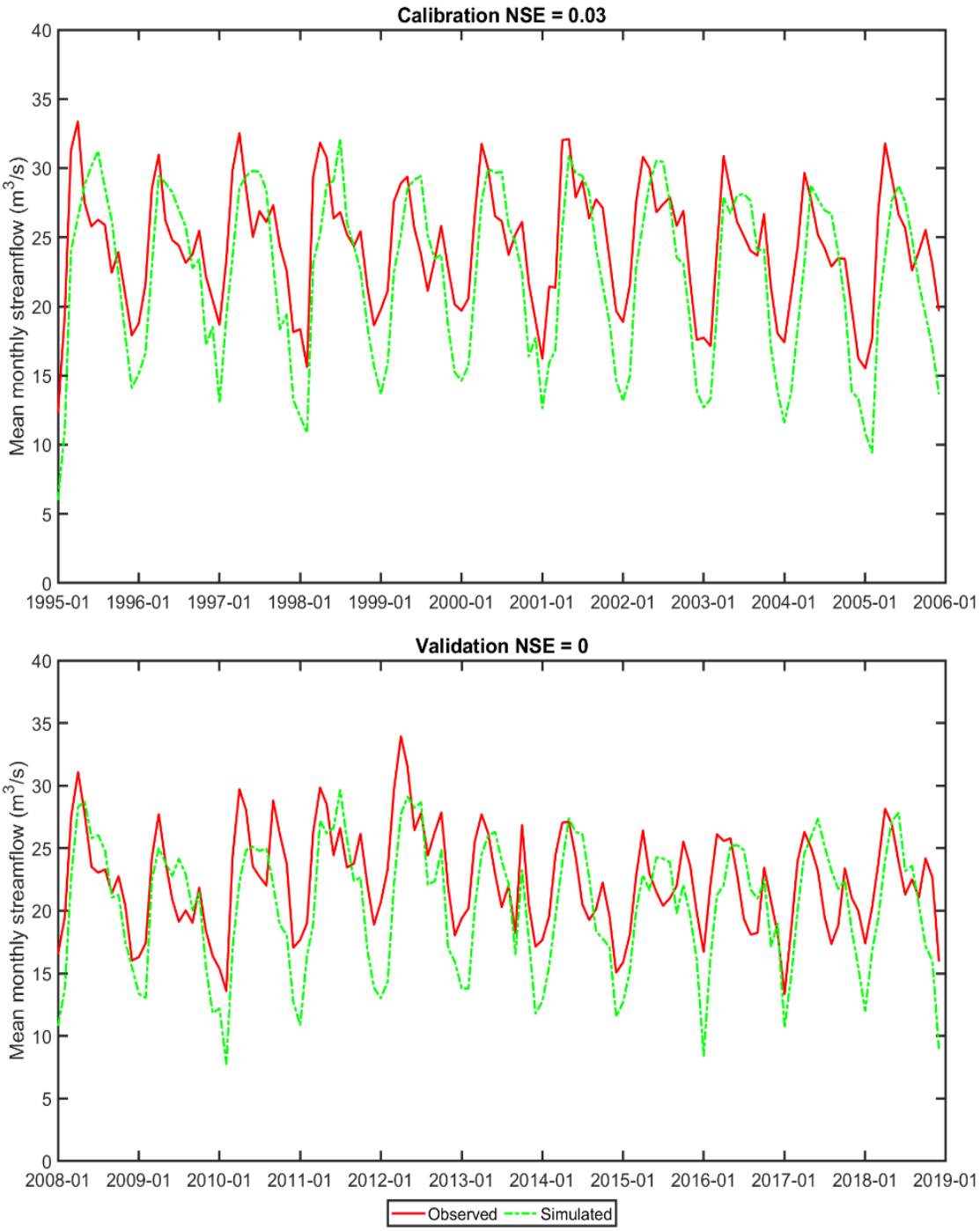

Figure 34. Alamo River (reach 98) mean monthly streamflow (mm/day) – Top Panel: calibration (1995 - 2005) and Bottom Panel: validation (2008 - 2018).

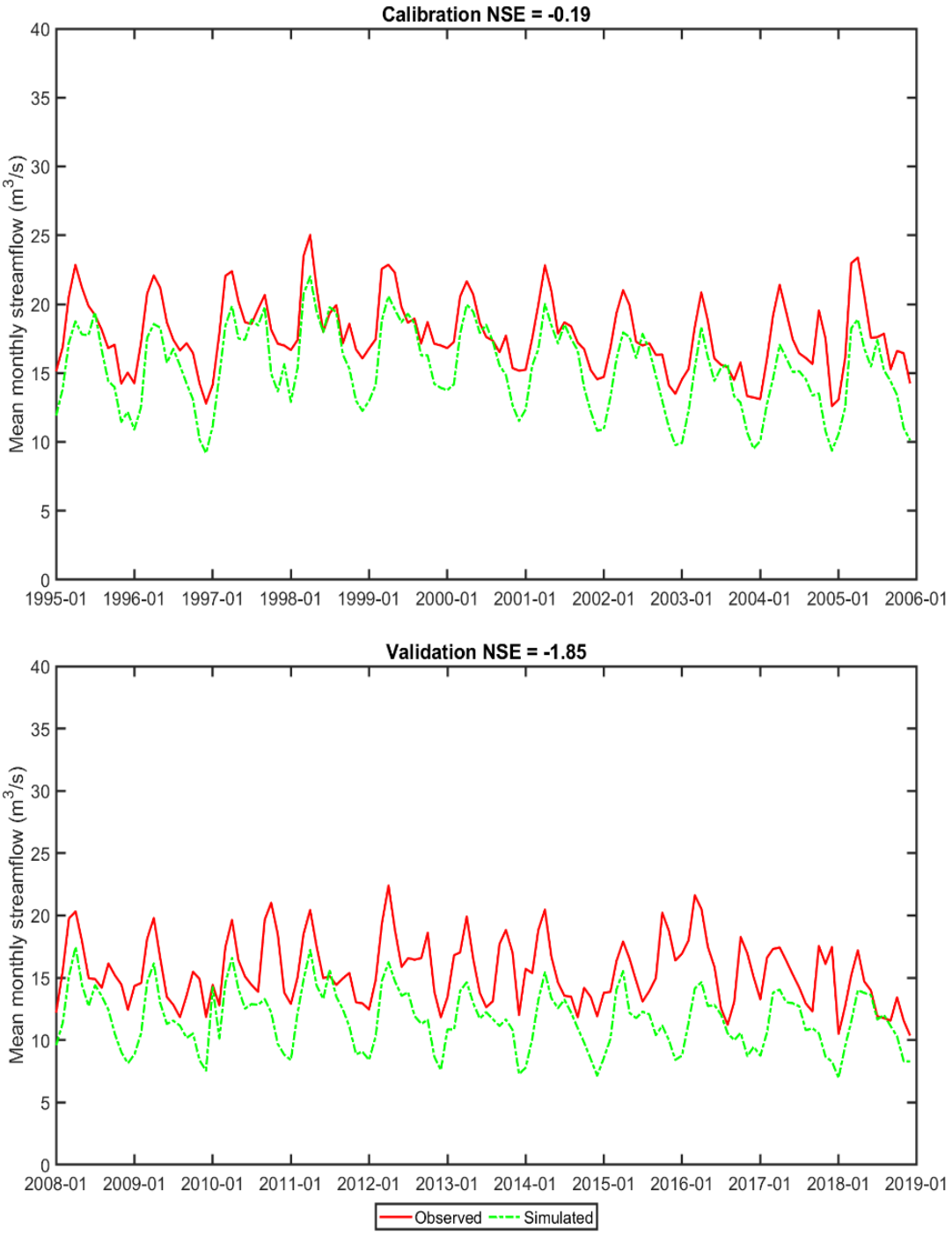

Figure 35. New River (reach 133) mean monthly streamflow (mm/day) – Top Panel: calibration (1995 - 2005) and Bottom Panel: validation (2008 - 2018).

Evapotranspiration was the dominant hydrologic flux within the 13 subbasins in IID, where it varied between 70% to 99% of applied irrigation and precipitation in the IID subbasins. The mean annual evapotranspiration rates (mm/year) were quantified for four major CFTs (Alfalfa, Bermuda grass, Small Grains and Field grains) that covered more than 90% of the agricultural area in IID (Table 20). These ET rates were compared to an independent dataset generated by the Bureau of Reclamation (BOR) for the Lower Colorado Region (BOR, 2014). It was found that these ET rates were comparable across the two datasets, with the SWAT model underestimating ET for Alfalfa, Bermuda and Field Grains and overestimating ET for Small Grains (Table 35).

Table 35. Mean annual evapotranspiration from 4 major Crop Functional Types (CFTs) in the IID region - Alfalfa, Bermuda Grass, Small Grains and Field Grains.

Crop	BOR (mm/year)	Calibration (mm/year)	Validation (mm/year)
Alfalfa	1561.34	1327.7	1212.52
Bermuda	1325.71	1063.59	966.95
Small grains	595.75	698.5	657.94
Field grains	884.74	732.24	681.74

3.2.3 Colorado River Inflow Scenarios

The calibrated model was run with three scenarios, where climatic forcings, land use, irrigation operations were kept constant, but Colorado River inflows to the IID were changed. This model was run for between 1995 and 2016, with 5 years of warmup between 1990 and 1995.

1) Baseline Model: this model was run with observed inflows from the AAC. The total inflow between 1995 and 2016 was 8.74E+10 (m^3) with a mean annual flow of 3.97E+09 m^3.
2) Scenario1: this model was run with the 1997 AAC data. This year had the maximum annual flow for the time period 1980 – 2018. The total inflow between 1995 and 2016 was 9.49E+10 (m^3), about 8.6% larger than the baseline. The mean annual flow for the 22 years was 4.31E+09 m^3.

3) Scenario 2: this model was run with the 1983 AAC data. This year had the minimum annual flow during the time period 1980 – 2018. The total inflow between 1995 and 2016 was 7.78E+10 (m^3), about 22% smaller than the baseline. The mean annual flow for the 22 years was 3.54E+09 m^3.

The relative change in the New River and Alamo River flows from the baseline scenario was calculated for scenario 1 and 2. It was observed that Alamo River flows were more sensitive to changes in inflows from the AAC, with larger changes observed in Alamo River flows for both scenarios (Table 36). We analyzed the change in total volumetric evapotranspiration flux and applied irrigation in the IID subbasins for all three scenarios. The total volumetric flux was calculated as the sum of monthly flux (m^3/month) for 13 subbasins in IID across all 22 years in each scenario. Results indicate that both fluxes had relatively small changes compared to the baseline (Table 36). As a result, despite a 15% decrease in the Colorado River inflow (Scenario 2), there was enough water in the canals to sustain the same level of irrigation as during the baseline scenario.

Table 36. Relative change in total flow out of Alamo and New Rivers for Scenario 1 and 2 with respect to flows in the Baseline scenario.

Scenario	AAC flow (86)	Alamo River (98)	New River (133)	Evapotranspiration	Irrigation
1 – Maximum flow	8.6%	7.4%	6.7%	1.0%	1.3%
2 – Minimum flow	-11.0%	-10.1%	-8.7%	-2.8%	-2.9%

This result raises the question as to why differences in Alamo and New Rivers are larger than changes in applied irrigation and evapotranspiration? Monthly flow (m^3/month) at the Colorado River inflow point at AAC (reach 86), Alamo (reach 98) and New Rivers (reach 133), were averaged for the months across all 22 simulation years for each scenario, and changes from the baseline scenario were calculated. This analysis revealed that the large changes observed at both

Alamo and New Rivers corresponded directly with seasonal changes in the Colorado River inflows (**Error! Reference source not found.**). It was observed that the largest changes occurred in F ebruary and March. This could be reflective of - 1) upstream management decisions with regards to reservoir releases or 2) climatological forcings that impact the availability of water in the Colorado River.

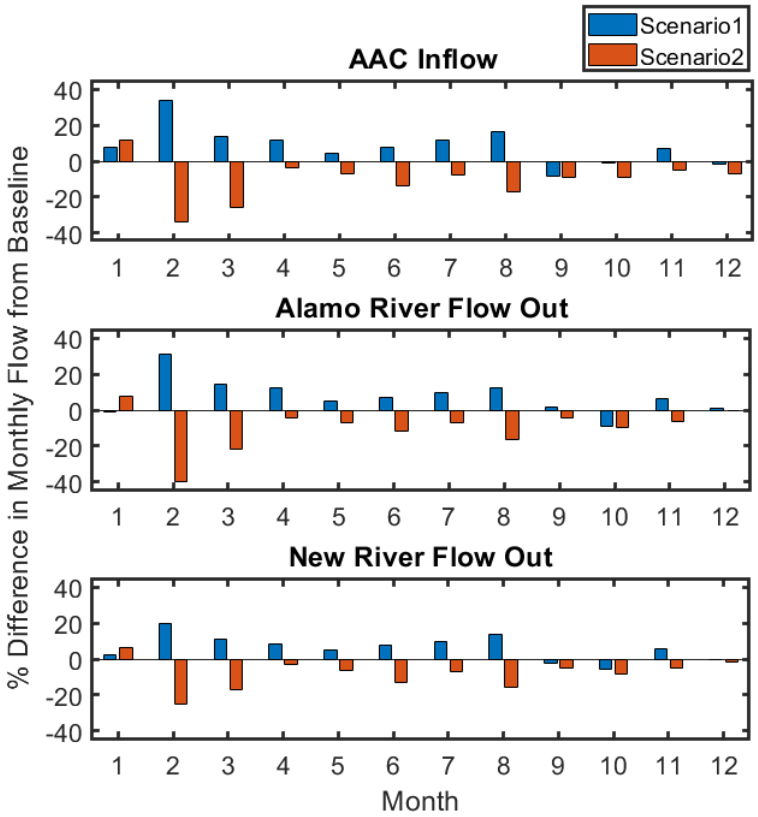

Figure 36. The percent difference in mean monthly flow across entire simulation time period for Scenario 1 and Scenario 2 from the Baseline Scenario. Top Panel: Percent difference in Colorado River inflows at AAC; Middle Panel: Percent difference in Alamo River flow; Bottom panel: Percent difference in New River flow.

4. DISCUSSION

This project demonstrates the application of a semi-distributed, process based hydrologic model for an irrigated, topographically closed watershed in Southern California. The Salton Sea Watershed is a highly managed, arid watershed, where all drainages are routed to the centrally

located terminal lake - the Salton Sea. Simulating hydrologic processes in this large arid watershed is challenging given the high topographic variability with elevation ranging from -87 m to 3498 m, diversity of agricultural crops and extensive canal networks distributing Colorado River water across the watershed. The SWAT model was chosen as the modeling platform given the flexibility that it provides in simulating irrigation practices, reservoirs, and crop growth. SWAT discretizes a watershed to Hydrologic Response Unit's (HRUs) based on the unique combinations of land use, soil, and slope. While delineating HRUs reduces computational time of large-scale watershed simulations, application of SWAT in large watersheds is still computationally expensive. We formulated a new methodology to capture the topographic variability within the watershed while reducing the computational time by conducting a series of sensitivity analysis to assess accuracy of watershed scale fluxes to the number of HRUs discretized based on number of slope classes, and area thresholds for HRU delineation. This methodology successfully determined the optimum number of HRUs that captured spatial variability in hydrologic response, while minimizing computational time.

Following HRU discretization and final model setup to incorporate Salton Sea and canal networks, we implemented a two-step calibration strategy by using observed streamflow data to calibrate the SWAT model for two distinct hydrologic systems within the watershed: 8 undisturbed headwater subbasins in mountain ranges, and 13 agricultural subbasins in the Imperial Irrigation District in the southern part of the watershed.

Model performance in undisturbed headwater subbasins: We applied two approaches to calibrate the 8 headwater subbasins. While the relative parameter change approach is advised to maintain spatial variability of model parameters, this approach did not result in satisfactory model performance (NSE $\geq$ 0.5) for 7 out of the 8 headwater subbasins after 6 successive iterations consisting of a total of 2400 model simulations (Table 22). While model performance was improved

from the default parameter values, the SUFI-2 optimization algorithm was unable to find optimum parameter sets for 7 out of 8 headwater subbasins. This result suggests that the initial parameter values from national soil and land cover databases were incorrect and perhaps more iterations are needed to improve model performance and uncertainty quantification. The relative change method utilizes this initial value of 4 parameters (in our case) as a starting point, and then changes the parameter's value relative to its initial value within a user defined range. Thus, the accuracy of the initial value can significantly impact the optimization algorithm performance. We utilized State Soil Geographic Database (STATSGO2) as the soil spatial layer and database for the American portion of the watershed. This database is a broad inventory of soils and non-soil areas that occur in a repeatable pattern over the landscape at a scale of 250 m (NRCS). The database consists of features that were created by generalizing and extrapolating more detailed soil maps. This could lead to simplification and misrepresentation of soil properties in mountainous areas and areas with lower frequency of soil surveys. In future work, this limitation can be overcome by using alternative datasets such as the finer resolution (30 m x 30 m) POLARIS (Chaney et al., 2019) dataset.

The second calibration approach in the 8 headwater subbasins replaced the values of all 15 parameters within specified ranges and had improved model performance. This approach was applied over 7 iterations with 400 simulations each, consisting of a total of 2800 simulations. The model performance was satisfactory for 4 of the 8 headwater subbasins. The 4 subbasins for which the model performed well had perennial flows and large mean annual flows (> 60 mm/year). These findings are consistent with results of other studies that reported difficulty in achieving satisfactory SWAT simulations for low flow conditions (Cibin et al., 2010; Liew & Garbrecht, 2003; Sudheer et al., 2007).

A limitation of our calibration approach was that all 8 subbasins were lumped into one category for which calibration was conducted simultaneously. However, the best parameter sets for different

subbasins are obtained from different simulations and spatial heterogeneity is still maintained. The replace parameter approach could be improved by first classifying subbasins based on subbasin level characteristics such as precipitation forcing, land cover and streamflow dynamics, and then calibrating each group based on similarity in subbasin level properties. This principle was demonstrated in calibration results where model performance was satisfactory only for the 4 headwater subbasins with similar hydrologic regimes. Cibin et al. (2010) demonstrated that different parameters are sensitive to different hydrologic regimes. They found that SURLAG was more sensitive to high flow regimes and CN2 was more sensitive to low flow regimes (Cibin et al., 2010). Therefore, by identifying clusters of subbasins, we could further refine subbasin parameterization by targeting parameters, and parameter ranges with sensitivity to specific flow regimes. This strategy can preserve spatial variability while maintaining computational efficiency.

Model performance in agricultural subbasins: Thirteen agricultural subbasins in the heavily irrigated Imperial Irrigation District (IID) were calibrated through a combination of manual and automated calibration techniques. Model calibration was conducted using observed streamflow from two USGS gages on two major rivers draining IID – Alamo River and New River. Model performance based on NSE of monthly flows was not satisfactory for either of the rivers. However, the performance was still better than default parameter values. An analysis of the KGE metric and its components (linear correlation, bias in variability and bias in mean), indicated that model predictions had high linear correlations with observed streamflow and the main discrepancy in model predictions was from large variability in model simulations. Due to lack of data on irrigation transfers, we applied a manual calibration approach where we assessed model performance (based on NSE) to varying levels of irrigation transfers and identified the best performing transfer ratio from AAC to major canals. We also used manual calibration to identify the best performing surface runoff ratio (ASQ) parameter, which determines the amount of applied irrigation that leaves as

surface runoff. A major limitation of this manual calibration approach was that it was conducted for one parameter at a time, and hence, ignored parameter interactions. Another limitation was that the SWAT model does not distinguish between different types of irrigation (for example, drip vs flood), and hence this information was not incorporated in the model.

We assessed the impacts of changes in Colorado River inflows by designing two scenarios. In scenario 1, inflows were 9% greater than the baseline model. In scenario 2, Colorado River inflows were 11% less than the baseline model. It was observed that while both rivers responded to changes in inflows, this response was a direct consequence of seasonal fluctuations of inflows, and differences in volumetric evapotranspiration and applied irrigation were relatively small. This result indicates that even with reduced flows, there is enough water in the system to support irrigation and plant growth at the baseline scenario levels. This finding demonstrates the application of such a model for water management in the region.

A major limitation of the overall calibration approach applied to both headwater and agricultural subbasins was that it was a single-objective calibration approach, where NSE was utilized as the sole performance metric to improve model predictions. The NSE metric has several limitations, including high sensitivity to extreme flows, and may not be the best metric to judge model performance in ephemeral streams with flashy streamflow events. The use of multiple objective functions can strengthen calibration by stressing on different performance metrics such as correlation and bias. Additionally, only streamflow was utilized to calibrate the model. Streamflow is the result of climatological forcings and multiple inter-connected processes occurring on the soil surface and subsurface. By utilizing only streamflow, we ignore other important fluxes (such as evapotranspiration) and state variables (soil moisture) that regulate streamflow. Therefore, a suggested improvement to this approach would be to utilize multiple objective functions based on remotely sensed evapotranspiration and soil moisture products.

5. CONCLUSION AND FUTURE WORK

A semi-distributed model was developed for the Salton Sea watershed in southern California and northern Mexico. Model calibration was conducted using observed streamflow for two distinct systems in the watershed – 1) undisturbed headwater subbasins in the mountainous regions, and 2) agricultural subbasins in the southern part of the watershed. Automatic calibration was conducted for 8 headwater subbasins using SWAT-CUP calibration software, and the SUFI-2 optimization algorithm. Literature review was used to identify 15 most commonly used parameters, and one-at-a time sensitivity analysis was used to identify initial parameter ranges for calibration. Calibration was conducted on a monthly basis using NSE as the objective function using two approaches. The first approach changed the values of 4 spatially distributed parameters (Curve Number, Alpha Baseflow, Soil Hydraulic Conductivity, and Soil Available Water Capacity) relative to their initial values, while replacing the values of the remaining parameters from within specified ranges. This relative parameter change approach was unable to find optimal parameter sets for 7 out of 8 headwater subbasins after 2400 model calibration simulations. This result indicated inaccuracy of initial parameter values.

The second calibration approach replaced the values of 15 parameters within specified ranges using monthly streamflow simulations. Optimum parameter sets were identified for each subbasin out of 2800 model simulations. Model performance was satisfactory for 4 out of 8 headwater subbasins during both calibration and validation time frames. It was found that model performance in headwater subbasins was strongly influenced by hydrologic flow regime, where model performance was satisfactory for the 4 subbasins with perennial flows and large mean annual flows (> 60 mm/year).

Model performance in 13 subbasins in the heavily irrigated Imperial Irrigation District (IID) in the southern portion of the watershed was quantified using observed streamflow from the two major

rivers that drain IID – Alamo and New Rivers. A combination of manual and automatic calibration was used to improve model performance. Manual calibration was used to identify optimal value of surface runoff ratio (ASQ) parameter and transfer ratio from the All-American Canal (AAC) to Central and Westside Main canals. Following this approach, the model was calibrated automatically on a monthly time step using SWAT-CUP SUFI-2 optimization algorithm for 1 calibration iteration consisting of 500 simulations. Model performance based on NSE was not satisfactory for both calibration and validation time frames. An analysis of KGE and its components revealed that this discrepancy in model performance came from large bias in simulated flow variability for the Alamo River, and underprediction of flows and low correlation in flows for the New River.

The calibrated model was run for 22 years between 1995 and 2016 (Baseline Scenario) using observed Colorado River inflows to the AAC representing dry and wet conditions. As expected, it was found that both Alamo River and New River were sensitive to changes in Colorado River inflows. This response was found to be a direct consequence of seasonal fluctuations in inflows as the differences in volumetric evapotranspiration and applied irrigation in 13 agricultural subbasins were relatively small between the two scenarios. This indicates that even with reduced Colorado River inflows, there is enough water in the system to support irrigation and plant growth at baseline scenario levels.

Further improvement to the current model can be made by testing multi-objective calibration techniques, calibrating for multiple model outputs such as remotely sensed ET and soil moisture in addition to streamflow. Furthermore, updating the soil database can improve calibration results. A longer-term application of this model would be to analyze the watershed scale water budget for the Salton Sea Watershed to inform management decisions regarding the Salton Sea. In order to achieve this goal, further model calibration should target three main areas – 1) inflows from

Mexico, 2) inflows from Coachella Valley, and 3) inflows from Salt Creek. The current model setup demonstrated the application of a semi-distributed model to two hydrologically distinct systems within the same watershed. The main findings of this model highlighted the underlying importance of flow regimes for successful model calibration. Additionally, the application of the model in understanding flux partitioning in highly managed subbasins in response to management decisions was also demonstrated.

6. REFERENCES

Abbaspour. (2015). *SWAT Calibration and Uncertainty Programs, User Manual*.

Abbaspour, K. C., Johnson, C. A., & Genuchten, M. T. van. (2004). Estimating Uncertain Flow and Transport Parameters Using a Sequential Uncertainty Fitting Procedure. *Vadose Zone Journal*, *3*(4), 1340–1352. https://doi.org/10.2136/vzj2004.1340

Abbott, M. B., Bathurst, J. C., Cunge, J. A., O'Connell, P. E., & Rasmussen, J. (1986). An introduction to the European Hydrological System — Systeme Hydrologique Europeen, "SHE", 1: History and philosophy of a physically-based, distributed modelling system. *Journal of Hydrology*, *87*(1), 45–59. https://doi.org/10.1016/0022-1694(86)90114-9

Awan, U. K., & Ismaeel, A. (2014). A new technique to map groundwater recharge in irrigated areas using a SWAT model under changing climate. *Journal of Hydrology*, *519*, 1368–1382. https://doi.org/10.1016/j.jhydrol.2014.08.049

Beven, K., & Binley, A. (1992). The future of distributed models: Model calibration and uncertainty prediction. *Hydrological Processes*, *6*(3), 279–298. https://doi.org/10.1002/hyp.3360060305

BOR. (2014). *Estimates of Evapotranspiration and Evaporation Along the Lower Colorado River: Calendar Year 2010*. Bureau of Reclamation. https://www.usbr.gov/lc/region/g4000/4200Rpts/LCRASRpt/2010/report10.pdf

Bosch, N. S., Allan, J. D., Dolan, D. M., Han, H., & Richards, R. P. (2011). Application of the Soil and Water Assessment Tool for six watersheds of Lake Erie: Model parameterization and calibration. *Journal of Great Lakes Research*, *37*(2), 263–271. https://doi.org/10.1016/j.jglr.2011.03.004

Boyle, D. P., Gupta, H. V., & Sorooshian, S. (2000). Toward improved calibration of hydrologic models: Combining the strengths of manual and automatic methods. *Water Resources Research*, *36*(12), 3663–3674. https://doi.org/10.1029/2000WR900207

Bucak, T., Trolle, D., Andersen, H. E., Thodsen, H., Erdoğan, Ş., Levi, E. E., Filiz, N., Jeppesen, E., & Beklioğlu, M. (2017). Future water availability in the largest freshwater Mediterranean lake is at great risk as evidenced from simulations with the SWAT model. *Science of The Total Environment*, *581–582*, 413–425. https://doi.org/10.1016/j.scitotenv.2016.12.149

Burt, C., Layous, S., & Feist, K. (2012). *Mexicali Valley Water Study*. California Polytechnic State University.

CH2M Hill. (2002). *IID Water Conservation and Transfer Project, Final Environmental Impact Report/Environmental Impact Statement*. https://www.iid.com/water/library/qsa-water-transfer/environmental-assessments-permits/final-eir-eis

CH2M Hill. (2018a). *Salton Sea Hydrological Modeling and Results* [Technical Report].

CH2M Hill. (2018b). *Salton Sea Hydrology Development*.

Chaney, N. W., Minasny, B., Herman, J. D., Nauman, T. W., Brungard, C. W., Morgan, C. L. S., McBratney, A. B., Wood, E. F., & Yimam, Y. (2019). POLARIS Soil Properties: 30-m Probabilistic Maps of Soil Properties Over the Contiguous United States. *Water Resources Research*, *55*(4), 2916–2938. https://doi.org/10.1029/2018WR022797

Chen, Y., Marek, G. W., Marek, T. H., Brauer, D. K., & Srinivasan, R. (2017). Assessing the Efficacy of the SWAT Auto-Irrigation Function to Simulate Irrigation, Evapotranspiration, and Crop Response to Management Strategies of the Texas High Plains. *Water*, *9*(7), 509. https://doi.org/10.3390/w9070509

Cibin, R., Sudheer, K. P., & Chaubey, I. (2010). Sensitivity and identifiability of stream flow generation parameters of the SWAT model. *Hydrological Processes*, *24*(9), 1133–1148. https://doi.org/10.1002/hyp.7568

Cohen, M. J. (2014). *Hazard's Toll: The Costs of Inaction at the Salton Sea*. Pacific Institute. https://pacinst.org/publication/hazards-toll/

Cohen, M. J., Christian-Smith, J., & Berggren, J. (2013, May). Water to Supply the Land: Irrigated Agriculture in the Colorado River Basin. *Pacific Institute*. https://pacinst.org/publication/water-to-supply-the-land-irrigated-agriculture-in-the-colorado-river-basin/

Cohen, M. J., & Hyun, K. H. (2006). *The Future of the Salton Sea With No Restoration Project.* Pacific Institute.

Daly, C., Taylor, G., & Gibson, W. (1997). *The Prism Approach to Mapping Precipitation and Temperature*. 4.

Dechmi, Burguete, J., & Skhiri, A. (2012). SWAT application in intensive irrigation systems: Model modification, calibration and validation. *Journal of Hydrology*, *470–471*, 227–238. https://doi.org/10.1016/j.jhydrol.2012.08.055

Dechmi, & Skhiri, A. (2013). Evaluation of best management practices under intensive irrigation using SWAT model. *Agricultural Water Management*, *123*, 55–64. https://doi.org/10.1016/j.agwat.2013.03.016

Dile, Y., Srinivasan, R., & George, C. (2018). *QGIS Interface for SWAT (QSWAT), Version 1.7*.

Dr. Aliasghar Montazar. (2020). *Personal communication, Dr. Aliasghar Montazar* [Personal communication].

Ficklin, D. L., Luo, Y., Luedeling, E., & Zhang, M. (2009). Climate change sensitivity assessment of a highly agricultural watershed using SWAT. *Journal of Hydrology*, *374*(1), 16–29. https://doi.org/10.1016/j.jhydrol.2009.05.016

Gassman, P. W., Arnold, J. g, Srinivasan, R., & Reyes, M. (2010). The Worldwide Use of the SWAT Model: Technological Drivers, Networking Impacts, and Simulation Trends. *21st Century Watershed Technology: Improving Water Quality and Environment Conference Proceedings, 21-24 February 2010, Universidad EARTH, Costa Rica*. 21st Century Watershed Technology: Improving Water Quality and Environment Conference Proceedings, 21-24 February 2010, Universidad EARTH, Costa Rica. https://doi.org/10.13031/2013.29418

Gassman, P. W., Reyes, M. R., Green, C. H., & Arnold, J. G. (2007). The Soil and Water Assessment Tool: Historical Development, Applications, and Future Research Directions. *Transactions of the ASABE*, *50*(4), 1211–1250. https://doi.org/10.13031/2013.23637

Githui, F., Selle, B., & Thayalakumaran, T. (2012). Recharge estimation using remotely sensed evapotranspiration in an irrigated catchment in southeast Australia. *Hydrological Processes*, *26*(9), 1379–1389. https://doi.org/10.1002/hyp.8274

Griensven, A. van, Ndomba, P., Yalew, S., & Kilonzo, F. (2012). Critical review of SWAT applications in the upper Nile basin countries. *Hydrology and Earth System Sciences*, *16*(9), 3371–3381. https://doi.org/10.5194/hess-16-3371-2012

Gupta, H. V., Kling, H., Yilmaz, K. K., & Martinez, G. F. (2009). Decomposition of the mean squared error and NSE performance criteria: Implications for improving hydrological modelling. *Journal of Hydrology*, *377*(1–2), 80–91. https://doi.org/10.1016/j.jhydrol.2009.08.003

Hengl, T., Jesus, J. M. de, Heuvelink, G. B. M., Gonzalez, M. R., Kilibarda, M., Blagotić, A., Shangguan, W., Wright, M. N., Geng, X., Bauer-Marschallinger, B., Guevara, M. A., Vargas, R., MacMillan, R. A., Batjes, N. H., Leenaars, J. G. B., Ribeiro, E., Wheeler, I., Mantel, S., & Kempen, B. (2017). SoilGrids250m: Global gridded soil information based on machine learning. *PLOS ONE*, *12*(2), e0169748. https://doi.org/10.1371/journal.pone.0169748

Homer, C., Dewitz, J., Jin, S., Xian, G., Costello, C., Danielson, P., Gass, L., Funk, M., Wickham, J., Stehman, S., Auch, R., & Riitters, K. (2020). Conterminous United States land cover change patterns 2001–2016 from the 2016 National Land Cover Database. *ISPRS Journal of Photogrammetry and Remote Sensing*, *162*, 184–199. https://doi.org/10.1016/j.isprsjprs.2020.02.019

Hopkins, F. M., Carranza, V., Ajami, H., Allison, J. E., Anderson, R. G., Barrows, C. W., Barth, M., Jenerette, D. R., Porter, W. C., Rolinski, T., Schwabe, K., Yáñez, C., & Yu, N. (2018). *Inland Deserts Summary Report. California's Fourth Climate Change Assessment.* https://www.energy.ca.gov/sites/default/files/2019-07/Reg%20Report-%20SUM-CCCA4-2018-008%20InlandDeserts.pdf

IID. (2018). *Imperial Irrigation District, 2016 Water Conservation Plan*. https://www.iid.com/home/showdocument?id=17259

Immerzeel, W. W., & Droogers, P. (2008). Calibration of a distributed hydrological model based on satellite evapotranspiration. *Journal of Hydrology*, *349*(3), 411–424. https://doi.org/10.1016/j.jhydrol.2007.11.017

Imperial Irrigation District. (2018, September). *Showdocument.pdf*. 2016 Water Conservation Plan. https://www.iid.com/home/showdocument?id=17259

ISRIC. (2005). *Soil and Terrain Database (SOTER) for Latin America and the Caribbean (SOTERLAC), version 2.0*. https://data.isric.org/geonetwork/static/api/records/436bd4b0-7ffc-4272-be57-686b7d7eea7d

Jalowska, A. M., & Yuan, Y. (2019). Evaluation of SWAT Impoundment Modeling Methods in Water and Sediment Simulations. *JAWRA Journal of the American Water Resources Association*, *55*(1), 209–227. https://doi.org/10.1111/1752-1688.12715

Jin, S., Homer, C., Yang, L., Danielson, P., Dewitz, J., Li, C., Zhu, Z., Xian, G., & Howard, D. (2019). Overall Methodology Design for the United States National Land Cover Database 2016 Products. *Remote Sensing*, *11*(24), 2971. https://doi.org/10.3390/rs11242971

Kannan, N., Roy, S. B., Rath, J. S., Munill, C. S., & Goldstein, R. A. (2019). Estimating Crop Consumption of Irrigation Water for the Conterminous U.S. *Transactions of the ASABE*, *62*(4), 985–1002. https://doi.org/10.13031/trans.13102

Kennedy, J., & Eberhart, R. (1995). Particle swarm optimization. *Proceedings of ICNN'95 - International Conference on Neural Networks*, *4*, 1942–1948 vol.4. https://doi.org/10.1109/ICNN.1995.488968

Khan, U., Ajami, H., Tuteja, N. K., Sharma, A., & Kim, S. (2018). Catchment scale simulations of soil moisture dynamics using an equivalent cross-section based hydrological modelling approach. *Journal of Hydrology*, *564*, 944–966. https://doi.org/10.1016/j.jhydrol.2018.07.066

Khoi, D. N., & Thom, V. T. (2015). Parameter uncertainty analysis for simulating streamflow in a river catchment of Vietnam. *Global Ecology and Conservation*, *4*, 538–548. https://doi.org/10.1016/j.gecco.2015.10.007

Kirchmeier-Young, M. C., & Zhang, X. (2020). Human influence has intensified extreme precipitation in North America. *Proceedings of the National Academy of Sciences*, *117*(24), 13308–13313. https://doi.org/10.1073/pnas.1921628117

Kollet, S. J., & Maxwell, R. M. (2006). Integrated surface–groundwater flow modeling: A free-surface overland flow boundary condition in a parallel groundwater flow model. *Advances in Water Resources*, *29*(7), 945–958. https://doi.org/10.1016/j.advwatres.2005.08.006

Koycegiz, C., & Buyukyildiz, M. (2019). Calibration of SWAT and Two Data-Driven Models for a Data-Scarce Mountainous Headwater in Semi-Arid Konya Closed Basin. *Water*, *11*(1), 147. https://doi.org/10.3390/w11010147

Kuczera, G., & Parent, E. (1998). Monte Carlo assessment of parameter uncertainty in conceptual catchment models: The Metropolis algorithm. *Journal of Hydrology*, *211*(1), 69–85. https://doi.org/10.1016/S0022-1694(98)00198-X

Liew, M. W. V., & Garbrecht, J. (2003). Hydrologic Simulation of the Little Washita River Experimental Watershed Using Swat1. *JAWRA Journal of the American Water Resources Association*, *39*(2), 413–426. https://doi.org/10.1111/j.1752-1688.2003.tb04395.x

Livneh, B., Bohn, T. J., Pierce, D. W., Munoz-Arriola, F., Nijssen, B., Vose, R., Cayan, D. R., & Brekke, L. (2015, August 18). *A spatially comprehensive, hydrometeorological data set for Mexico, the U.S., and Southern Canada 1950–2013 | Scientific Data*. https://www.nature.com/articles/sdata201542

Luo, Y., Zhang, X., Liu, X., Ficklin, D., & Zhang, M. (2008). Dynamic modeling of organophosphate pesticide load in surface water in the northern San Joaquin Valley watershed of California. *Environmental Pollution*, *156*(3), 1171–1181. https://doi.org/10.1016/j.envpol.2008.04.005

Marek, G. W., Gowda, P. H., Marek, T. H., Porter, D. O., Baumhardt, R. L., & Brauer, D. K. (2017). Modeling long-term water use of irrigated cropping rotations in the Texas High Plains using SWAT. *Irrigation Science*, *35*(2), 111–123. https://doi.org/10.1007/s00271-016-0524-6

McInerney, D., Thyer, M., Kavetski, D., Githui, F., Thayalakumaran, T., Liu, M., & Kuczera, G. (2018). The Importance of Spatiotemporal Variability in Irrigation Inputs for Hydrological Modeling of Irrigated Catchments. *Water Resources Research*, *54*(9), 6792–6821. https://doi.org/10.1029/2017WR022049

Medellín-Azuara, J., Vergati, J. A., Sumner, D. A., Howitt, R. E., & Lund, J. R. (2012). *Analysis of effects of reduced supply of water on agricultural production andirrigation water use in Southern California.*

Mesinger, F., DiMego, G., Kalnay, E., Mitchell, K., Shafran, P. C., Ebisuzaki, W., Jović, D., Woollen, J., Rogers, E., Berbery, E. H., Ek, M. B., Fan, Y., Grumbine, R., Higgins, W., Li, H., Lin, Y., Manikin, G., Parrish, D., & Shi, W. (2006). North American Regional Reanalysis. *Bulletin of the American Meteorological Society*, *87*(3), 343–360. https://doi.org/10.1175/BAMS-87-3-343

Molina-Navarro, E., Nielsen, A., & Trolle, D. (2018). A QGIS plugin to tailor SWAT watershed delineations to lake and reservoir waterbodies. *Environmental Modelling & Software*, *108*, 67–71. https://doi.org/10.1016/j.envsoft.2018.07.003

Moriasi, D. N., Arnold, J. G., Liew, M. W. V., Bingner, R. L., Harmel, R. D., & Veith, T. L. (2007). Model Evaluation Guidelines for Systematic Quantification of Accuracy in Watershed Simulations. *Transactions of the ASABE*, *50*(3), 885–900. https://doi.org/10.13031/2013.23153

Muleta, M. K. (2012). Model performance sensitivity to objective function during automated calibrations. *Journal of Hydrologic Engineering*, *17*(6), 756–767.

MWH. (2012). *Coachella Valley Water Management Plan 2010 Update*. MWH.

Natural Resources Conservation Service. (2006). *A REVIEW OF AGRICULTURAL WATER USE IN THE COACHELLA VALLEY*.

https://www.nrcs.usda.gov/wps/PA_NRCSConsumption/download?cid=nrcseprd336811&ext=pdf

Nazemi, A., & Wheater, H. S. (2015). On inclusion of water resource management in Earth system models – Part 1: Problem definition and representation of water demand. *Hydrology and Earth System Sciences*, *19*(1), 33–61. https://doi.org/10.5194/hess-19-33-2015

Neitsch, S. L., Arnold, J. G., Kiniry, J. R., & Williams, J. R. (2009). *Soil and Water Assessment Tool: Theoretical Documentation, Version 2009*.

Nrcs141p2_017781.pdf. (n.d.). Retrieved April 18, 2020, from https://www.nrcs.usda.gov/Internet/FSE_DOCUMENTS/nrcs141p2_017781.pdf

Paul, M., & Negahban-Azar, M. (2018). Sensitivity and uncertainty analysis for streamflow prediction using multiple optimization algorithms and objective functions: San Joaquin Watershed, California. *Modeling Earth Systems and Environment*, *4*(4), 1509–1525. https://doi.org/10.1007/s40808-018-0483-4

Post, D. F., Fimbres, A., Matthias, A. D., Sano, E. E., Accioly, L., Batchily, A. K., & Ferreira, L. G. (2000). Predicting Soil Albedo from Soil Color and Spectral Reflectance Data. *Soil Science Society of America Journal*, *64*(3), 1027–1034. https://doi.org/10.2136/sssaj2000.6431027x

Ross, C. W., Prihodko, L., Anchang, J., Kumar, S., Ji, W., & Hanan, N. P. (2018). HYSOGs250m, global gridded hydrologic soil groups for curve-number-based runoff modeling. *Scientific Data*, *5*(1), 180091. https://doi.org/10.1038/sdata.2018.91

Salton Sea Authority. (2017). *Salton Sea Facts*. http://saltonseaauthority.org/get-informed/facts/

Saxton, K. E., & Willey, P. H. (2006). *THE SPAW MODEL FOR AGRICULTURAL FIELD AND POND HYDROLOGIC SIMULATION*. USDA.

Shabani, A., Zhang, X., & Ell, M. (2017). Modeling Water Quantity and Sulfate Concentrations in the Devils Lake Watershed Using Coupled SWAT and CE-QUAL-W2. *JAWRA Journal of the American Water Resources Association*, *53*(4), 748–760. https://doi.org/10.1111/1752-1688.12535

Simunek, J., van Genuchten, M. T., & Sejna, M. (2006). *The HYDRUS software package for simulating two- and three-dimensional movement of water, heat, and multiple solutes in variably-saturated media, version 1.0, technical manual,*. PC Progress.

Sudheer, K. P., Chaubey, I., Garg, V., & Migliaccio, K. W. (2007). Impact of time-scale of the calibration objective function on the performance of watershed models. *Hydrological Processes*, *21*(25), 3409–3419. https://doi.org/10.1002/hyp.6555

Swamee, P. K., Mishra, G. C., & Chahar, B. R. (2000). Design of Minimum Seepage Loss Canal Sections. *Journal of Irrigation and Drainage Engineering*, *126*(1), 28–32. https://doi.org/10.1061/(ASCE)0733-9437(2000)126:1(28)

Tan, M. L., Gassman, P. W., Yang, X., & Haywood, J. (2020). A review of SWAT applications, performance and future needs for simulation of hydro-climatic extremes. *Advances in Water Resources*, *143*, 103662. https://doi.org/10.1016/j.advwatres.2020.103662

Tarboton, D. G. (2008). *TERRAIN ANALYSIS USING DIGITAL ELEVATION MODELS (TAUDEM)*. Utah State University. http://hydrology.usu.edu/taudem/taudem3.1/

Thornton, P. E., Thornton, M. M., Mayer, B. W., Wei, Y., Devarakonda, R., Vose, R. S., & Cook, R. B. (2016). *Daymet: Daily Surface Weather Data on a 1-km Grid for North America, Version 3.* ORNL DAAC. https://doi.org/10.3334/ornldaac/1328

Tompson, A., Demir, Z., Moran, J., Mason, D., Wagoner, J., Kollet, S., Mansoor, K., & McKereghan, P. (2008). *Groundwater Availability Within the Salton Sea Basin* (LLNL-TR-400426). Lawrence Livermore National Laboratory.

Uniyal, B., Dietrich, J., Vu, N. Q., Jha, M. K., & Arumí, J. L. (2019). Simulation of regional irrigation requirement with SWAT in different agro-climatic zones driven by observed climate and two reanalysis datasets. *Science of The Total Environment*, *649*, 846–865. https://doi.org/10.1016/j.scitotenv.2018.08.248

USGS. (2019). *National Water Information System*. https://maps.waterdata.usgs.gov/mapper/?state=ca

van Griensven, A., & Meixner, T. (2007). A global and efficient multi-objective auto-calibration and uncertainty estimation method for water quality catchment models. *Journal of Hydroinformatics*, *9*(4), 277–291. https://doi.org/10.2166/hydro.2007.104

Wada, Y., Wisser, D., & Bierkens, M. F. P. (2014). Global modeling of withdrawal, allocation and consumptive use of surface water and groundwater resources. *Earth System Dynamics*, *5*(1), 15–40. https://doi.org/10.5194/esd-5-15-2014

Wang, R., Chen, H., Luo, Y., Moran, P., Grieneisen, M., & Zhang, M. (2019). Nitrate Runoff Contributing from the Agriculturally Intensive San Joaquin River Watershed to Bay-Delta in California. *Sustainability*, *11*(10), 2845. https://doi.org/10.3390/su11102845

Wei, X., Bailey, R. T., & Tasdighi, A. (2018). Using the SWAT Model in Intensively Managed Irrigated Watersheds: Model Modification and Application. *Journal of Hydrologic Engineering*, *23*(10), 04018044. https://doi.org/10.1061/(ASCE)HE.1943-5584.0001696

Xiao, M., Udall, B., & Lettenmaier, D. P. (2018). On the Causes of Declining Colorado River Streamflows. *Water Resources Research*, *54*(9), 6739–6756. https://doi.org/10.1029/2018WR023153

Xie, X., & Cui, Y. (2011). Development and test of SWAT for modeling hydrological processes in irrigation districts with paddy rice. *Journal of Hydrology*, *396*(1), 61–71. https://doi.org/10.1016/j.jhydrol.2010.10.032

Xiong, L., Xu, X., Ren, D., Huang, Q., & Huang, G. (2019). Enhancing the capability of hydrological models to simulate the regional agro-hydrological processes in watersheds with shallow groundwater: Based on the SWAT framework. *Journal of Hydrology, 572*, 1–16. https://doi.org/10.1016/j.jhydrol.2019.02.043

Yang, L., Jin, S., Danielson, P., Homer, C., Gass, L., Bender, S. M., Case, A., Costello, C., Dewitz, J., Fry, J., Funk, M., Granneman, B., Liknes, G. C., Rigge, M., & Xian, G. (2018). A new generation of the United States National Land Cover Database: Requirements, research priorities, design, and implementation strategies. *ISPRS Journal of Photogrammetry and Remote Sensing*, *146*, 108–123. https://doi.org/10.1016/j.isprsjprs.2018.09.006

Zhang, L., Xue, B., Yan, Y., Wang, G., Sun, W., Li, Z., Yu, J., Xie, G., & Shi, H. (2019). Model Uncertainty Analysis Methods for Semi-Arid Watersheds with Different Characteristics: A Comparative SWAT Case Study. *Water*, *11*(6), 1177. https://doi.org/10.3390/w11061177